UNIVERSITÉ DE REIMS CHAMPAGNE-ARDENNE

ÉCOLE DOCTORALE Choisissez un élément.

THÈSE

Pour obtenir le grade de

DOCTEUR DE L'UNIVERSITÉ DE REIMS CHAMPAGNE-ARDENNE

Discipline : ***MÉCANIQUE DES FLUIDES, ÉNERGÉTIQUE, THERMIQUE, COMBUSTION, ACOUSTIQUE***

Spécialité : Energétique et Génie des procédés

Présentée et soutenue publiquement par

PATRICIA AL ALAM

Le 11 juillet 2018

Microscopie thermique à sonde locale : vers une analyse thermique des nanomatériaux

---

Thèse dirigée par **NATHALIE TRANNOY**

JURY

M. Jonathan WEAVER**,**	Professeur,	Université de Glasgow,	**Président**
M. Francesc ALZINA**,**	Directeur de Recherche,	Institut de Nanoscience et Nanotechnologie,	**Rapporteur**
Mme Nathalie TRANNOY,	Professeur,	Université de Reims,	**Directeur de thèse**
Mme Severine GOMES,	Chargé de Recherche HDR,	CNRS - CETHIL,	**Examinateur**
M. Petr KLAPETEK,	Chargé de Recherche HDR,	Institut de métrologie Tchèque,	**Examinateur**
M. Jaona RANDRIANALISOA,	Maître de Conférences,	Université de Reims,	**Examinateur**
M. David LACROIX,	Professeur,	Université de Lorraine,	**Invité**

Abstract

Scanning thermal microscopy is a promising tool to investigate material's thermal measurements and heat transfer mechanisms at the micro/nanoscale. The probe thermal response was explored using two different resistive probes: Wollaston and Palladium probes. A 3D realistic model was developed for the Wollaston probe-sample system with their surrounding medium. The simulation of tip wire takes into account its holder and considers that the surrounding medium between the probe and the sample is convective and diffusive. The probe's response was evaluated during the approach toward a sample of copper. The comparison with experimental results showed that considering natural air convection for the surrounding medium is a valid assumption. We then present a methodology to characterize the thermal signal of probe in contact with a nanostructured sample. For that, we used a sample composed of buried silicon steps under SiO_2. SThM proves to be a powerful tool to perform subsurface imaging. We showed that the thermal signal obtained by the probe is influenced by the presence of internal structures and corresponds to a scanned volume which takes into account material's thermal properties. With our modelling, we were able to rebuild the experimental profile obtained by SThM. For the Palladium probe, the probe's response was studied experimentally under ambient conditions in the AC mode for different frequencies. The analysis of the results pointed on a phenomenon which can be described as a thermal wave resonance which takes place at micro/nanoscale. This phenomenon is suggested to be related to the thermal diffusion length of the surrounding medium (air) and independent of the sample thermal properties.

Keywords: Scanning thermal microscopy, Characterization, nanostructured sample, thermal probe, convective medium, thermal wave, modelling, experiments

Résumé

La microscopie thermique est un outil prometteur permettant d’étudier les mesures thermiques de matériaux et les mécanismes de transfert de chaleur aux micro/nanoéchelles. La réponse thermique de la sonde a été étudiée en utilisant deux sondes résistives : Wollaston et Palladium. Un modèle en 3D réaliste a été développé pour la sonde Wollaston et l’échantillon avec leur milieu environnant. La simulation de la sonde prend en compte son support et considère que le milieu environnant est convectif et conductif. La réponse de la sonde a été évaluée lors de l'approche vers un échantillon de cuivre. La comparaison avec les résultats expérimentaux montre que la prise en compte de la convection naturelle pour le milieu environnant est une hypothèse qui semble pourrait être prise. Nous présentons ensuite une méthodologie pour étudier le signal thermique de la sonde en contact avec un échantillon nanostructuré. Pour cela, nous avons utilisé un échantillon composé de marches de silicium sous une couche de SiO_2. SThM s'avère être un outil puissant pour effectuer de l'imagerie sub-surfacique. Nous avons montré que le signal thermique obtenu par la sonde est influencé par la présence de structures internes et correspond à un volume sondé qui prend en compte les propriétés thermiques des matériaux. Avec notre modèle, nous avons pu reconstruire le profil expérimental obtenu par SThM. Pour la sonde en Palladium, la réponse de la sonde a été étudiée expérimentalement sous conditions ambiantes en mode alternatif. L'analyse des résultats a mis en évidence la présence d’un phénomène que nous interprétons comme une résonance d'onde thermique qui prend place au micro/nanoéchelle. Ce phénomène est lié à la longueur de diffusion thermique du milieu environnant (air) et indépendant des propriétés thermiques de l'échantillon.

Mots clés: Microscopie thermique à balayage, Caractérisation thermique, échantillon nanostructuré, sonde thermique, milieu convectif, onde thermique, modèle, expérimental

Acknowledgments

I would like to thank all members of jury for their participation in the thesis defense. I thank the reviewers Jonathan Weaver and Francesc Alzina for their comments and reports also for traveling all the way from Glasgow and Spain for the thesis defense. I thank Severine Gomes, Petr Klapetek (thank you for traveling from Czech Republic) and Jaona Randrianalisoafor the examination of the manuscript and their participation in the thesis defense. It was a pleasure working with all of you in the frame of QuantiHeat project and I hope that we will meet again in the near future.

I would like to thank infinitely my supervisor Nathalie Trannoy for being a great advisor. I will be always grateful for your precious advices, for the opportunities you gave me, for teaching me how to be a good researcher and how to be autonomous during this research work. Thank you also for your support not only in my research works but also during my journey in this lab.

I would also like to thanks Jaona Randrianalisoa for all the advices and the help in the modelling part of my thesis and for all the group meetings which increased my knowledge in this domain. I would like to thank also some collaboration partners with whom I worked during this thesis: Petr Klapetek from CMI Brno, Mika Prunnila from VTT Finland and a special thanks to the research group of Professor Jonathan Weaver from Glasgow University for their warm welcome and for giving me the opportunity to visit their lab and to learn from their expertise.

I would like to thank Champagne-Ardennes region (A2101-03-Excellence) and European project QuantiHeat (ProgramFP7-NMP-2013-LARGE-7) for funding this research work.

I appreciate the great moments I had with different persons in the lab. Thanks to Clarisse for her support and for the moments we shared together. Big thanks go also to Tala for her support, for listening to my problems and always being there to help me out. I also mention Naima and the actual and former PhD students and postdoctoral researchers.

Big thanks to Georges Costantine for those 3 years full of positive energy and positive vibes because of him!! Thanks for all the support you gave and for being such a great friend!! Huge thanks goes also to Manel, thank you for being who you are and for always being there for me when I needed! I highly appreciate the moments of laziness and laughter we spent together... lots of love to you.

I would like to especially thank Georges Hamaoui (my office colleague) who was always there for me, for all the times he encouraged me and made my thesis journey easier, for the moments we shared in and outside the lab, without him this journey wouldn't be the same!! Many thanks go also to Carmen for being the most caring person I ever met, for having a pure heart, for taking care of me when I needed!! You two form a great couple I wish you the best in your lives.. lots of love to you.

I especially would like to mention Stephanie my sister!! There are no enough words to describe the gratitude and the love that I hold for you!! You are the greatest sister/friend that a person can ever have! Your support to me, your encouragements were not restricted to the PhD journey only, I had your support all along my life journey!! I am so lucky to have you!! Love u so much!!

Special thanks goes to my heart, my future Doctor Charbel (babu) for being always there for me, for the infinite support and encouragement you gave me, for all the efforts that you made and you're keep doing from the day I met you!! For all the funny ways you do to make me happy (and all the preparations you did to keep me entertained!! ;)). Thank you for the positive shift you made to my life!! I am so lucky to have a man like you!! I love you loads!!

I would like to thank my parents (Léona and Raymond) for all their infinite support and encouragement. Due to their suffering and the sacrifices they made in their lives, I was able later to follow my ambitions. Hopefully, one day I will be able to give them back just a little from what they gave me all time. I also thank my Brothers (Rony, Pierre, Paul - and their wives Carole (ya albiii..), Ronza (sushii time), Julie) for being the greatest people and support (by all means :D) I can have, my lovely nephew Chriss and my princesses, my cutie pie nieces Perla and Christy. A big and huge special thanks goes to my beautiful sister inside/out and my best friend by choice Pamela (Pampoumtii – Miss Lebanon :D) for being the best sister that someone can ever have in the world, for her infinite support and encouragements, I am one of the luckiest people in the world to have you in my life.. I love you all so much. Big thanks also go to my Cousins (Maria, Melissa, Maria (our nutritionist) and Tony) for your special kind of support by gossiping, being funny and sharing lots of food experiences together :D Many thanks also go to my big family including Grandparents, Cousins, Aunts and Uncles (lots of love to you…).

Table of contents

Table des matières

List of figures

Liste des figures

Figure 4 - 1 : Représentation du dispositif expérimental mis en place et utilisée pour les mesures. Il est composé d’un pont de Wheatstone et d’une détection synchrone. Ce dispositif est utilisé pour le mode de fonctionnement AC

Figure 4 - 2 : Représentation schématique du dispositif expérimental mis en place comportant le support de la sonde, une camera grandissante et un porte-échantillon avec une platine motorisée.

Figure 4 - 3 : Évolution de la réponse de la sonde s’approchant et se rétractant d’un échantillon de cuivre sous condition ambiante pour une fréquence de 1 500 Hz avec un courant de 530 µA

Figure 4 - 5 : Evolution en amplitude et en phase de la réponse de la sonde à la troisième harmonique en fonction de la distance entre la sonde et un échantillon de cuivre pour quatre fréquences. Les mesures ont été effectuées dans des conditions ambiantes pour un courant de µA 530

Figure 4 - 6 : Evolution normalisée en amplitude et en phase de la réponse de la sonde à la troisième harmonique en fonction de la distance entre la sonde et un échantillon de cuivre pour 4 fréquences. Les mesures ont été effectuées sous conditions ambiantes avec un courant de 530 µA

Figure 4 - 7 : Comparaison des distances caractéristiques dR de la courbe d’amplitude à la longueur de diffusion thermique de l’air sec en fonction de la fréquence d’excitation

Figure 4 - 8 : Comparaison de l’évolution de la réponse de sonde en amplitude et en phase à la troisième harmonique en fonction de la distance pour deux échantillons ayant des conductivités thermiques différentes (cuivre, verre) pour une fréquence de 3 000 Hz à température ambiante avec un courant de 530 µ A

Figure 4 - 9 : Représentation schématique de la nanosonde de silicium a proximité d’un échantillon de silicium

Figure 4 - 10 : Cartographie de la température de la sonde en silicium et de l’échantillon où la sonde est placée à 1 nm de l’échantillon et zoom de la sonde.

Figure 4 - 11 : Comparaison des résultats obtenus FEM avec la littérature pour le flux de chaleur dissipée de la demi-sphère en fonction de la distance qui sépare la sonde et l’échantillon.

Figure 4 - 12 : Représentation schématique d’un matériau massif avec une source de chaleur placée en surface de l’échantillon

Figure 4 - 13 : Evolution de la conductivité thermique a) du silicium et b) du dioxyde de silicium en fonction de la température. Conductivité thermique du silicium dopé avec dopant B en fonction de la densité à une température de 300 K.

Figure 4 - 14 : Flux de chaleur total de la source de chaleur en fonction de la variation de son diamètre pour a) silicium b) SiO2 c) B-dopé avec une densité de zéro, d) B dopé de silicium avec une densité de $1^{e}25$.

List of tables

Liste des tableaux

Nomenclature

Abbreviation	*Term*
AFM	Atomic Force Microscope
SThM	Scanning Thermal Microscopy
TCU	Thermal Control Unit
CVD	Chemical Vapor Deposition
PECVD	Plasma Enhanced Chemical Vapor Deposition
MFP	Mean Free Paths
FEM	Finite Element Method
SEM	Scanning Electron Microscope

Symbol	*Variable*	*Unit*
b	Thermal exchange radius	m
d	Probe-sample distance	m
g	Ratio	
G_{th}	Total thermal conductance	$\mathrm{W.K^{-1}}$
h	Heat transfer coefficient	$\mathrm{W/m^2.K}$
k_{film}	Thermal conductivity of film	$\mathrm{W.m^{-1}.K^{-1}}$
k_{sub}	Thermal conductivity of substrate	$\mathrm{W.m^{-1}.K^{-1}}$
l	Thickness	m
P	Pressure	bar
P_a	Probe Joule power (in contact with sample)	W
P_c	Probe Joule power – Probe in air	W
Q	Heat flux	W

R_C	Thermal contact resistance	$K.W^{-1}$
R_s	Spreading thermal resistance	$K.W^{-1}$
T_a	Ambient Temperature	K
u	Velocity	m/s
$V_{3\omega}$	Third harmonic voltage	V
C_p	Heat capacity	$J.Kg^{-1}.K^{-1}$
D	Dielectric loss	
V	voltage	V
J	Current density	
E	Electric field	
R	Electrical resistance	Ω
I	Electrical current	A
G_{air}	Thermal conductance through air	$W.K^{-1}$
a_a	Thermal diffusivity of air	m^2s^{-1}
f_{th}	Thermal frequency	
t	Thin film thickness	m
T_m	Mean temperature of the probe	K

Greek letters

$\Delta P/P_a$	Probe Joule power relative difference	
ΔT_p	Temperature difference	K
$\theta_{2\omega}$	Second harmonic relative temperature	K
μ	Dynamic viscosity	
ω	Angular frequency	Rad/s
μ_{th}	The thermal diffusion length	
η	Doping density	$1/m^3$

Nomenclature

Abbreviation	***Term***
AFM	Microscope à Force atomique
SThM	Microscopie thermique a sonde locale
TCU	Unité de contrôle thermique
CVD	Depôt chimique en vapeur
PECVD	Depôt chimique en vapeur par plasma
MFP	Libre parcours moyen
FEM	Méthode par elements finis
SEM	Microscopie électronique à balayage

Symbole	***Variable***	***Unité***
b	Rayon d'échange thermique	m
d	Distance entre la sonde et l'échantillon	m
g	Rapport de flux	
G_{th}	Conductance thermique totale	$\mathrm{W.K^{-1}}$
h	Coefficient d'échange themique	$\mathrm{W/m^2.K}$
k_{film}	Conductivité thermique du film mince	$\mathrm{W.m^{-1}.K^{-1}}$
k_{sub}	Conductivité thermique du substrat	$\mathrm{W.m^{-1}.K^{-1}}$
l	Epaisseur	m
P	Pression	bar
P_c	Puissance dissipée par la sonde (en contact avec l'echantillon)	W

P_a	Puissance dissipée par la sonde – sonde dans l'air	W
Q	Flux de chaleur	W
R_C	Résistance thermique de contact	$K.W^{-1}$
R_s	Résistance thermique de l'échantillon	$K.W^{-1}$
T_a	Température ambiante	K
u	Vitesse	m/s
$V_{3\omega}$	Tension à la troisième harmonique	V
C_p	Capacité calorifique	$J.Kg^{-1}.K^{-1}$
D	Pertes diélectriques	
V	Tension	V
J	Densité de courant	
E	Champ électrique	
R	Résistance électrique	Ω
I	Courant électrique	A
G_{air}	Conductance thermique de l'air	$W.K^{-1}$
a_a	Diffusivité thermique de l'air	m^2s^{-1}
f_{th}	Fréquence thermique	
t	Epaisseur du film mince	m
T_m	Température moyenne de la sonde	K

Greek letters

$\Delta P/P_a$	Ecart relative de la puissance de Joule	
ΔT_p	Ecart de température	K
$\theta_{2\omega}$	Température à la deuxième harmonique	K
μ	Viscosité dynamique	
ω	Fréquence angulaire	Rad/s

μ_{th}	Longueur de diffusion de l’air	
η	Densité de dopage	$1/m^3$

General Introduction

Modern materials technology and device miniaturization are increasingly dedicated to the control of heat management at the nanoscale since thermal properties play an important role in materials used for electronic devices. Tools capable to perform thermal measurements at the nanoscale are needed to aboard this problem. Scanning thermal microscopy (SThM) is a promising technique to explore nanoscale thermal measurements in nanostructures, nano-electronic devices and modern semiconductor. Investigating thermal properties at the micro/nanoscale is crucial for understanding heat transfer in nanostructured materials [1-3]. SThM is an Atomic Force Microscopy (AFM) based technique that enables mapping of temperature or thermal properties of a sample surface. The key element of SThM is its thermal probe that acts as a source and heating components. This manuscript is dedicated to the characterization of probe-sample thermal system to improve the interpretation of thermal measurements. Different resistive probes were used to study thermal interactions that occur between the probe and the sample. The work presented in this thesis is in the frame of the European project QuantiHeat (FP7-NMP-2013-LARGE-7). This project deals with problems linked to thermal metrology at the nanoscale. It aims to provide methods and modelling tools for nanoscale thermal measurements. Several laboratories collaborated to deal with heat management problems at the nanoscale and to provide reliable quantitative measurements. URCA is involved in this project and it focuses on using scanning thermal microscopy method to aboard this problem. Various samples were developed and used to elaborate calibration methods and methodologies for the probe/sample system to characterize the probe thermal signal.

The first chapter introduces the principle of SThM technique. It presents the different resistive probes used in this work. Measurement methods given by researchers are presented for each probe. The chapter focuses on investigations that explored the heat transferred by the probe to the environment while working under ambient conditions. Special attention was given to studies that considered the surrounding medium between the probe and the sample as conductive. Thermal interactions of the probe/sample system depend on material’s thermal properties and their dimensions. Based on the literature, thermal conductivities of materials such as Silicon and Silicon dioxide that will be used in this study are given from experimental and simulation results.

The second chapter consists of developing a 3D realistic model for the Wollaston probe-sample system in COMSOL Multiphysics based on finite element method (FEM). A model for the Wollaston wire based on experimental results was developed in order to evaluate the heat exchange coefficient to the environment. This coefficient was used for the simulation of thermal probe. The probe/sample system was then modeled with their surrounding medium. The simulation treated the surrounding medium as a convective one. Heat fluxes of the probe/sample system are evaluated via the numerical models which gives access to the probe relative Joule power and the overall thermal conductance at the solid-solid contact.

The third chapter describes a methodology to study the thermal signal obtained by thermal probe while scanning across a sample surface. In the frame of the European project QuantiHeat, URCA has proposed a design of a nanostructured sample composed of silicon steps under polished CVD silicon dioxide. It was fabricated by VTT from Finland and used in this chapter. A 3D realistic model was developed for the probe-sample system which takes into account materials thermal properties at nanoscale. The thermal profile obtained by the probe is rebuilt by modelling and compared to experimental results. A free topography sample also provided by VTT is modeled in its realistic geometry. The sample is composed of a buried silicon dioxide with oblique interface on a silicon substrate. The thermal signal obtained by the probe was reconstituted by simulation. The last section of this chapter discusses investigations of polymer particles coated with various thicknesses of Silver with Wollaston probe. Polymers are provided by the industrial company Compart. In a first step, the study was done on single polymer particles which presented a difficulty in the interpretation of results due to inappropriate sample preparation. Therefore, a new set of polymer particles in an adhesive matrix was considered for the next step. Experimental results performed by SThM are presented and discussed.

The last chapter is dedicated to probes of nanoscale tip radius. In the first part, we studied experimentally the probe’s response at the third harmonic in the AC mode using Palladium probe. The probe-sample interactions are analyzed for the probe out of contact while approaching toward a sample of copper.

The second part deals with modelling of Silicon nanoprobe in the frame of QuantiHeat. It aims to check the validity domain of probe/sample modelling. For this a Silicon probe was modelled in FEM while approaching toward a sample of Silicon. The heat flux dissipated from the probe is evaluated and compared to results obtained with different methods such as finite element and finite difference methods.

The last part of this chapter consists on developing a material library in COMSOL Multiphysics based on data from the literature. Various materials were investigated such as Silicon and Silicon dioxide bulk materials, Silicon free standing thin films and polymers with various inclusions. The modeling approach is presented and discussed.

Introduction générale

La technologie des matériaux modernes et la miniaturisation des dispositifs électroniques nécessitent l'étude du transfert de chaleur à l'échelle nanométrique. Les propriétés thermiques des matériaux jouent en effet un rôle important dans le comportement des matériaux, et ceci d'autant plus aux petits échelles. Des outils capables d'effectuer des mesures thermiques à l'échelle micro/nanométrique sont donc nécessaires pour aborder ce problème. La microscopie thermique (SThM) est une technique prometteuse pour l'investigation à ces échelles les propriétés thermiques des matériaux nanostructuré et pour comprendre les mécanismes du transfert de chaleur [1-3]. La microscopie thermique est une technique basée sur la Microscopie à Force Atomique (AFM) qui permet d'obtenir une cartographie de la température ou des propriétés thermiques de la surface de l'échantillon. L'élément clé du SThM est la sonde thermique qui agit comme une source et/ou détecteur de chaleur. Ce manuscrit est dédié à la caractérisation du système thermique sonde-échantillon. Différentes sondes thermorésistives ont été utilisés pour étudier les interactions thermiques qui se produit entre la sonde et l'échantillon. Le travail présenté dans cette thèse est dans le cadre du projet européen QuantiHeat (FP7-NMP-2013-grand-7) et soutenue par la région Champagne Ardennes. Ce projet traite des problèmes liés à la métrologie thermique à l'échelle nanométrique. Il vise à fournir des méthodes expérimentales et outils de modélisation pour les mesures thermiques. L'URCA (Université de Reims Champagne Ardennes) est impliqué dans ce projet et se concentre plus particulièrement sur les méthodes basées sur la microscopie thermique. Divers échantillons ont été développés et utilisés pour l'élaboration de méthodologies afin de caractériser le signal thermique de la sonde.

Le premier chapitre introduit le principe de la technique de la microscopie thermique. Il présente les différentes sondes résistives utilisées dans ce travail. Les méthodes de mesures présentées dans la littérature sont détaillées pour chaque sonde. Ce chapitre se concentre sur les études qui ont exploré le transfert de chaleur transmis par la sonde vers le milieu environnant en travaillant dans des conditions ambiantes. Une attention particulière a été portée sur des études qui traitent le milieu environnant comme conductif entre la sonde et l'échantillon. Les interactions thermiques du système sonde/échantillon dépendent également des propriétés thermiques du matériau. Les conductivités thermiques des matériaux (Silicium et de dioxyde de Silicium) sont données expérimentalement et par simulation comme évaluer dans la littérature.

Le deuxième chapitre consiste à développer un modèle 3D réaliste pour le système de la sonde en Wollaston et l'échantillon. Nous avons utilisés un logiciel basé sur la méthode des éléments finis (FEM). Un modèle pour le filament en Wollaston, basé sur des résultats expérimentaux a d'abord été développé afin d'évaluer le coefficient d'échange thermique effectif de la sonde vers le milieu environnant. Ce coefficient a été utilisé pour la simulation complète de la sonde thermique. Ensuite, le système sonde/échantillon a été modélisé avec son milieu environnant. La simulation considère que le milieu environnant est conductif. Les flux de chaleur du système sonde/échantillon sont évalués à partir du modèle numérique qui permet d'accéder à la puissance Joule relative de la sonde et la conductance thermique totale au contact solide-solide.

Le troisième chapitre décrit une méthodologie pour étudier le signal thermique obtenu par la sonde thermique balayant la surface d'un l'échantillon. Dans le cadre du projet européen QuantiHeat, l'URCA a proposé la conception d'un échantillon nanostructuré composé de marches de silicium sous une couche de dioxyde de silicium poli. Cet échantillon a été fabriqué par l'institut VTT de Finlande. Un modèle réaliste 3D a été développé pour le système sonde-échantillon qui tient compte des propriétés thermiques des matériaux à l'échelle nanométrique. Un profil thermique obtenu par la sonde est reconstruit par modélisation et comparé aux résultats expérimentaux. Un second échantillon a été également fourni par VTT et modélisé avec sa géométrie réelle. L'échantillon est constitué d'une interface SiO2/Si ayant une pente douce sur substrat de silicium. Le signal thermique obtenu par la sonde a été également reconstitué par simulation et comparé aux résultats expérimentaux. La dernière partie de ce chapitre est dédié aux investigations par SThM avec une sonde en Wollaston de particules de polymère enrobées d'une couche d'argent. Les polymères sont fournis par la compagnie industrielle Compart. Dans un premier temps, l'étude a été réalisée sur des particules de polymère libres ayant différentes épaisseurs d'Argent. L'échantillon a été préparé au sein de notre laboratoire selon les instructions données par Compart. L'étude de cet échantillon a présenté des difficultés dans l'interprétation des résultats due à une préparation des échantillons inappropriés. Par conséquent, un nouveau lot d'échantillons composés de particules de polymère fixées dans une matrice adhésive a été fourni. Les résultats expérimentaux effectués par SThM sont présentés et discutés.

Le dernier chapitre est consacré à l’étude des sondes ayant une extrémité avec un rayon de courbure nanométriques. Dans la première partie, la réponse thermique d’une sonde en Palladium a été étudiée expérimentalement en mode AC. L’évolution du signal thermique sonde-échantillon est analysée pour la sonde hors contact. Ils ont mis en évidence la présence d’un phénomène déjà observé avec la sonde Wollaston. Les résultats sont présentés et discutés.

La deuxième partie se situe dans le cadre du projet QuantiHeat, elle traite de la modélisation de nanosonde en Silicium. Elle vise à vérifier le domaine de validité de modélisations du système sonde-échantillon par différentes méthodes. Pour cela, une sonde de silicium a été modélisée dans la méthode de FEM lors de son approche et vers un échantillon de silicium. Le flux de chaleur dissipé par la sonde est évalué et comparé aux résultats obtenus avec différentes méthodes telles que la méthode des éléments finis et des différences finies d’autres partenaires du projet.

La dernière partie de ce chapitre consiste à élaborer une bibliothèque de propriétés thermiques des matériaux issus des données de la littérature. Différentes matériaux ont été étudiés tels que les matériaux massifs en Silicium et en dioxyde de Silicium, les films minces suspendus en Silicium et les polymères avec différentes densités. L’approche de cette étude est présentée et discutée.

Résumé du chapitre 1

La caractérisation locale des propriétés thermophysiques des nouveaux matériaux ou systèmes nécessite des techniques expérimentales qui permettent des mesures thermiques locales à l'échelle nanométrique. Plusieurs techniques et méthodes ont été développées pour atteindre cet objectif tel que la spectroscopie Raman. La microscopie thermique (SThM) basée sur le principe de la microscopie à force atomique (AFM) s'avère être un outil à fort potentiel pour étudier les propriétés thermiques du matériau à l'échelle micro/nano. La quantification des mesures obtenues par SThM exige toutefois une investigation adéquate des mécanismes de transfert de chaleur entre le système sonde-échantillon et le milieu environnant.

Ce chapitre est consacré à une étude bibliographique sur l'analyse du transfert thermique entre une sonde et un échantillon par SThM. Plusieurs types de sondes ont été développés au cours des années précédentes, comme les thermocouples ou des sondes thermo-résistives. Dans ce travail nous nous intéressons plus particulièrement aux sondes thermo-résistives. La première partie de ce chapitre, présente la description de ces sondes thermiques utilisées ainsi que leurs méthodes de mesures. Trois types de sondes ont été étudiées : sonde en Wollaston, en Palladium et celle en Silicium. La sonde Wollaston a été développée en 1994 par Dinwiddie, elle est composée d'un filament en Wollaston de 75 µm de diamètre et son élément résistif est formé d'un filament Platine-Rhodié de 5 µm de diamètre et de 200 µm de longueur avec un rayon de courbure de 15 µm. La sonde en Palladium est une nanosonde, composée de 1µm de film mince de Palladium considéré comme résistance déposé sur un microlevier en Nitrure de Silicium de 150 µm de longueur et de 0.4 µm d'épaisseur. Cette sonde a un rayon de courbure inférieur à 100 nm

Le transfert de chaleur entre la sonde et l'échantillon dépend de plusieurs facteurs tels que la taille des sondes, des propriétés thermiques des éléments de la sonde et de l'échantillon, la température de la sonde, le milieu environnant du système sonde/échantillon et bien d'autres paramètres. Par conséquent, l'interprétation du signal thermique de la sonde et l'investigation des propriétés thermiques des matériaux nécessitent une bonne modélisation du système sonde-échantillon. Cette modélisation passe par l'étude de l'interaction thermique qui peut être interprétée à travers un réseau des conductances thermiques du système.

Jusqu’à présent, les études publiées précédemment traitent le système sonde-échantillon en considérant le milieu environnant comme diffusif. Mais une étude expérimentale a monté que le milieu environnant de la sonde s’échauffe à larges distances ce qui peut engendrer un phénomène de convection pour l’air environnant. En se basant sur cette étude, nous avons considéré l’hypothèse du le milieu environnant comme convectif. Les interactions thermiques entre la sonde et l’échantillon dépendent de plusieurs grandeurs thermiques comme la résistance thermique de l’échantillon, résistance thermique du contact... Ainsi, un état de l’art des recherches qui ont étudié ces quantités est donné d’un point de vue expérimental et théorique. Les valeurs de la résistance thermique du contact évaluées dans la littérature varie entre $10^4 K.W^{-1}$et$10^7 K.W^{-1}$ dépendant de la taille de la sonde et du matériau utilisé.Ces travaux nous ont donné une idée de l’ordre de grandeur évaluée dans la littérature. L'interaction thermique entre la sonde et l'échantillon dépend également des propriétés thermiques de l'échantillon. Ainsi, la dernière partie de ce chapitre présente les études qui caractérisent les propriétés thermiques des matériaux à l'échelle macro / nanométrique. Différentes méthodes ont été utilisées telles que la méthode 3ω, la microscopie thermique à sonde locale et bien d'autres. Ces travaux de recherche ont montré la différence entre les propriétés thermiques des matériaux massifs et celles des films minces d’où l’importance d’utiliser ces propriétés dans notre étude.

Chapter 1: Scanning thermal microscopy: Heat transfer measurements at micro and nanoscale

The characterization of material’s thermophysical properties requires a powerful technique that enables local thermal measurements at the nanoscale. Several techniques and methods are developed to address this problem such as Raman spectroscopy, IR thermal emission or photo reflectance [1]. Scanning thermal microscopy (SThM) is proved to be a well-established tool to study the material’s thermal properties at the micro/nanoscale [1-3]. However, quantifying measurements obtained by SThM requires a proper investigation of the heat transfer mechanisms between the probe-sample system and the surrounding medium.

Therefore, this chapter presents an introduction of SThM technique and a description of thermal probes used in this work. A state of the art of works presented in the literature of thermal interactions between the probe and the sample are presented. A special attention was given to studies that investigated the heat transferred by the probe to the surrounding medium. The last part of this chapter consists on presenting works that investigated thermal properties of nanostructured materials using different techniques such as 3ω method, SThM and many others.

1. Scanning Thermal microscopy (SThM)

Scanning thermal microscopy is a promising technique for thermal measurements that allows the characterization of sample’s thermal properties by scanning their surface. This technique was improved by Majumdar *et al.* in 1993 [4] by associating a thermocouple probe to atomic force microscope (AFM).In general, a scanning thermal microscope is established by adding a thermal probe and a control module to a standard AFM. This allows obtaining a thermal image simultaneously with a topographical image.

1.1. Principle of Atomic Force Microscopy

The atomic force microscope (AFM) principle of measurement relies on the analysis of interaction forces that appears between micrometric or nano-metric probes and the material surface. Regardless the origin of the force, whether it's repulsive when probe is in contact or attractive by capillarity effect due to the presence of a water meniscus on surface, the probe deflection is detected by the displacement of laser beam on the photodetector surface (figure 1-1). The photodetector is composed of four segments, so it's possible to identify the direction of displacement by subtracting or adding different signals obtained by the photodetector.

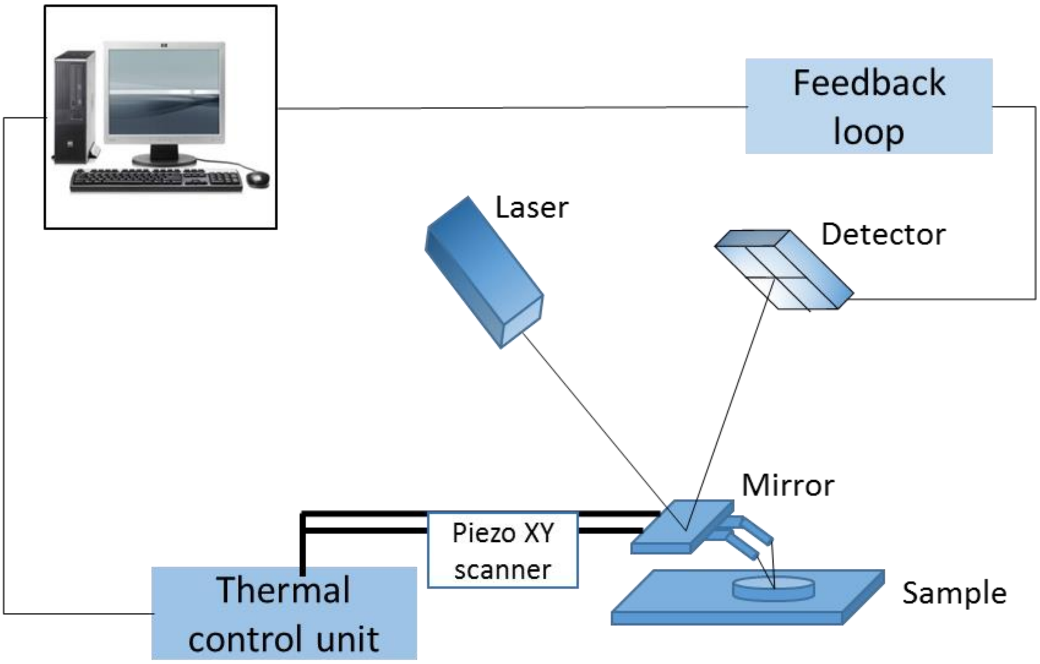

Figure 1- 1: Description of the principle of AFM technique.

When the probe is out of contact, the laser beam reflected via the mirror of the probe hit the photodetector at a certain point. The detected current is than used for reference. A current set point is fixed via the control interface as a function of the probe type and the desired applied force. This procedure is done in two steps. In the first step the motor move the probe toward the sample with little steps. The laser beam is detected once it moves in a significant way, the feedback loop then stops the movement of the motor. A piezoelectric system allows the movement of the probe slightly with respect to the sample in the space dimensions x,y (in plane) and z perpendicular to the surface. The voltage applied to the Piezo-electric affected to the vertical position of the probe is adjusted in a way to respect the value of the set point.

While scanning, the piezo-electric is always adjusted in order to maintain the position of the laser beam constant thus the probe deflection. Therefore, variations of the applied voltage on the piezo are characteristics of the sample topography.

The sensibility of measurements is strongly affected by the value of cantilever spring constant. In fact, when the probe spring constant is low (5 to 6 $N.m^{-1}$) even little deformations affects the probe deflection. Therefore, the spring constant of the probe affects variations of the electric-piezo [5].

1.2. Signal acquisition

The electrical supply of the probe is ensured by an electronic unit (Thermal Control Unit in figure1-1) which provides also different operating modes. The first mode called temperature contrast is a passive mode and the second one called thermal conductivity contrast is an active mode. They are described as:

- The passive mode is when the current flowing through the probe is sufficiently small to avoid any additional heating of the thermal probe. This mode is to map the temperature at the surface of a sample. The sample is locally heated by the probe that plays the role of thermometer (few articles exists in the literature for this mode [6, 7]).

- The active mode allows mapping contrast in thermal conductivity. The current flowing through the probe heats the resistive element by Joule effect. The probe plays then a double role of a source and sensing component. Measuring the probe voltage simultaneously allows evaluating the heat flux transmitted from the probe to the sample. This flux depends on parameters such as the roughness, on sample’s thermal properties such as thermal conductivity and on the localized thermal conductance of the scanned sample.

In the thermal conductivity contrast mode, the probe temperature is controlled by a feedback loop. It should be mentioned that this temperature represents the mean temperature of the whole resistive probe. And the temperature of the tip apex cannot be deduced directly from measurements. Figure 2-2 illustrates a schematic of SThM acquisition system. It is composed of:

- Wheatstone bridge
- Amplification chain
- Feedback loop

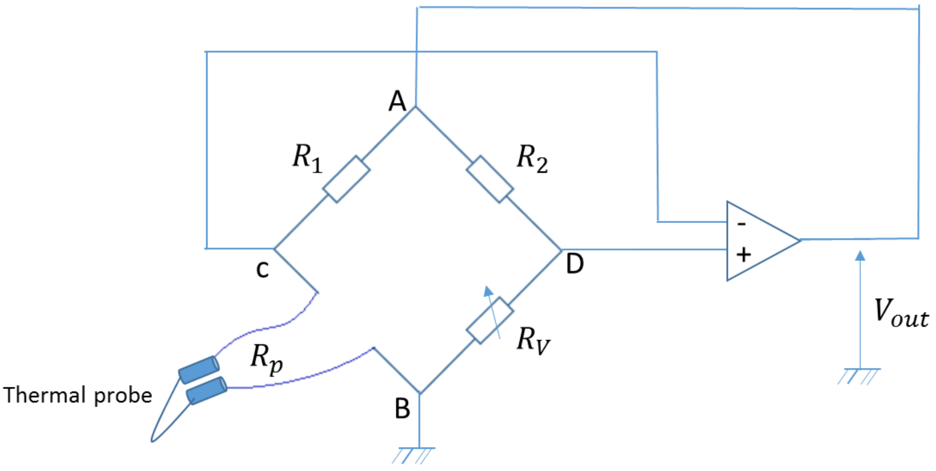

Figure 1- 2: Schematic of the thermal signal acquisition of scanning thermal microscopy.

The thermo-resistive probe R_p forms one of the legs of a whetstone bridge. The other legs are composed of 2 resistances R_1 and R_2 which values depends on the used probe. And one last leg that forms the control resistance which is selected by the user.

The amplification chain compares every moment the potentials at points C and D to indicate the balance of the bridge. When the equilibrium of the bridge is lost, the difference of potential V_{C-D} is no longer zero. The amplifier generates then a proportional voltage that is applied to the bridge through a feedback loop. Thus the Wheatstone bridge finds its balance again.

The Wheatstone bridge is powered by a DC voltage. The voltage across the bridge is amplified by an isolator amplifier. The system seeks to compensate the potential difference obtained from the gap between the probe resistance and the control resistance. Therefore it increases the output voltage V_{out}. The increased current heats the probe by

Joule effect and increases its electrical resistance. The equilibrium is reached when the probe's resistance is equal to one-fifth of the control resistance.

1.3. Resistive Probes

The key element of SThM is its thermal probe. Different probes were developed for SThM in the last decade. The first category of probes is described by thermocouple; they were presented by Majumdar *et al.* in 1993 [4]. They are composed of chromium/alumel wire with 25 µm in diameter. The resolution in temperature for this kind of probes was estimated to 1 K. In order to improve the lateral resolution, a diamond tip was added to the extremity of thermocouple junction to obtain a finer tip [8]. Later on in 1994 Dinwiddie *et al.* developed a thermoresistive probe based on Wollaston wire with 5 µm in diameter and 200 µm in length [9]. The particularity of the resistive probes is that their electrical resistance is linked to their temperature. The resolution of topographic measurements depends on the shape therefore the curvature radius of the probe. While the thermal resolution depends on dimensions and the thermal properties of the active element [9].Several probes were developed in the last few years, in this study we are interested in three different types of resistive probes: Wollaston in particular, Palladium and Silicon.

1.3.1. Wollaston wire probe

In this study the probe used is a thermo-resistive probe developed by Dinwiddie *et al.* in 1994 [9]. It's composed of a Wollaston wire with 75 µm in diameter. This material is composed of a wire of an alloy of Platinum-rhodium coated with a thickness of silver. This alloy is made with 90 % of platinum and 10 % of rhodium. The thermal tip is obtained by electrochemical etching of the Wollaston wire over a length of 200 µm in a way to have only the Pt-Rh wire appearing. This wire is bent in its middle to form a V shape thermal probe with a radius of curvature of 15 µm (figure 1-3). The probe cantilever is made by fixing extremities of the Wollaston wire parallel to each other.

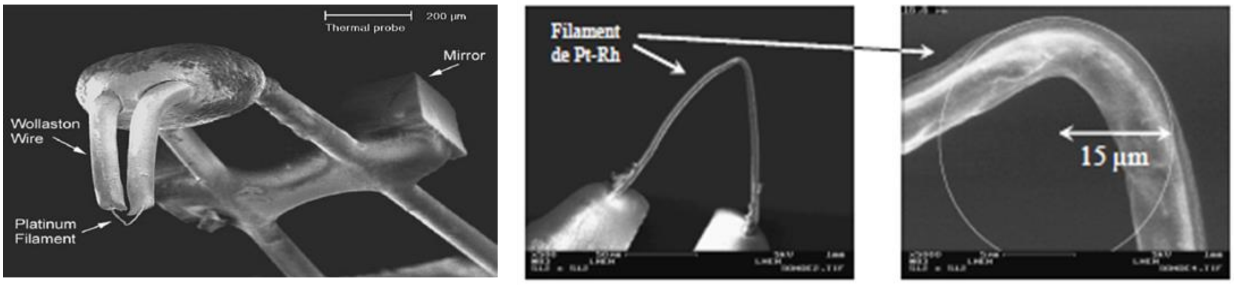

Figure 1- 3: SEM image of the Wollaston probe with a zoom on the pt-rh tip apex and its curvature radius [10].

The spring constant of the Wollaston probe is about 5 to 6 $N.m^{-1}$and its resonance is about 10 KHz [11]. The thermal properties of Silver and the Pt-Rh alloy exists in the literature [12]. Those values presented in (table 1-1) will be used in this study.

Table 1- 1: Thermophysical characteristic of the Wollaston probe at ambient temperature

	Density Kg.m^{-3}	Heat capacity J/(kg.K)	Thermal conductivity $W.m^{-1}k^{-1}$	Electrical resistivity Ω.m	Resistivity coefficient K^{-1}
	ρ	C_p	k	ρ_e	α
Silver	10500	235	429	$1.63.10^{-8}$	$4.1.10^{-3}$
Pt-Rh	19970	130	38	$18.8.10^{-8}$	$1.65.10^{-3}$

These kinds of probes are manually produced, so they are not identical. Previous studies showed that dimensions of probes vary from one to another [10].O. Raphael in his thesis has used SEM technique to evaluate dimensions of Pt-Rh wires for different probes. He found that the length varies from 244µm to 251 µm and the diameter varies from 4.61 µm to 5 µm. In this work Wollaston probes manufactured by Bruker and CMI (Czech Metrology Institute) are used to perform SThM measurements.

1.3.2. The Palladium probe

The palladium probe (Pd/SiO2) is essentially fabricated for the characterization of thin films and polymer layers [13]. It is composed of 1 µm in width of thin film Palladium as resistor and gold pads deposited on a cantilever as presented in figure 1-4. The cantilever is made of Silicon Nitride (Si3N4) [14] with a length of 150 µm, a width of 60 µm and a thickness of 0.4 µm. The tip is 10 µm in height and 40 nm in thickness. The tip radius for this kind of probes is smaller than 100 nm [13-14]. Palladium probes used in this work are commercialized by Anasys instruments.

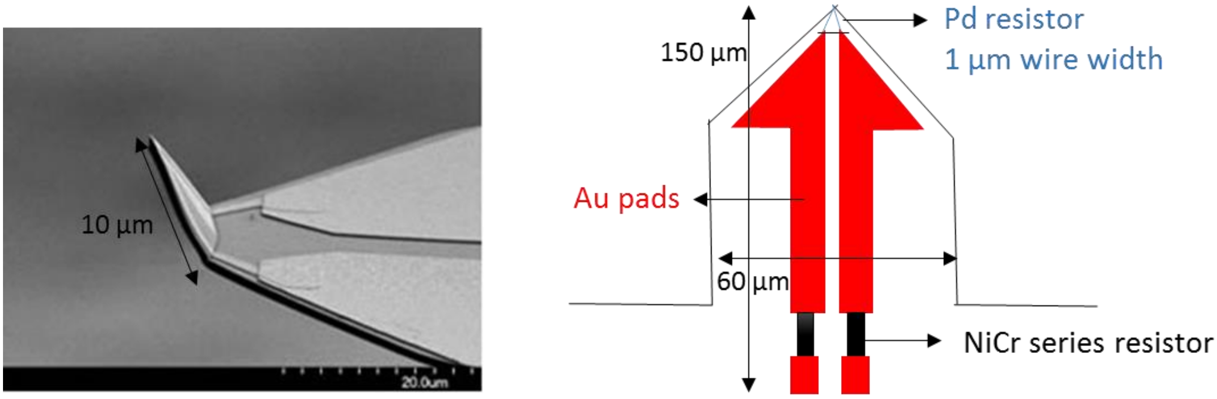

Figure 1-4: SEM image of the Palladium probe [62] and its description.

1.3.3. Silicon probes

Silicon nanoprobes are widely used in high density data storage, nanometer thermal measurements and in investigations of polymers [15]. Gostman *et al.* used silicon nanoprobe to perform measurements on a 20 nm thin film of polystyrene deposited on silicon wafer. They identified wear modes which depend on characteristics of tip temperature [16]. The cantilever is composed of two legs fabricated with doped crystal Silicon with different doping levels. The legs have a length of 300 µm, a width of 20µm and a thickness of 2 µm. The tip have a pyramidal shape and a radius smaller than 30 nm with a tip height varying from 3 to 6 µm [17]. Figure 1-5 illustrates a SEM image of the silicon probe by Anasys instuments. These kinds of probes have a spring constant varying between 0.5 and 3 $N.m^{-1}$and a resonant frequency between 15 and 30 KHz.

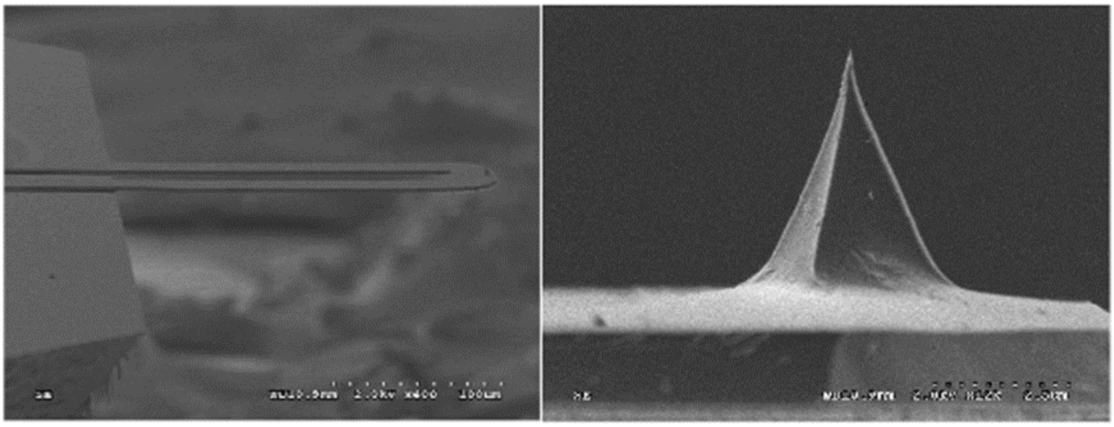

Figure 1-5: SEM images of the silicon probe from Anasys Instruments.

Each probe of those listed above has its own measurement method depending on its characteristics. In this study the Wollaston probe was mainly used in the DC mode while the Palladium probe was used in the AC mode. The next section describes the approach of measurements with the DC and AC modes.

1.4. Measurement methods

1.4.1. Wollaston probe in DC regime

Wollaston probes enable two types of operating modes: DC and AC. In this study the measurements were performed in the DC operating mode. In this case, the probe is powered with a constant current that increases its initial temperature $T_0 + \Delta T$.Where ΔT is the temperature rise of the heated probe out of contact. When the probe is in contact, part of the heat is dissipated from the probe into the sample. The probe temperature changes once the equilibrium is reached, we use the fact that the electrical resistance of the probe depends on temperature.

$$R(T) = R_0(1 + \alpha(T - T_0)) \tag{1}$$

Where R_0 is the electrical resistance of the resistive element at a temperature T_0, R is the resistance at temperature T and α is the temperature coefficient of the platinum-rhodium wire with a value of 0.00165 $\Omega(\Omega.K)^{-1}$ [18]. A precise measurement of the electrical voltage for a given applied current allows the determination of the temperature by using the following expression [19]:

$$U(T) = R_0 I(1 + \alpha(T - T_0)) \tag{2}$$

A calibrated Wheatstone bridge allows us to simplify the measurement and to access the temperature directly, in this case the heating of probe is given by the following expression:

$$\Delta T = \frac{\Delta U(T)}{\alpha R_0 I} \tag{3}$$

1.4.2. The Palladium probe in AC regime

The palladium probe was recently used in many studies for the investigation of nanostructures and the nanoscale thermal management. In this study we are interested to study the performance of the Palladium probe using the 3ω method [20, 21]. Working in AC regime presents some good advantages like the use of a lock in amplifier that allows to increase the ratio signal-noise compared to other static measurements. The 3ω technique is a non-linear mode in which the probe plays the dual role of heat source and sensor at the same time. In fact, an alternating current of pulsation ω flows into the probe heated by Joule effect. The dissipated power P_J in the form of heat is expressed as follows:

$$P_J = \frac{R_p I_0^2}{2}(1 + \cos(2\omega t)) \tag{4}$$

Where I_0 is the amplitude of the induced current with:

$$I = I_0 \cos(\omega t) \tag{5}$$

Then, the temperature rise ΔT of the probe by Joule effect, with respect to the ambient, has a static component T_{DC} and a component at 2ω $T_{2\omega}$:

$$\Delta T(t) = T_{DC} + T_{2\omega} \cos(2\omega t + \emptyset) \tag{6}$$

With$\emptyset$ is the phase shift of thermal signal with respect to the electrical excitation. The voltage V across the probe is then written as:

$$V = R_p I = R_0\big[1 + \gamma\big(T_{DC} + T_{2\omega} \cos(2\omega t + \phi)\big)\big] I_0 \cos(\omega t) \tag{7}$$

$$V = R_0(1 + \gamma T_{DC}) I_0 \cos(\omega t) + \frac{R_0 I_0 \gamma T_{2\omega}}{2} \cos(\omega t + \phi) + \frac{R_0 I_0 \gamma T_{2\omega}}{2} \cos(3\omega t + \phi) \tag{8}$$

As mentioned before, the probe is the fourth leg of a Wheatstone bridge. As observed in the above equation the third harmonic is directly proportional to the harmonic temperature at 2ω. Therefore the expression of the voltage at the third harmonic is given by:

$$V_{3\omega} = \frac{R_0 I_0 \gamma T_{2\omega}}{2} \cos(3\omega t + \phi) \tag{9}$$

Using this assumption, the probe average temperature can be experimentally calculated.

Temperature variations depend on sample thermal properties with which the probe is in contact. The more the sample is conductive, the more the heat transmitted to the sample will increase thus the temperature of the probe will decrease compared to where it’s out of contact.

2. Thermal interactions between the probe and the sample

The thermal resistance at the contact which is the inverse of the thermal conductance $R = \frac{1}{G}$ depends on mechanisms of the heat transfer from the thermal probe to the sample. When the probe is far away from any sample, under ambient conditions, the heat transfer to the sample is made via radiation and conduction through air. When the probe is in contact with the sample the conduction through solid-solid contact and the conduction/convection via the water meniscus are added to the heat transfer modes. Figure 1-6 illustrates the heat transfer mechanisms between a Wollaston probe and a sample.

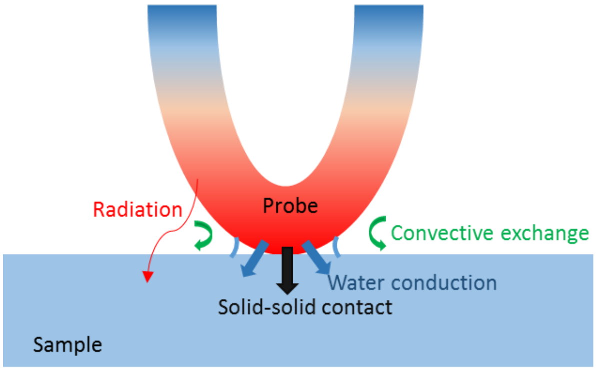

Figure 1-6: Schematic of heat transfer mechanisms between the probe and the sample.

Previous studies stated that the heat transfer through radiation is neglected compared to other modes. Lefevre *et al.* found that the radiation thermal conductance is about 10^{-3} µW.K^{-1} which is 1000 times smaller than the other transfer modes [22]. Therefore, while modelling the contact between the probe and the sample under ambient conditions this mechanism is not taken into account [23]. Kim *et al.* also stated that the radiative heat transferred from the cantilever of the silicon probe to its surrounding medium is predicted to be only 0.5% of the total heat transfer in the tip when the cantilever is heated up to 570 K [24]. This value is calculated from the Stefan Boltzman law [25]. Hence the radiation percentage becomes 1% of the total heat loss when the cantilever is heated to 700 K.

When working under ambient conditions, a film of water is formed on the sample surface due to the relative humidity presented in air. When the probe gets into contact with the sample, a water meniscus takes place between the tip and the sample. Gomes *et al.* were among the first who investigated the water meniscus effect on measurements with the Wollaston probe. They studied experimentally the thermal signal obtained by the probe for different samples (glue, duralumin and copper) at different temperatures [26]. They reported that for probe temperature higher than 90°C capillary effects are not observed. In their work the thermal conductance of water was not determined. Later on A. Assy *et al.* [27] studied the heat transfer between the Wollaston probe, the Palladium probe and the doped Silicon probe and the sample through water meniscus. They calculated the total thermal conductance of water meniscus as a function of the probe mean temperature. Their results showed that the heat transfer through water meniscus is not predominant and it is neglected for probe mean temperature higher than 100°C because the water evaporates.

2.1. Heat transfer through the environment

The heat transfer mechanisms between the probe and the sample are a complex phenomenon that requires a deep study. The heat flows from the thermal probe into the sample through air under atmospheric conditions. A part of the cantilever remains in contact with the surrounding air. Thus the probe heat up the surrounding environment. The probe power dissipation increases once the tip approaches the sample. It was proven that the separation distance d between the probe and the sample plays an important role in the modes of air transferred into the sample [26, 28, 29].

When d is much smaller than air molecules mean free path l_m a ballistic regime is considered. Thus the air gap conductance should be estimated from local conductances and not from the continuum assumption. When d is much larger than l_m the heat transfer becomes diffusive. Thus the heat is transferred by successive collision of air molecules. Majumdar*et al.* stated that since the probe and the sample can't be considered as two parallel plates, a geometry factor α should be added [23]. Considering the separation distance between the tip and the sample is given by $(d + y)$, Majumdar wrote the air conductance coefficient in the ballistic regime as:

$$h_{ballistic} = \frac{\alpha k_a}{y + d} \tag{10}$$

Where k_a, is the thermal conductivity of bulk air.

While the air conductance coefficient for a diffusive regime is written as:

$$h_{diffusive} = \frac{\alpha k'_a}{(y + d)(1 + 2f)} \tag{11}$$

With
$$k'_a = \frac{CV(y + d)}{3} \tag{12}$$

And $$f = \frac{2(2-A)\gamma}{A(\gamma+1)Pr} \tag{13}$$

Where k'_a is the thermal conductivity of air in the free phonon flow regime, C is the heat capacity and V is the heat velocity of air phonon, A is a thermal accommodation coefficient which is about 0.9 for air, γ is the heat capacity and Pr is the Prandtl number.

An intermediate regime takes place between the diffusive and ballistic one. Majumdar presented it as the slip regime. The equation of air coefficient in this case is written as follows:

$$h_{slip} = \frac{\alpha k_a/(y+d)}{1+2fl_m/(y+d)} \tag{14}$$

The different mechanisms of conduction through air have been accounted for unidirectional conductance formulas, where the tip shape is represented by a geometrical factor. The thermal conductance through air is the written as:

$$G_{gas} = \iint h_{(diffusive,ballistic\ or\ slip\ regime)} dxdy \tag{15}$$

Once the contact occurs, the value of thermal conductance increases, according to Lefevre it is estimated to $2.5.10^{-6} W/K$ when working with AC operating mode [30]. For experiments done under ambient conditions, the order of magnitude of air thermal conductance can vary between $10^{-6} - 10^{-8}\ W/K$ depending on the geometry of the probe.

S Gomes *et al.* [26] David *et al.* [31] and Lefevre *et al.* [32] operated SThM measurements with probe temperature higher than 100°C to eliminate the contribution of water meniscus. They estimated G_{air} using an equation of calibration for the Wollaston probe with DC operational mode. Several samples with known thermal conductivities were used for the calibration. The estimated values of G_{air} is around $5.10^{-6} W/K$.

Measuring the thermal signal as a function of the probe/sample distance allows to determine the equivalent conductance G_{eq} (equation (13)).

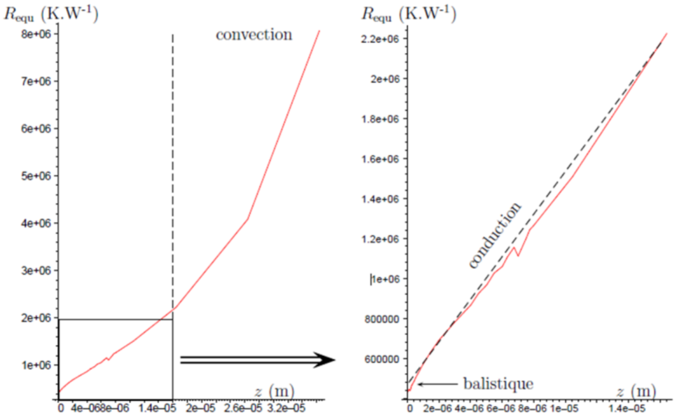

Figure 1-7: Variation of the equivalent thermal resistance versus the distance between the Wollaston probe and a sample of silver [30].

Figure 1-7 shows curves of the equivalent resistance measured by Lefevre. $R_{eq}$is measured as a function of the distance separating the probe from the sample down to 300 nm.

These curves show two distinct behaviors, the first, which is visible for high distances, follows a law of 1/z characteristic of the slip and diffusive regime where a linear domain in observed. The second appears from a distance of 300 nm where measurements show a plateau that may indicates the presence of a ballistic regime.

Later in 2006 Lefevre *et al.* investigated the evolution of the probe response as a function of the probe/sample distance in order to evaluate the heat mechanisms involved in the thermal equilibrium of the probe [33]. To do this, they used the head of the microscope to automate and evaluate the approach of the probe to the sample surface from an altitude of 150 µm using small steps for the approach. Figure 1-8 shows the evolution of the equivalent thermal resistance noted $1/G_{eq}$ as a function of the distance (equation 13).

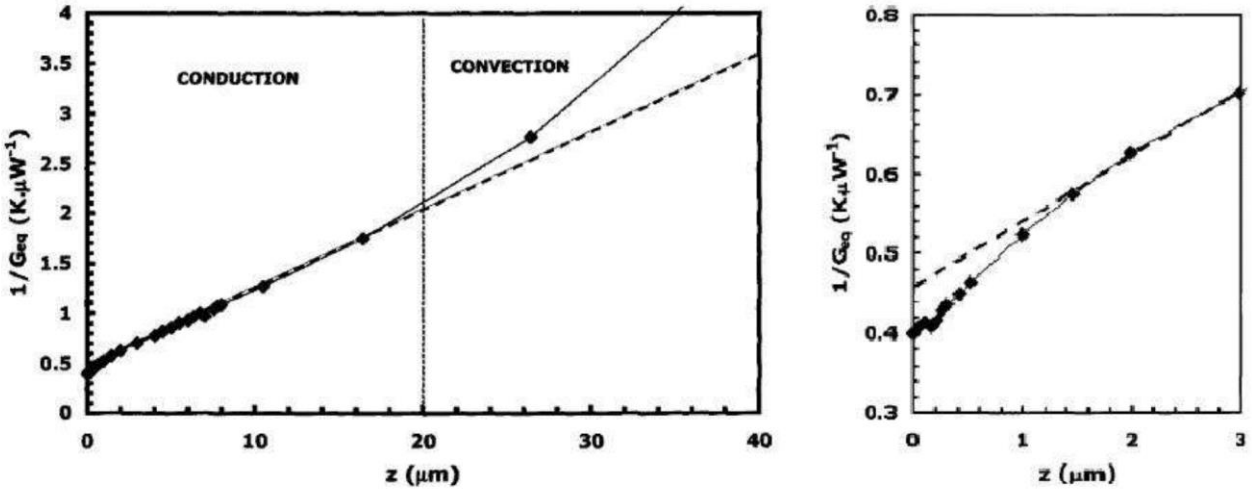

Figure 1-8: Evolution of the equivalent thermal contact resistance characterizing the heat transfer between the probe and the sample as a function of the probe/sample distance. This resistance takes into account the exchanges by solid-solid conduction and through the surrounding air where three regimes (convective, diffusive and ballistic) are highlighted [33].

A sample of silver was taken into account in this study in a way to keep the air thermal resistance greater than that of the sample. Thus the equivalent thermal conductance G_{eq} becomes equivalent to the thermal conductance relative to the surrounding environment G_a. It is evaluated from the response 3ω and from the second harmonic expression of the probe temperature:

$$\theta_{2\omega} = \frac{J}{Lm^3} \cdot \frac{AG_{eq} + BG_s mL}{(e^{2mL} - 1)G_{eq} + (e^{2mL} + 1)G_s mL} \tag{16}$$

Where $$A = -2 - mL + 4e^{mL} - 2e^{mL} + mLe^{2mL} \tag{17}$$

And $$B = 1 + mL - e^{2mL} + mLe^{2mL} \tag{18}$$

Where G_s is the probe thermal conductance, J represents the electrical resistivity of the probe, L is the ½ length of the platinum rhodium wire and m denotes the probe fin parameter and it is given by:

$$m = \frac{hp}{\lambda S} + \frac{2i\omega}{a} \tag{19}$$

Where h is the heat transfer coefficient between the probe and its surrounding environment, S, p and a, λ represents respectively the probe area, perimeter, thermal diffusivity and thermal conductivity.

The analysis of these experimental results leads the authors to evaluate three regimes of heat transfer between the probe and the sample via the surrounding environment. They observed a changed in the evolution of the equivalent resistance for distances higher than 20 µm. Thus they stated that beyond 20 µm the convective regime dominates by the thickness of the viscous layer which is estimated from the equation $\lambda_a/h = 25\ \mu m$ where, λ_a is the thermal conductivity of air and h is the heat transfer coefficient between the probe and the nearby air. Beyond the viscous layer, the evolution of the thermal resistance becomes linearly dependent on the distance z and characteristic of a heat diffusion mechanism. As seen in figure 7, a deviation appears for distances below 1µm. This deviation would be significant of the slip regime. This type of regime is characterized by the appearance of temperature discontinuities at the solid-gas interfaces and it is explained by an imperfect transfer of molecule energy to the solid interface. The authors observe stabilization in the variation of the equivalent thermal resistance for distances below 300 nm. They interpret this plateau by the predominance of a ballistic transfer for which the molecules transport the energy of the probe towards the sample without interacting with each other.

They also developed a model for the Wollaston probe while approaching toward a sample using FEM. Figure 1-9 represents a comparison between experimental and simulation results. It report sthat experimental data and FEM have the same evolution but the simulation

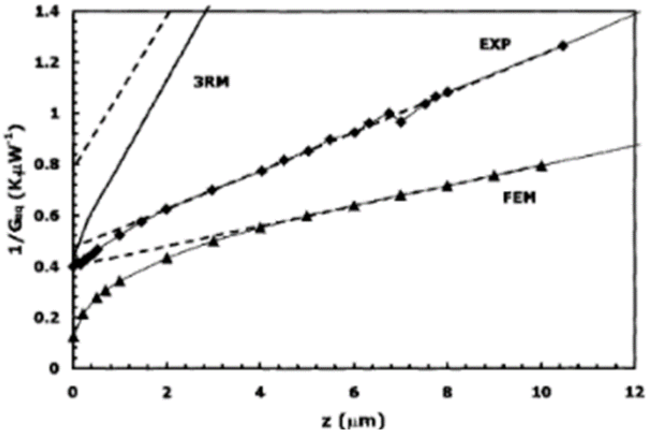

Figure 1- 9: Comparison between experimental and simulation results of the equivalent thermal resistance as a function of the distance between the Wollaston probe and the sample. [33].

Heat transfer mechanisms at short distances were investigated by Raphael *et al.* [10]. They studied the thermal response of the probe as a function of the probe/sample distance. He used a monitoring device with high precision (resolution of 20 nm) to approach the probe toward the sample. Figure 1-10 illustrates an experimental evolution of the normalized voltage of the probe's response while approaching toward three different samples as a function of the probe/sample distance under ambient conditions in the DC operating mode.

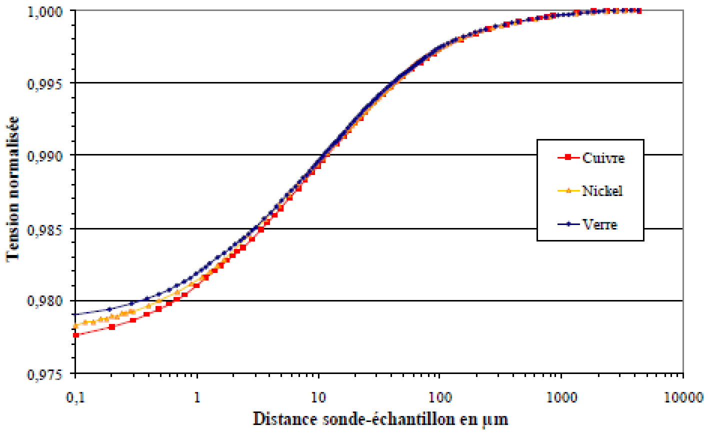

Figure 1- 10: Experimental evolution of the voltage at the extremity of the Wollaston probe as a function of probe/sample distance in the DC operating mode at ambient pressure. The current used is fixed to 50 mA [10].

Their experiments revealed that the presence of the sample is detected from distances lower than 2 mm. It is well shown that three different regimes takes place for the heat transfer mechanisms between the probe and the sample. A diffusive regime appears for distances between 1 and 100 µm, for distances higher than 100 µm the probe response becomes stable, an intermediate regime for distances between 0.5 and 1 µm and a linear behavior for distances lower than 0.5 µm.

An interesting phenomenon was observed while approaching the Wollaston probe toward a sample. This phenomenon can be translated by a resonance of thermal waves [29]. Olivier *et al.* performed curves of approach in AC mode at the third harmonic using a sample of copper (figure 1-11).

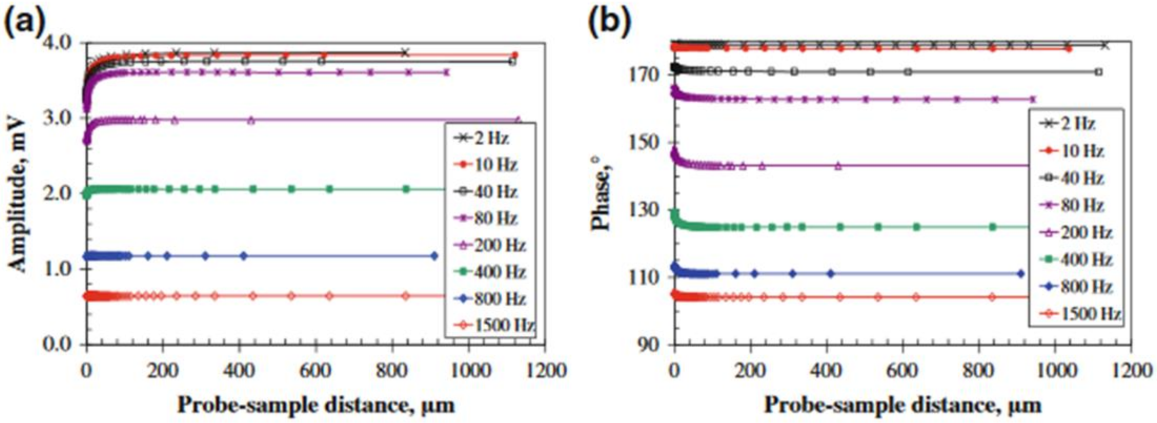

Figure 1-11: Evolution of the a) magnitude and b) phase of 3ω signal of the Wollaston probe as a function of the distance between the probe and the sample for different frequencies [29].

The distance 'zero' represents the contact point with the sample where a sudden decrease in the amplitude is observed. The thermal response of the probe, thus its temperature is not influenced by the presence of the sample for distances higher than 300 µm. For a good comparison of the results the amplitude was normalized by the values obtained for distances far from the sample. Figure 1-12 shows results obtained for several frequencies.

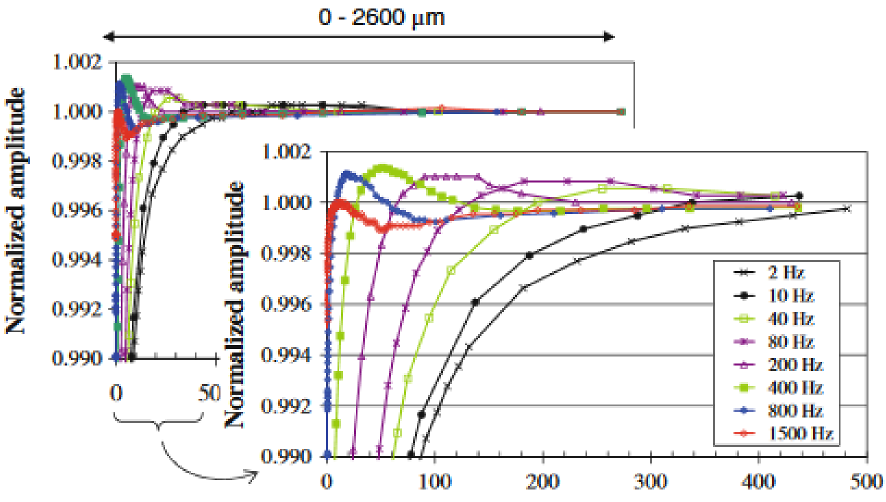

Figure 1-12: Normalized amplitude of the 3ω signal for different frequencies and an enlarged graph at small distances [29].

The normalization curves are very useful to particularly focus on the evolution signals that may be hidden by a large graph scale. While approaching the probe toward the sample, the magnitude of the temperature changes. This amplitude reaches a maximum value that depends on the used frequency. The temperature behavior of the probe response can be translated as a resonance phenomenon of thermal waves. This study with respect to frequency allows considering the system of the probe, air and the sample as a cavity of resonance at the microscale.

To date this kind of experiments was only performed for the Wollaston probe and there is no published data in the literature that shows if this phenomenon is observed for the nanoprobes. Therefore in chapter four a study of this type will be presented and discussed using the Pd/SiO2 nanoprobe.

2.1.1. Contribution of the cantilever in the heat transferred from the probe into the environment

The heat transferred from the cantilever of the probe into the surrounding medium plays its role in the heat transfer mechanisms. Therefore the contribution of cantilever needs to be investigated. Few works considered the study of heat transferred within and from the cantilever [34-36]. When operating in air environment with the tip in contact with a sample, the heat flowing into the sample is much larger than the heat transferred into the nearby air. Therefore most of the studies explored the heat transferred from the cantilever into the sample and ignored the heat flow to the nearby air [37]. Lee *et al.* investigated the heat transferred from a single-crystal Silicon cantilever into the air environment far away from any substrate under partial vacuum conditions. They found a value about $2000\ W/m^2K$ for the effective heat transfer coefficient [38]. Park *et al.* studied the thermal response of a heated Silicon microcantilever in frequency dependent measurements. They estimated the effective heat transfer coefficient to be in the range of $1000 - 3000\ W/m^2K$ [39].

In 2008 Kim *et al.* simulated the thermal conduction from a Silicon microcantilever into the environment. They reported that for a steady state heat generation, the heat transfer coefficient of the legs is around $7000\ W/m^2K$ and near the heater it is about $2000\ W/m^2K$ [24]. While Chapuis *et al.* reported that the heat losses through air are in the order of $3000\ W/m^2K$ which accounts for both convection and conducting in air [40].

Trannoy *et al*. used experimental data obtained from Infrared imaging to calculate the heat fluxes dissipated from the probe based on Wollaston [41]. They evaluated the heat flux dissipated into the Wollaston wire when the probe is out of contact to 13.7 mW which corresponds to 67 % of the total dissipated power. In chapter 2 we base on experimental results obtained by this study to calculate the heat exchange coefficient of the Wollaston wire to the environment.

2.2. Thermal sample resistance and thermal exchange radius

Investigating heat transfer mechanisms between the probe and the sample is often ensured through evaluating an equivalent thermal conductance that depends on the thermal contact resistance and the sample resistance [22]. Therefore, the interpretation of results can be done through thermal resistances of the probe-sample system. In scanning thermal microscopy the AC and DC thermal responses of the probe may be associated with the probe/sample thermal contact resistance, the thermal resistance of the probe and the sample's thermal resistance. Figure 1-13 illustrates a schematic of interactions between the probe and the sample with the thermal exchange radius b and a schematic of thermal resistances network of the probe-sample system.

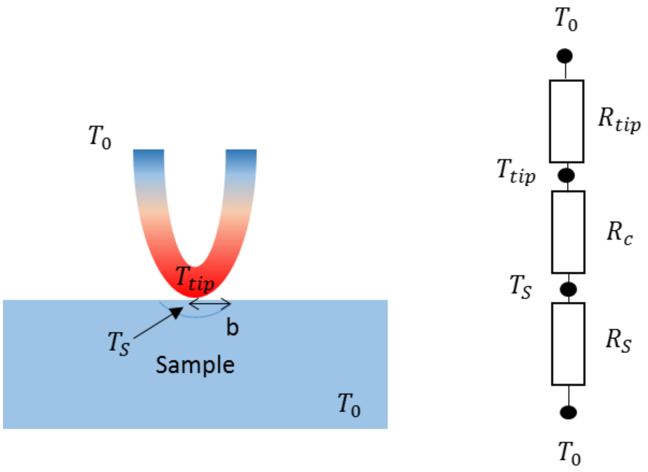

Figure 1-13: Schematic of thermal interactions between the probe and the sample showing the thermal exchange radius b and schematic diagram of the network of the thermal resistances of the probe-sample system.

Regarding the sample thermal resistance, we consider that it corresponds to the superposition of a constriction resistance of the sample's flux lines and an intrinsic sample resistance. The curvature of the lines flux or constriction is due to the passage of the flow through a circular orifice that represents the surface of the thermal exchange radius b.

The heat transferred from the heated probe into the sample is given by Q_S:

$$Q_S = \frac{T_{tip} - T_0}{R_S} \tag{20}$$

Where T_{tip} represents the temperature of the probe apex, T_0 is the temperature of the sample at ambient temperature and R_S is the sample thermal resistance.

If the sample studied is bulk, the thermal conductivity is determined from R_S where the area of contact between the probe and the sample is defined by the circular radius b. R_S is written as [42]:

$$R_S = \frac{1}{4k_{sample}b} \tag{21}$$

Where k_{sample} is the thermal conductivity of the bulk sample.

When the sample considered is a thin film over a substrate, the thermal spreading resistance is given as a function of the series thermal resistance crossing the film and the substrate. And as a function of the thin film thickness, in this case R_S is given as [42]:

$$R_S = \frac{1}{4k_{sub}b} + \frac{l}{\pi k_{film}b^2} \tag{22}$$

Where k_{sub} the thermal conductivity of the substrate is, k_{film} is the thermal conductivity of the thin film and *l* is the film thickness.

The determination of the thermal exchange radius b is very important since the sample thermal resistance depends on this value. In the literature, this parameter has been identified from a theoretical model [22,43] or by measuring the curvature radius of the probe apex on a SEM image [44]. The assimilation of the thermal exchange radius to a simple probe apex radius of curvature [44] seems approximate when considering all the possible heat transfer mechanisms. Y. Zhang *et al*. considered that this value is constant and it was estimated to 2.45 µm for a Wollaston probe in contact with a sample of Bi2Te3 on glass substrate [43]. K. Kim et *al.* took the assumption that the heat is transmitted from the thermal probe to a single point on the sample [45]. While E. Puyoo *et al*. considered that the heat transferred is incorporated in the disc of radius b at a constant temperature. Using the Wollaston probe with a sample of SiO2 thin film (200 nm) on Silicon substrate, b was evaluated to 820 nm [46]. Moreover, concerning the values of b identified from the modelling [22, 43], we observe, according to the authors, a difference of an order of magnitude where Lefevre *et al.* found a value of 300 nm and Zhang *et al.* found a value of 2.26 µm whereas the evaluation was done for the same type of probe (Wollaston) and under the same environmental conditions.

It therefore seems that the interpretation of measurements when the probe is in contact should pass through an accurate determination of the thermal exchange radius and the thermal contact resistance.

2.3. Thermal contact resistance

The contact between the probe and the sample is not considered perfect due to their surface roughness. The contact between two rough surfaces consists of a multitude of contact points between asperities. Figure 1-14 illustrates a schematic representation of the probe/sample contact. As seen the contact surface between the probe and the sample is not continuous and the surface is divided into small contact areas. These areas can be quantified by a thermal conductance (inverse of thermal resistance) that depends on the size of contact areas and the phonon mean free path [47].

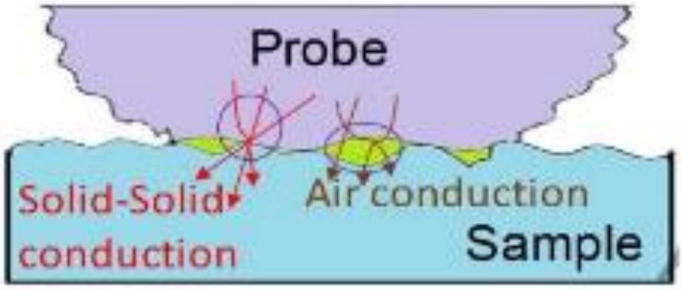

Figure 1-14: Schematic representation of heat transfer mechanisms showing contact areas between the probe and the sample [47].

The thermal contact resistance limits the amount of heat exchanged between the probe and the sample. So quantifying this heat transferred requires an evaluation of the contact resistance. Therefore to obtain quantitative measurements in SThM it is crucial to evaluate the thermal contact resistance. The estimation of sample's thermal properties requires a precise knowledge of the heat transferred into the sample. In the following we present methods found in the literature for the calculation of thermal contact resistance.

Lefèvre *et al.* proposed an analytical model to evaluate the thermal contact resistance. The contact between the probe and the sample was introduced via a boundary condition applied on the extremity of the probe apex [22]. They introduced an equivalent thermal conductance G_{eq}that links the sample conductance G_s and the tip-sample contact G_c and it is written as:

$$G_{eq} = \frac{G_c G_s}{G_c + G_s} \tag{23}$$

Where $G_s = {}^{1}\!/_{R_s}$can be written in different configurations depending on the sample and the heat source. The authors proved that in both alternative and direct operational modes the measurement with Wollaston probes is limited to the materials having thermal conductivities below $30\, W.m^{-1}K^{-1}$. Furthermore, neglecting the temperature dependence of thermophysical sample's properties allows to reduce the sensitivity of the equivalent thermal conductance to the ambient temperature variations. Results issued from equation 13 shows a linear dependence of the thermal contact resistance $R_c = \frac{1}{G_c}$ and the inverse of sample's thermal conductivity. By fitting experimental data Lefevre *et al.* found a value of 4.6 – $6.10^{-6}\ W.K^{-1}$for the thermal contact conductance G_c [22].

Later studies considered constant values for the thermal contact resistance and the thermal exchange radius. Kim *et al.* considered that when the contact occurs between the probe and the sample, the heat is transferred from the probe to a single point on the sample [45]. The probe used is composed of a V-shaped SiN_x cantilever with a Gold-Chromium thermocouple integrated at the end of a silicon dioxide tip.

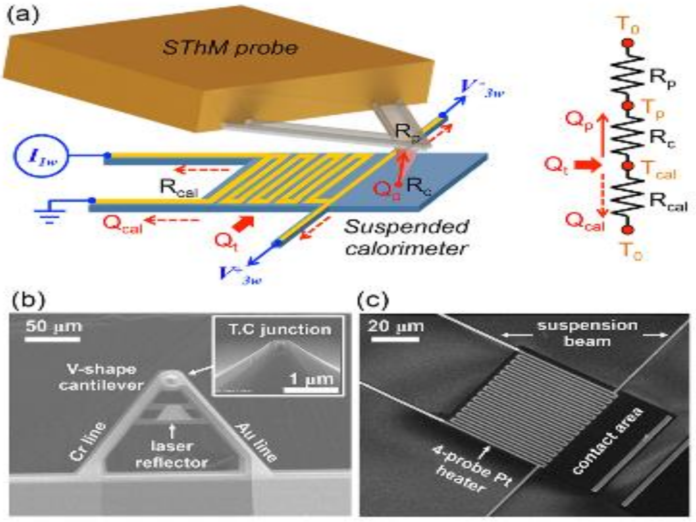

Figure 1-15: a) Schematic diagram of the probe in contact with a calorimeter, b) and c) SEM images of the SThM probe used in the experiments and the suspended calorimeter [45].

They used a calorimeter in order to quantify thermal resistances of the heat within the probe and the thermal contact resistance between the probe and the sample (figure 1-15). The work was performed in ultra-high vacuum environment to neglect the convection through air and heat conduction. The thermal contact resistance R_c was obtained from the equation:

$$R_c = \frac{\Delta T_{cal} - \Delta T_p}{Q_p} \tag{24}$$

Where $\Delta T_{cal}$is the temperature rise of the calorimeter, ΔT_p denotes the temperature rise within the probe and Q_p is the heat flow through the probe. The value of R_c was found to be $4.96.10^7\ K.W^{-1}$.

Wilson et *al.* developed a calibration method of the probe to investigate the dependence of thermal contact resistance and the thermal exchange radius on the sample's thermal conductivity [49]. Measurements were performed for bulk samples and thin film on a substrate for both low and high thermal conductivities. It was proven that R_c and b remains constant for samples with low thermal conductivity ranging between 0.3 $W.m^{-1}.K^{-1}$and 1.08 $W.m^{-1}.K^{-1}$. The value of R_c computed for a bulk sample with low thermal conductivity is 44927 $K.W^{-1}$. While for a bulk sample of thermal conductivity ranging between 15 $W.m^{-1}.K^{-1}$and 54 $W.m^{-1}.K^{-1}$the thermal contact resistance is estimated to $R_c = 40191\,K.W^{-1}$.

Timofeeva et *al.* proposed an analytical model complemented by finite element method (FEM) in order to estimate the thermal contact resistance for the probe/sample system. For this, in FEM they added a thin resistive layer between the probe and the sample with a thickness much smaller than the contact diameter. The comparison between modelling and experimental method allowed to give an estimation of the contact resistance which was estimated to $6.10^{-8}\ K.m^2.W^{-1}$ between multiwall carbon nanotube and Al interface [50].

In scanning thermal microscopy and under ambient conditions (pressure, temperature and humidity), the thermal contact resistance is divided in four heat fluxes: the heat exchanged by solid-solid contact, the heat transferred via the water meniscus, and the heat transferred to the air environment and the heat transferred through radiation. The resulting thermal conductance respectively noted G_{ss}, G_w, G_a,G_{rad} are presented as following:

$$G_c = G_{ss} + G_w + G_a + G_{rad} \tag{25}$$

Previous studies estimated the solid-solid thermal conductance for the Wollaston probe ranging between $10^{-4}W.K^{-1}$ and$10^{-6}W.K^{-1}$, the conduction via the meniscus of water also in the range of $10^{-6}W.K^{-1}$[51]. While the thermal conductance of the heat exchanged through air was estimated to be in the order of $10^{-6}W.K^{-1}$ and for the heat exchanged through radiation it was estimated to be $10^{-9}W.K^{-1}$ [30].

As seen in this section the thermal contact resistance for the probe sample system varies between $10^4\ K/W$ and $10^7\ K/W$. In chapter 2, a methodology will be presented to calculate the total thermal conductance by developing a model based on finite element method.

3. Thermal measurements of materials at the micro/nanoscale

The heat transfer mechanism is a complex system that requires careful investigations. When working with micro/nanoelectronic devices the material's thermal properties are not the same as for the bulk. In this thesis work, the thermal probe was used to study nanostructured materials. Therefore for an accurate interpretation of measurements, a special attention was given to earlier studies that investigated the material's thermal properties particularly their thermal conductivity at the micro/nanoscale. The following paragraph study the thermal conductivity of some materials used in this study.

3.1. Thermal conductivity measurements

The thermal conductivity is a critical property in several applications such as thermoelectric, microelectronics for thermal management: thermal isolation or heat dissipation. The thermal conductivity of thin films could be very different from that of bulk material. This difference comes from phonon scattering at the interfaces sides and from the imperfections in the structure [52]. A lot of numerical methods such as Monte Carlo, discrete ordinate and experimental method such as the 3ω were used for measurement of thin films thermal conductivity and have been reported in the literature[53, 54, 55, 56]. In the following we discuss methods that have been useful for this work.

Several studies were done on silicon dioxide (SiO_2) thin films since they are essential insulating materials in the development of semiconductor devices. Many methods for growing silicon dioxide thin films such as evaporation, thermal oxidation, chemical vapor deposition (CVD) and sputtering have been developed. T. Yamane *et al.* studied the dependence of microstructures of SiO2 thin films thermal conductivities prepared with different methods. Measurements were executed using 3ω method, where a metal line supplied by a current was produced on the surface of a sample composed of SiO2 thin film deposited on a Si substrate. The supplied current produces temperature oscillation in the sample from which the thermal conductivity of the sample is evaluated for various thickness of SiO_2 [53, 54, 57].

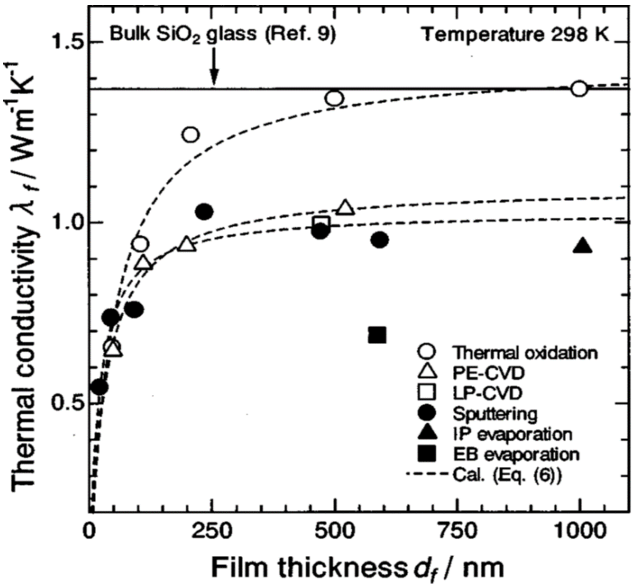

Figure 1-16: Thermal conductivities of SiO_2 thin films over Si substrate as a function of thickness. The solid line illustrates the thermal conductivity of bulk silicon. Dashed lines are the fit of results obtained with different methods of deposition for SiO_2 thin film on Silicon substrate [57].

Figure 1-16 illustrates the thermal conductivity of SiO_2 thin films obtained in their study versus the film thickness [57]. It reports that the SiO_2 thin films prepared with thermal oxidation and for thickness above 500 nm agrees with the values of bulk silicon dioxide. The same results have been found with other group of researchers [58]. For PECVD the thermal conductivity for thicknesses above 500 nm tends to lower values than that of the bulk SiO_2.

Later on H. Chieh *et al.* investigated the cross-plane thermal conductivity of silicon dioxide thin films using a method based on an electrical sensing/heating mechanism and a steady state technique [55]. They used three different methods to prepare the SiO_2 thin films: thermal oxidation, plasma enhanced chemical vapor deposition (PECVD) and E-beam evaporation. Figure 1-17 represents results obtained by different methods compared to results from the literature. As seen for the thermal oxidation method, the value of thermal conductivity for thin films with thickness above 500 nm tends to values of bulk silicon [55].

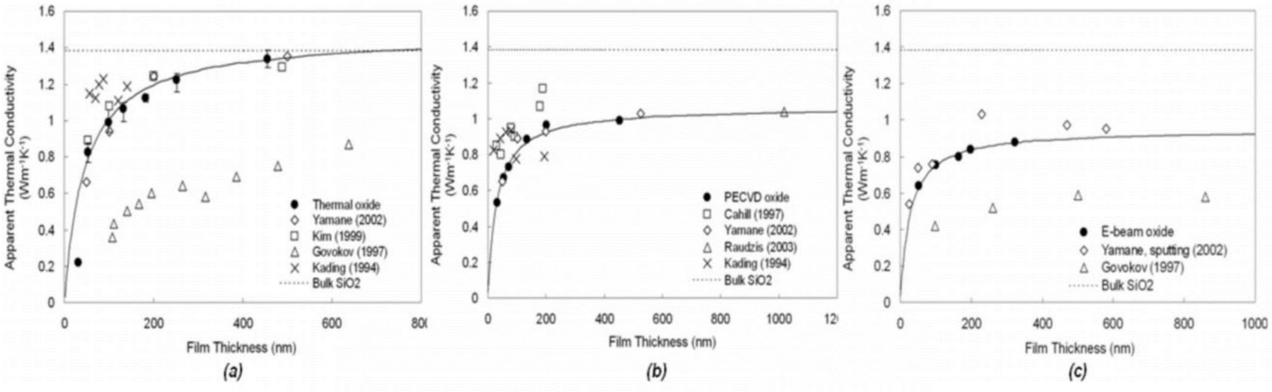

Figure 1- 17: Variation of thermal conductivity as a function of SiO2 thin films thickness compared to results published previously in literature using different methods of thin films preparation [55].

While for PECVD the thermal conductivity of silicon dioxide thin films are lower than the values found with thermal oxidation method. It was reported that the thermal conductivity of SiO_2 thin films firmly correlates with their porosity thus a higher porosity of SiO_2 thin film corresponds to a lower thermal conductivity [57, 59].

In chapter 3, a sample composed of different thicknesses of SiO_2 will be investigated in detail. Thus values of thermal conductivity will be incorporated in the modelling of silicon dioxide thin films over silicon substrate to have a well-designed model for the study of the probe thermal response while in contact with such structure.

Several studies were done in order to estimate the thermal conductivity of bulk silicon and silicon thin films. It is well known that the thermal conductivity of Si thin film decreases with decreasing the film thickness. This is due to the influence of surface roughness scattering [60].

D. Baillis *et al.* investigated the in-plane and out-of-plane thermal conductivity of silicon thin films and nanowires [56]. They used the approximations of Holland dispersion and the Brillouin zone boundary condition (BZBC). The thermal conductivity was obtained by solving Boltzman transport equation. The study of thermal conductivity was done as a function of the temperature ranging from 150 to 1000 K for several thickness of Silicon films.

Figure 1-18 represents the results obtained for the out of plane thermal conductivity using different methods: Monte Carlo (MC) and Discrete ordinate method (DOM) simulations using both Holland dispersion and Brillouin zone boundary condition approximation. The results show that the thermal conductivity of Si thin film decreases with increasing the temperature. When the thickness of the film higher than 100 nm, the out of plane thermal conductivity is lower than the in plane one and they both tends to the same value at 150 K.

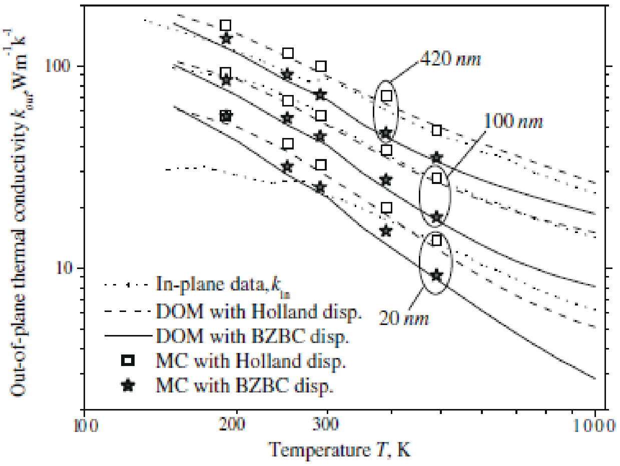

Figure 1-18: Variation of out of plane and in-plane thermal conductivity of different silicon thin films thickness (20 nm, 100 nm, 420 nm) as a function of the temperature using different methods (DOM, MC) [56].

For temperatures higher than 300 K, the in plane thermal conductivity is larger than the out of plane due to the fact that the phonon mean free path in the in plane direction much bigger than that in the out of plane direction.

Later on, C. Jeong *et al.* investigated the in-plane (diffusive transport) and cross-plane (quasi ballistic transport) thermal conductivity of silicon thin film at room temperature [61]. For the in plane measurements they used a frequency dependent specularity parameter to model the surface roughness influence.

Figure 1-19 illustrates results of thermal conductivity calculated as a function of silicon film thickness. As illustrated, at room temperature, the in plane thermal conductivity is higher than the cross-plane one. For the in-plane direction, fifty percent of the heat is transmitted by phonons with mean free paths (MFP) smaller than in the bulk. When the thickness of thin films is smaller than about 0.2 µm, 50% of the heat is transmitted by phonons with MFP larger than the film thickness.

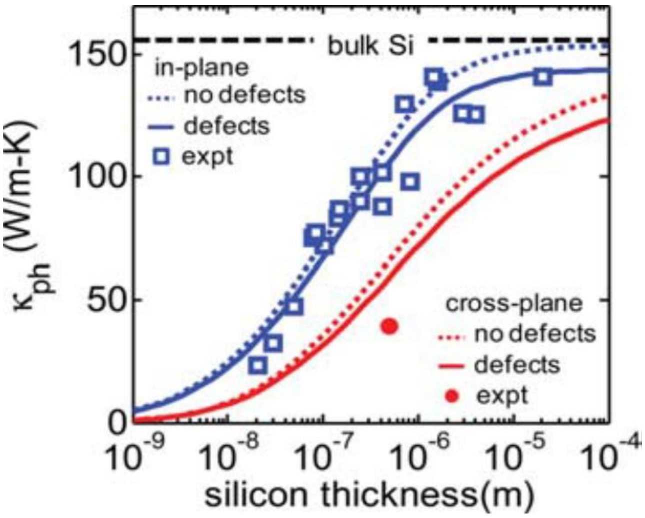

Figure 1-19: Variation of the cross plane and in plane thermal conductivity of different thicknesses of silicon thin films at room temperature. The black dashed line represents the thermal conductivity for bulk Si. Blue and red curves correspond respectively to the in-plane and cross plane results where: squares and circles correspond to experimental results, dashed line to the absence of defects, solid line to the presence of defects [61].

3.2. Measurements on nanostructured materials by SThM method

The miniaturization of modern electronic devices to the order of nanometers requires a good characterization of their thermal properties. Scanning thermal microscopy is widely used in this domain for its ability to perform topographic and thermal imaging of the sample surface. In the active mode the measurements obtained by SThM represents an image of the sample surface that doesn’t truly represent the real thermal properties of the specimen due to the presence of some artifacts that are obtained by changes in the probe/sample thermal contact surface resulting from the sample surface roughness [62]. When the probe scans the sample surface and encounters some sharpness the probe-sample contact area decreases, which also decreases the heat transferred from the probe to the sample. Thus a decrease in the power provided to the probe is required in order to maintain its temperature constant. The decrease in the power provided to the probe is translated on thermal image by a decrease in sample local thermal conductivity. Therefore, the comparison between topographic and thermal images is needed to observe whether the features in the thermal image are obtained from topographic variations or not.

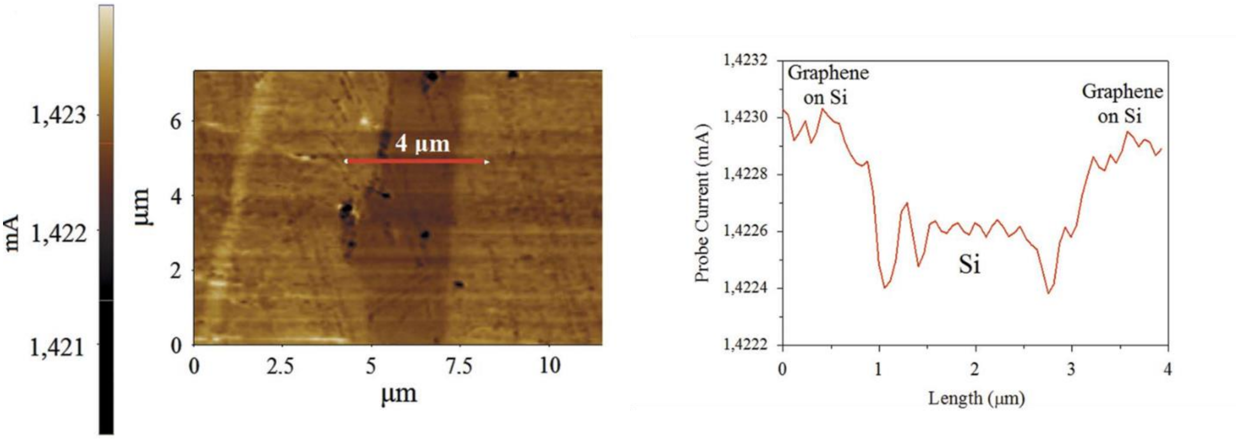

Figure 1-20: Thermal image and its corresponding line profile performed with SThM on a sample of graphene deposited on a silicon substrate showing covered and uncovered area of graphene [63].

Pereira *et al.* have performed SThM measurements on materials with various thermal properties; the thermal conductivity of the used materials ranged between 0.13 $W.m^{-1}.K^{-1}$for a polymeric sample and 1000 $W.m^{-1}.K^{-1}$for a graphene layer [63]. They aimed to illustrate the use of scanning thermal microscopy for microstructures and thermal investigation at the nanoscale. They used a sample formed of graphene deposited on silicon substrate. The sample was prepared in a way to leave some area of the silicon substrate uncovered by graphene. SThM imaging was performed over an area composed of covered and uncovered silicon. Figure 1-20 illustrates the thermal scan and line profile of the sample surface. It was demonstrated that SThM is a very powerful tool to distinguish between materials with different thermal conductivity. Thus the authors showed that SThM is a consistent tool to study locally the thermal properties of the materials.

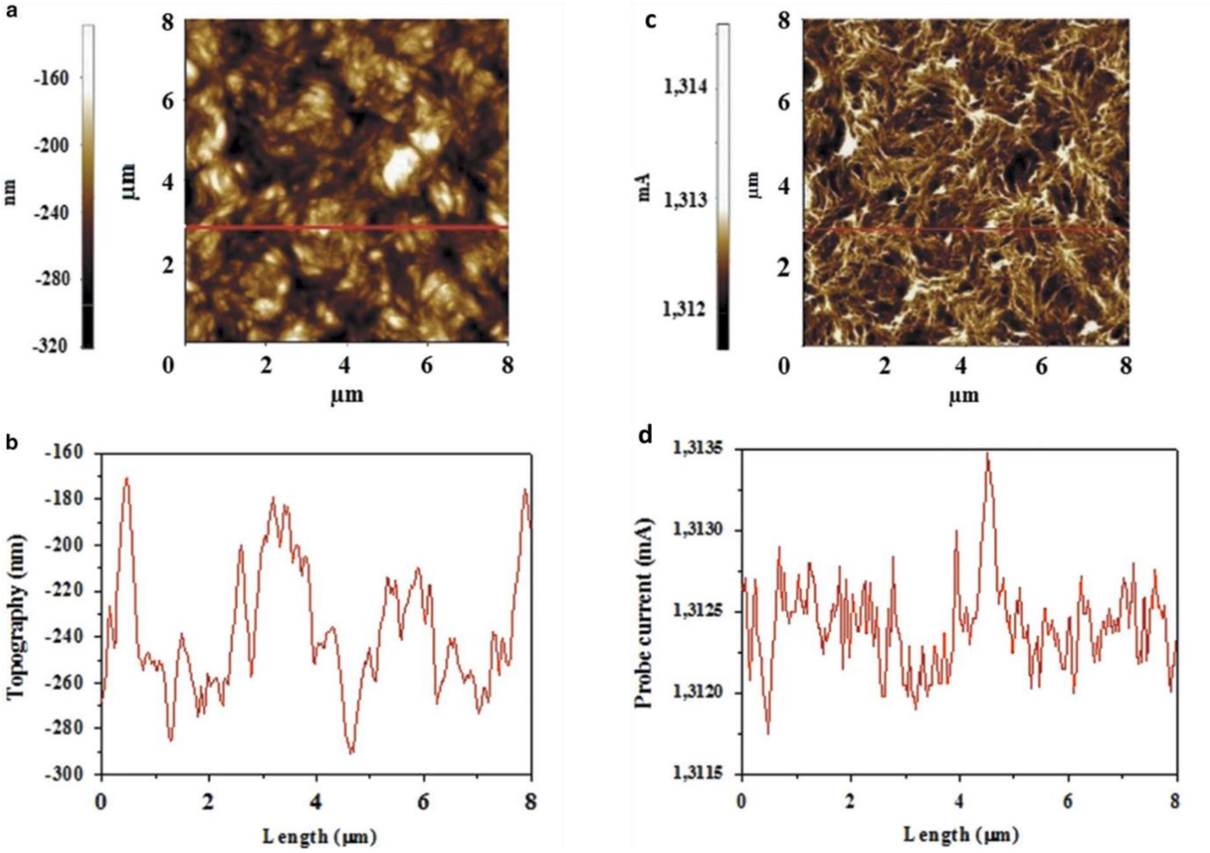

Figure 1- 21:a) topography and c)thermal images with their corresponding line profiles b and d obtained by SThM on a polymeric sample composed of polylactic acid (PLA) with 0.5% graphene oxide [63].

Measurements were also performed on polymeric sample composed of polylactic acid (PLA) with 0.5% graphene oxide [63]. Figure 1-21a and b represent the topographic and thermal image performed by SThM on a polymeric sample composed of polylactic acid with 0.5% of graphene oxide, while figure 1-21c and d illustrate their corresponding line profiles. The comparison between topographic and thermal line profiles shows that SThM is able to perform sub-surface imaging.

The capability to perform subsurface imaging is very important for semiconductor industry where it is necessary in some applications to build multi- level structures. Hammiche *et al*. performed SThM imaging using the Wollaston probe to investigate a sample composed of copper particles embedded in a polymer matrix [64]. A theoretical model was developed for copper particles embedded in a matrix at different depth. Figure 1-22a represents the geometry of the simulated material where material 2 corresponds to the buried structure under different distance of depths (material 1) in a semi-infinite matrix. The heat flow of the probe was simulated while scanning in x direction across the sample surface over an area containing 2 particles of 1 µm in length and width, with different distance of separation between them and buried at different depths. Figure 1-22b shows results obtained for this simulation.

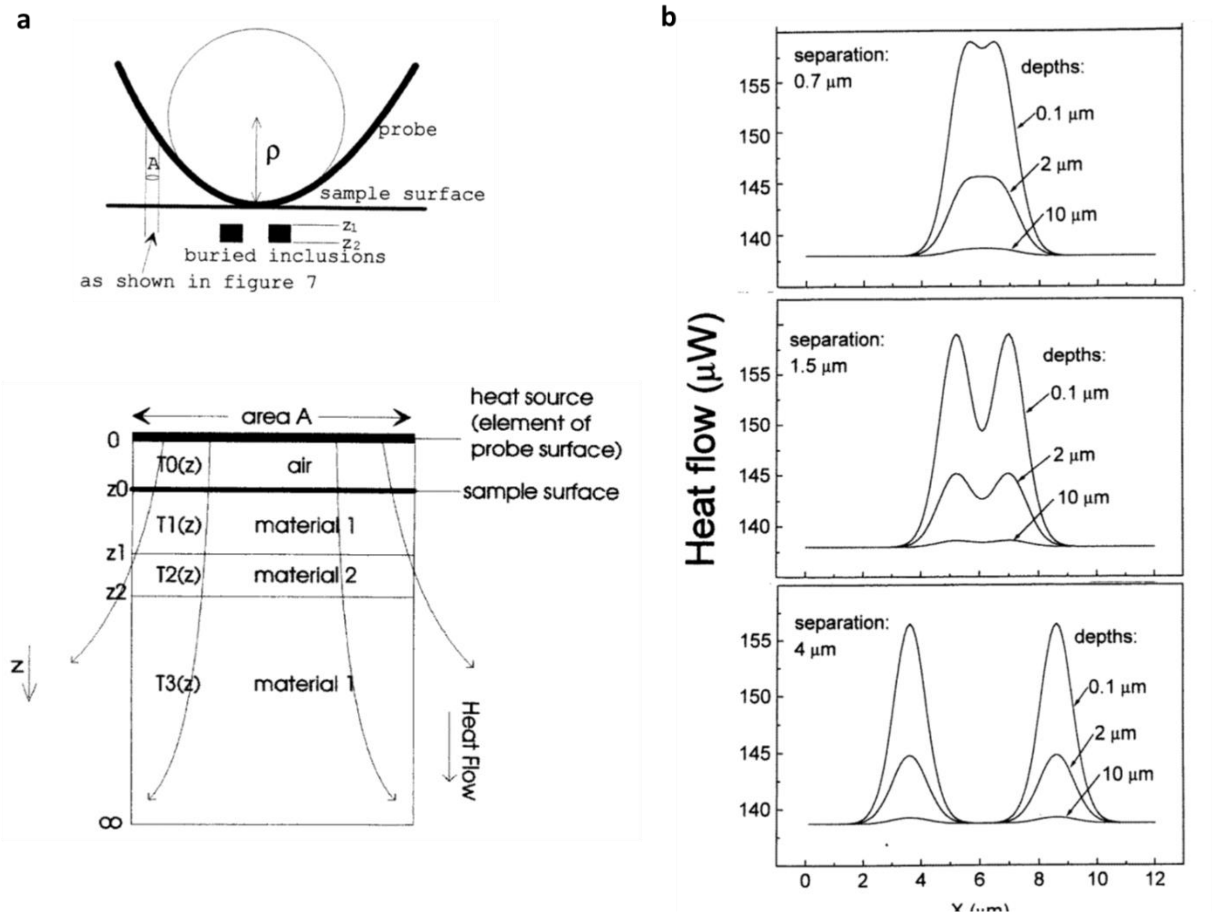

Figure 1- 22: a) illustration of the probe in contact with sub-surface inclusions with a schematic of the modelled semi-infinite volume. b) Results of the simulated heat flow in the direction x along two particles with 1µm in width, buried at different levels (0.1 µm, 2µm and 10 µm) [64].

As observed the heat flow decreases with increasing the depth of the buried particle. For a depth of 10 µm the signal is almost flat. These results indicate that SThM is a powerful technique to perform subsurface imaging by scanning thermal contrast correlated with thermal conductivity variation below the sample surface.

3.3. Heat transfer measurement with nanoscale probes

Nanoprobes were recently used to thermally characterize micro/nano-devices for their reduced tip apex which is in the range of few nanometers. This kind of probe has superior spatial resolution than the Wollaston probes, but their thermal behavior is still not perfect since they are not sensitive to materials having high thermal conductivities. This is due to the weak thermal contact between the sample and the probe and the low thermal conductivity of the apex. Yet it is very important to understand the thermal behavior between the probe and the sample.

When working with nanoscale probes the heat transferred from the probe through air is difficult to determine. Thus, evaluating the probe/air/sample conductances require appropriate experimental and modelling approaches. For this Puyoo *et al.* performed experimentally approach and retract curves in the AC mode using the 3ω method [65]. This kind of experiment consists of approaching the probe toward the sample surface until the contact point and then retracting it back to a certain point away from the sample surface. Puyoo *et al.* have performed this kind of experiments using the Pd/SiO_2 nanoprobe. Figure 1-23 illustrates the curves of approach/retract under ambient and vacuum conditions [65].

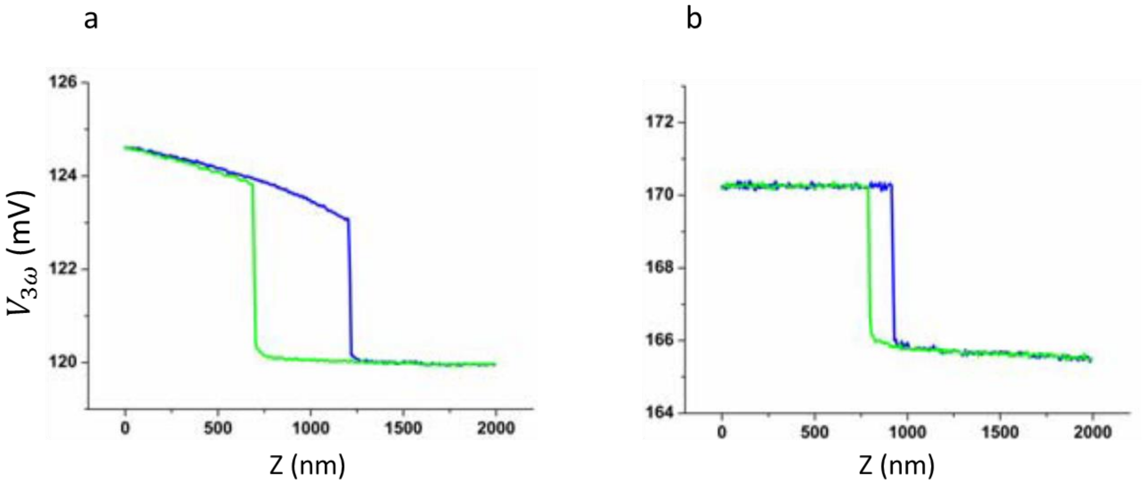

Figure 1-23: Evolution of the 3ω signal in amplitude a) under ambient conditions b) under vacuum of the palladium probe while approaching (blue curve) and retracting (green curve) toward a sample of silicon [65].

The sample considered here is bulk silicon. The blue and green curves represent the thermal signal obtained by the probe while approaching toward the sample corresponding successively to the approach and retract curves. For the approach curve the thermal signal decreases while moving the probe toward the sample until a sudden drop where the contact takes place. The signal remains constant after the contact. As observed curves present a hysteresis due to the presence of adhesion forces between the probe and the sample. It is necessary to provide an additional force to remove the probe from the contact. The adhesion forces are mainly attributed to capillary phenomena due to the presence of water meniscus at the very end of the tip. As observed under ambient conditions the probe needs more time to be retracted from contact comparing to vacuum conditions. This indicates the absence of water meniscus under vacuum.

Tovee *et al.* developed a model based on finite element method to investigate the sensitivity of the Palladium probe under ambient conditions. As the first approximation, they considered a continuity of temperature for the tip-sample boundaries [13]. The simulation results showed that material with high thermal conductivity such as silicon (130 $W.m^{-1}.K^{-1}$), the tip apex and surface contact hinder the heat transfer to the sample and to the probe. This fact limits SThM ability to investigate nanostructures made of such materials [49]. Therefore they also studied the sensitivity of the probe to under ambient conditions. Figure 1-24 represents the heater temperature change as a function of sample thermal conductivity. The results show that this kind of probe is sensitive to materials with thermal conductivity ranging between 0.1 and 10 $W.m^{-1}.K^{-1}$.

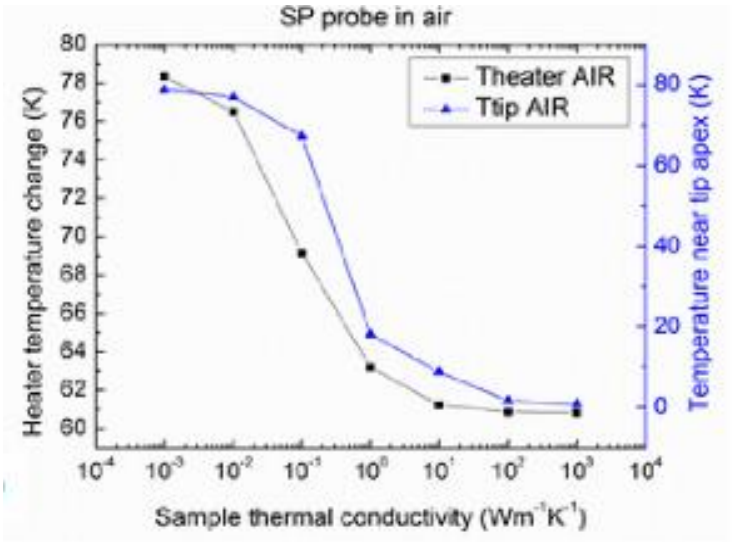

Figure 1-24: Heater temperature change (black curve) and temperature near tip apex (blue curve) as a function of thermal conductivities under ambient conditions with the Silicon probe [13].

Pumarol *et al.* used an ultra-high vacuum scanning thermal microscope with a Silicon probe to explore heat transport in supported and suspended graphene layers. The thermal conductivity of suspended graphene is 6600 $W.m^{-1}.K^{-1}$. The thermal contact resistance of the probe in contact with the supported graphene layers was estimated to$3.35.10^{6}\ K.W^{-1}$and $2.75.10^{6}\ K.W^{-1}$ for the suspended bilayer graphene. They showed that the thermal conductance of the suspended graphene layer is higher than the supported layer due to ballistic phonon propagation [66].

Assy *et al.* investigated the heat transferred from the Palladium probe to a silicon sample under vacuum conditions. They calculated the thermal resistance of the contact between the probe and the sample ($R_{s-s} = 10^{5}K.W^{-1}$) from which the thermal boundary resistance was estimated ($R_b = 14.1.10^{-9}m^{2}.K.W^{-1}$).

4. Conclusion

This chapter is dedicated to the investigation of heat transfer between SThM probes and samples. It was shown that the heat transfer depends on several factors such as the size of probes, thermal properties of the sample, the probe temperature, the medium surrounding the probe/sample system, and many others. Therefore, the interpretation of probe thermal signal and the investigation of materials thermal properties require a proper modelling of the probe-sample system. This modelling passes through the study of thermal interaction that can be interpreted through the network of thermal conductance of the system. Three different probes were studied: Wollaston, Palladium and Silicon probe.

This chapter consists describing the different thermal probes used in this chapter and the measurement methods given in the literature for each of probes. The heat transfer between the probe and the sample depends on the environment medium. Therefore, we showed that to date, researchers studied the probe sample system considering the surrounding medium as diffusive. Based on experimental studies we raised the hypothesis to consider the surrounding medium as convective. Thermal interactions between the probe and the sample depend on several thermal quantities such as sample thermal resistance, thermal contact resistance… Thus, a state of the art of the research that studied those quantities is given through experimental and theoretical methods. These works gave us an idea about the order of magnitude evaluated in the literature.

The thermal interaction between the probe and the sample depends also on sample thermal properties. Thus, the last part of this chapter deals with studies that characterized materials thermal properties at the macro/nanoscale. This characterization was done using experimental methods such as 3ω and scanning thermal microscopy and theoretical methods. Researchers works presented in the literature showed that thermal conductivity of a bulk material is not the same as for thin film material which will be used in the following chapters.

5. References

[1] M. Timofeeva, A. Bolshakov, P. Tovee, D. Zeze, V. Dubrovskii and O. Kolosov, Scanning thermal microscopy with heat conductive nanowires probes, Ultramicroscopy 162, 42-51 (2016)

[2] A. Hammiche, H. M. Pollock, M. Song, D. J. Hourston, Sub-surface imagingby scanning thermal microscopy, Meas. Sci. Technol. 7, 142-150 (1996)

[3] E. Puyoo, S. Grauby, J. M. Rampnoux, E. Rouvière and S. Dilhaire,Thermal exchange radius measurement: application to nanowire thermal imaging Rev. Sci. Instrum, 81 (7), (2010)

[4] A. Majumdar, J. P. Carrejo, and J. Lai, Thermal imaging using the atomic force microscope. Appl. Phys. Lett., vol 62, (1993)

[5] S. Gomès, Ali Assy and Pierre-Olivier Chapuis, Scanning thermal microscopy, Phys. Status Solidi A 212,No. 3, 477–494, (2015)

[6] J. Altet, S. Dilhaire, S. Volz, J.-M. Rampnoux, A. Rubio, S.Grauby, L. D. Patino Lopez, W. Claeys, and J.-B. Saulnier,Microelectron. J.33(9), 689–696 (2002).

[7] J. Altet, W. Claeys, S. Dilhaire, and A. Rubio, Dynamic surface temperature measurements in ICs Proc. IEEE94 (8), 1519–1533 (2006)

[8] A. Majumdar, M. Chandrachood, J. Lai, O. Nakabeppu, Y. Wu, Z. Shu, Thermal imaging by atomic force microscopy using thermocouple cantilever probes, Rev. Sci. Instr. 66-6, 3584-3592 (1995)

[9] R. B. Dinwiddie, R. J. Pylkki, P. E. West, Thermal conductivity contrast imaging with a scanning thermal microscope, Thermal Conductivity 22, 668-677 (1997)

[10] O. Raphael, Contribution à la microscopie thermique à sonde locale en mode alternatif : Caractérisation de la réponse et de l'interaction sonde échantillon, Thesis, Reims university (2008)

[11] Specification Scanning Thermal Microscope Option, User's Manual Addendum, Topometrix Corporation (1997)

[12] S. Gomès, Contribution théorique et expérimentale à la microscopie thermique à sonde locale : calibration d'une pointe thermorésistive, analyse des divers couplages thermiques, Thèse de doctorat, Université de Reims (1999)

[13] Tovee, P., et al., Nanoscale spatial resolution probes for Scanning Thermal Microscopy of solid state materials. Journal of Applied Physics,112(11), 114317-114317-11 (2012)

[14] Dobson, P.S., J.M. Weaver, and G. Mills. New Methods for Calibrated Scanning Thermal Microscopy (SThM). inSensors, 2007 IEEE. (2007)

[15] M. Despont, J. Brugger, U. Drechsler, U. Durig, W. Haberle, M. Lutwyche, H. Rothuizen,R. Stutz, R. Widmer, G. Binnig, H. Rohrer, P. Vettiger, VLSI-NEMS chip for parallel AFM data storage Sensors and Actuators, Sensors and Actuators (80) 100–107, (2000)

[16] Gotsmann, B. and U. Dürig, Thermally activated nanowear modes of a polymer surface induced by a heated tip. Langmuir, 20(4): p. 1495-1500, (2004).

[17] Anasys instruments, NanoTA and SThM Manual (2013).

[18] S. Lefevre, J.-B.Saulnier, C.Fuentes, S.Volz Probe calibration of the scanning thermal microscope in the AC mod, Superlattices and Microstructures (35) 283–288, (2004)

[19] B. SAMSON, Imagerie thermique par microscopie en champ proche à sonde fluorescente, PhD thesis université pierre et marie curie, (2009)

[20] D.G.Cahill, 'Thermal conductivity measurement from 30 to 750K: the 3ωmethod', Rev. Sci. Instrum., 61(2), 802, (1990).

[21] S. Lefèvre, S. Volz, '3ω-scanning thermal microscope', Rev. Sci. Inst. 76, 033701 (2005)

[22] S. Lefèvre, S. Volz, 3ωscanning thermal microscope, Rev. Scientific Instrum. 76, 033701 (2005)

[23] Majumdar, A., Scanning thermal microscopy. Annual review of materials science, 29(1), p. 505-585, (1999).

[24] K. Kim, W P King, Thermal conduction between a heated microcantilever and a surrounding air environment, App. Thermal engineering (29) 1631-1641, (2009)

[25] J.R. Howell, R. Siegel, M. Pinar, Thermal radiation heat transfer, Taylor and francis Group, 6th edition, (2015)

[26] S. Gomès, N. Trannoy, P. Grossel, DC thermal microscopy: study of the thermal exchange between a probe and a sample, Meas. Sci. Technol. 10, 805-811 (1999)

[27]A. Assy, S. GomèsTemperature-dependent capillary forces at nano-contacts for estimating the heat conduction through a water meniscus, Nanotechnology, 26, (2015).

[28] J.B. Xu, K. Läuger, R. Möller, K. Dransfeld, I.H. Wilson, Heat transfer between two metallic surfaces at small distances, J. Appl. Phys. 76-11, 7209-7216 (1994).

[29] O. Raphael, N. Trannoy and P. Grossel, thermal resonance at the microscale in AC scanning thermal microscopy with a thermal resistive probe, International Journal of Thermophysics 33, 1259-1269 (2012).

[30] S. Lefèvre, Modélisation et élaboration des métrologies de microscopie thermique à sonde locale résistive, Université de Poitiers (2004),

[31] David, L., S. Gomes, and M. Raynaud, Modelling for the thermal characterization of solid materials by dc scanning thermal microscopy. Journal of Physics D: Applied Physics, 40(14): p. 4337, (2007).

[32] Lefevre, S., et al., Thermal conductivity calibration for hot wire based dc scanning thermal microscopy. Review of scientific instruments, 2003. 74(4): p. 2418-2423.

[33] S. Lefèvre, S. Volz, P.O. Chapuis, Nanoscale heat transfer at contact between a hot tip and a substrate, Int. J. Heat Mass Transfer 49, 251-258 (2006)

[34] W.P. King, T.W. Kenny, K.E. Goodson, G. Cross, M. Despont, U. Durig, H. Rothuizen, G.K. Binnig, P. Vettiger, Atomic force microscope cantilevers for combined thermomechanical data writing and reading, Applied Physics Letters(78) 1300–1302 (2001).

[35] B.W. Chui, T.D. Stowe, Y.S. Ju, K.E. Goodson, T.W. Kenny, H.J. Mamin, B.D. Terris, R.P. Ried, Low-stiffness silicon cantilever with integrated heaters and piezo resistive sensors for high-density data storage, Journal of Microelectromechanical Systems (7) 69–78, (1998).

[36] N. Masters, W. Ye, W.P. King, The Impact of sub-continuum gas conduction on the sensitivity of heated atomic force microscope cantilevers, Physics of Fluids17, 100615, (2005).

[37] W.P. King, T.W. Kenny, K.E. Goodson, G.L.W. Cross, M. Despont, U. Durig, H. Rothuizen, G. Binnig, P. Vettiger, Design of atomic force microscope cantilevers for combined thermomechanical writing and thermal reading in array operation, Journal of Micro electromechanical Systems 11, 765–774, (2002).

[38] J. Lee, T.L. Wright, M.R. Abel, E.O. Sunden, A. Marchenkov, S. Graham, W.P. King, Thermal conduction from microcantilever heaters in partial vacuum, Journal of Applied Physics 101, 014906, (2007).

[39] K. Park, J. Lee, Z.M. Zhang, W.P. King, Frequency-dependant electrical and thermal response of heated atomic force microscope cantilevers, Journal of Micro electromechanical Systems 16, 213–222, (2007).

[40] O. Chapuis, E. Rousseau, A. Assy, S. Gomès, S. Lefèvre, and S. Volz, Heat transfer between a hot AFM tip and a cold sample: impact of the air pressure MRS Online Proc. Libr. 1543,159–164 (2013)

[41] N. Trannoy, J-F Henry, Investigation of thermal resistive probe behaviour used in Scanning Thermal Microscope by infrared imaging system. QIRT Journal (5) 27-44 (2008).

[42] Yovanovich, M. and E. Marotta, Thermal spreading and contact resistances. Heat Transfer Handbook, 1: p. 261-394, (2003).

[43] Y. Zhang, E. E. Castillo, R. J. Mehta, G. Ramanath and T. Borca-Tasciuc, A new class of doped nanobulk high-figure-of-merit thermoelectrics by scalable bottom-up assembly, Rev. Sci. Instrum., 82,2, (2011).

[44]K. Kim, W.H. Jeong, W.C. Lee, P. Reddy, Ultra-high vacuum scanning thermal microscopy for nanometer resolution quantitative thermometry, Acs Nano (6) 4248–4257, (2012).

[45] K. Kim, W. Jeong, W. Lee, S. Sadat, D. Thompson, E. Meyhofer and P. Reddy, Quantification of thermal and contact resistances of scanning thermal probes Appl. Phys. Lett., 105, 20, (2014).

[46] E. Puyoo, S. Grauby, J. M. Rampnoux, E. Rouvièreand S. Dilhaire,Thermal exchange radius measurement: application to nanowire thermal imaging, Rev. Sci. Instrum., ,81,7, (2010).

[47] B. Gotsmann and M. Lantz, Quantized thermal transport across contacts of rough surfaces. Nature Mater.12(1), 59–6 (2013)

[48] D.Pratap, R. Islam, P. Al-Alam, J.Randrianalisoa and N.Trannoy, Effect of air confinement on thermal contact resistance in nanoscale heat transfer, J. Phys. D: Appl. Phys.51 125301, (2017)

[49] A. Wilson, M. Rojo, B. Abad, J. Perez, J. Maiz, J. Schomacker, M Gonzalez, D. Borca-Tasciuc and T. Borca-Tasciuc, Thermal conductivity measurements of high and low thermal conductivity films using a scanning thermal hot probe method in the 3ω mode and novel calibration strategies, Nanoscale, 7 15404 (2015)

[50] M. Timofeeva, A. Bolshakov, P. Tovee, D. Zeze, V. Dubrovskii and O. Kolosov, Scanning thermal microscopy with heat conductive nanowires probes, Ultramicroscopy 162, 42-51 (2016)

[51] K. Luo, Z. Shi, J. Varesi, A. Majumdar Sensor nanofabrication, performance, and conduction mechanisms in scanning thermal microscopy. Journal of Vacuum Science & Technology B, 15(2): p. 349-360, (1997).

[52] D. G. Cahill, W. K. Ford, and K. E. Goodson, A generalized 3ω method for extraction of thermal conductivity in thin films,J. Appl. Phys. 93, 793 (2003).

[53] D. G. Cahill, M. Katiyar, and J. R. Abelson, Thermal conductivity of *a*-Si:H thin films Phys. Rev. B 50, 6077, (1994).

[54] D. G. Cahill, Thermal conductivity measurement from 30 to 750 K: the 3ω method Rev. Sci. Instrum. 61, 802, (1990).

[55] H Chieh, D. Yao, M. Huang and T. Chang, Thermal conductivity measurement and interface thermal resistance estimation using SiO2 thin film, REVIEW OF SCIENTIFIC INSTRUMENTS 79, 054902, (2008).

[56] D. Baillis, J. Randrianalisoa, Prediction of thermal conductivity of nanostructures: Influence of phonon dispersion approximation (11), 2516-2527, (2009)

[57] T. Yamane, N. Nagai, and S. Katayama, Measurement of thermal conductivity of silicon dioxide thin films using a 3ω method, J. Appl. Phys. 91, 9772, (2002).

[58] M. Okuda and S. Ohkubo, A novel method for measuring the thermal conductivity of submicrometre thick dielectric films, Thin Solid Films 213, 176 (1992).

[59] B. Y. Tsui, C. C. Yang, and K. L. Fang, Anisotropic thermal conductivity of nanoporous silica film IEEE Trans. Electron Devices 51, 20, (2004).

[60] W. Liu and M. Asheghi,J., Thermal conduction in ultrathin pure and doped single-crystal silicon layers at high temperatures, Appl. Phys.98, 123523 (2005)

[61] C.Jeong, S. Datta, and M.Lundstrom, Thermal conductivity of bulk and thin-film silicon: A Landauer approach, Birck and NCN Publications.Paper, 111 (2012)

[62] Cretin B., Gomès S., Trannoy N. and Vairac P. 2007 Microscale and Nanoscale Heat Transfer (Springer) 181-238

[63] M. J. Pereira, J. S. Amaral, N. J. O. Silva and V. S. Amaral, Nano-localized Thermal Analysis and Mapping of Surface and Subsurface Thermal Properties using scanning thermal microscopy, Microanal. 22, 1270-1280 (2016)

[64] A. Hammiche, H. M. Pollock, M. Song, D. J. Hourston, Sub-surface imaging by scanning thermal microscopy, Meas. Sci. Technol. 7, 142-150 (1996)

[65] E. Puyoo, Caractérisation thermique de nanofils de silicium pour des applications à la thermoélectricité, University of Bordeaux (2010)

[66] Manuel E. Pumarol, Mark C. Rosamond, Peter Tovee, Michael C. Petty,Dagou A. Zeze, Vladimir Falko, and Oleg V. Kolosov, Direct Nanoscale Imaging of Ballistic and Diffusive Thermal Transport in Graphene Nanostructures, Nano Letters 12, (2012).

[67] A. Assy, Developpement of two techniques for thermal characterization of materials: Scanning thermal Microscopy (SThM) and 2ω method, PhD thesis (2015)

[68] M.Hinz, O.Marti, B.Gotsmann, M.A.Lantz, U.Durig, ‘High resolution vacuum scanning thermal microscopy of HO2 and SiO2’, Appl. Phys. Lett., 92, 043122, (2008).

[69]A. Soudi, R.D. Dawson, Y. Gu, Quantitative heat dissipation characteristics incurrent-carrying GaN nanowires probed by combining scanning thermal mi-croscopy and spatially resolved Raman spectroscopy, Acs Nano (5) 255–262, (2011).

[70] K. Kim, J. Chung, G. Hwang, O. Kwon, J.S. Lee, Quantitative measurement with scanning thermal microscope by preventing the distortion due to the heat transfer through the air, Acs Nano 5 (2011) 8700–8709.

Résumé du chapitre 2

Ce chapitre a pour but d’étudier les transferts de chaleur entre la sonde en Wollaston et un échantillon et d’interpréter le signal thermique obtenu expérimentalement. Pour ce faire un modèle réaliste en 3D du système sonde/échantillon a été développé par la méthode des éléments fini (FEM) à l’aide de COMSOL. Une étude expérimentale par thermographie infrarouge a montré l’échauffement du microlevier en Wollaston ainsi que l’échauffement de l’air environnant. Tout d’abord nous nous sommes intéressés à la modélisation du filament en Wollaston qui a été basée sur des données issues de cette étude expérimentale. Cette modélisation a permis d’évaluer un coefficient d’échange thermique équivalent du microlevier vers le milieu environnant. Ce coefficient a été utilisé par la suite pour la modélisation complète de la sonde thermique. La sonde thermique est modélisée en tenant compte de ces dimensions réelles (filament du Pt/Rh et support en Wollaston). L'approche théorique de la réponse de la sonde a nécessité un couplage thermo-électrique basé sur l’équation du transfert de la chaleur et les équations de la densité de courant et du champ électrique. Les simulations ont été réalisées en mode DC à pression atmosphérique. Le modèle numérique permet aussi d’accéder aux flux de chaleur dissipés par le filament de Pt/Rh vers l’environnement. Les résultats obtenus ont été comparés aux résultats expérimentaux issus de la littérature montrant que les puissances mises en jeu étant du même ordre de grandeur.

Ce modèle nous a permis d’étudier l’évolution de la réponse de la sonde en fonction de la distance séparant celle-ci d’un échantillon en Cuivre. La simulation de la sonde à l'air ambiant prend en compte son support et considère que le milieu environnant (air) est convectif. Le milieu environnant est représenté par une boite ayant les propriétés thermiques de l’air. Lors de la réalisation de simulations, les résultats peuvent être influencés par des paramètres géométriques tels que la taille de la boîte ou la dimension des mailles. Pour cela, une étude paramétrique a été effectuée pour déterminer la taille de la boite optimale (compromis entre le temps de calcul et convergence des résultats) conduisant à un choix de 1 mm pour sa largeur. De la même façon, une étude paramétrique a été menée pour l’épaisseur de l’échantillon, le choix s’est porté pour une valeur de 800 nm. Les simulations sont faites à pression atmosphérique dans le mode de fonctionnement DC avec un courant d’excitation de 50 mA. Les résultats de l’évolution de la réponse de la sonde lorsque celle-ci s’approche de l’échantillon montrent la présence de trois régimes de transfert qui s’installent entre la sonde et l’échantillon : pour des distances supérieures à 1 µm, un régime diffusif régit les mécanismes du transfert, un régime intermédiaire est observé pour des distances comprises entre 0.5 et 1 µm, un comportement linéaire est observé pour des distances inférieures à 0.5 µm.

Les résultats ont été comparés à ceux d’une étude précédente comportant des données expérimentales à la même température de sonde et des données obtenues par FEM où le milieu environnant est considérée conductif. Ils montrent que nos résultats sont plus proches des données expérimentales. Pour des distances inférieures à 1 µm, les deux évolutions obtenues par FEM convergent. Pour des distances comprises entre 1 et 10 µm, nos résultats ont la même tendance que les résultats expérimentaux et sont relativement proches, contrairement à ceux obtenus par FEM en considérant le milieu environnant conductif. Pour des distances comprises entre 10 µm et 100 µm, nous obtenons un bon accord avec les données expérimentales, tandis que les résultats obtenus par FEM pour l'air diffusif sous-estiment les résultats expérimentaux. Pour des distances comprises entre 1 µm et 0,5 µm, un régime intermédiaire est observé pour les deux résultats par FEM et une variation linéaire prend place pour des distances inférieures à 0,5 µm. Plusieurs hypothèses peuvent être annoncées à partir de l'interprétation des résultats. Considérer l’hypothèse d’un milieu environnant comme convectif donne des résultats plus fiables pour des distances supérieures à 10 µm. Pour les distances plus faibles, un autre mécanisme de transfert de chaleur tend à s'opposer aux transferts entre la sonde et l'échantillon.

Par la suite, la sonde a été modélisée en contact avec un échantillon. Une étude paramétrique a été faite pour déterminer les dimensions de l’échantillon d’une façon à ce qu’elles n’influencent pas les résultats. Le modèle numérique permet d’obtenir plusieurs caractéristiques thermiques (flux de chaleur, température) du système sonde échantillon. La variation de la puissance électrique dissipée par la sonde a été calculée et présentées en fonction de la conductivité thermique de divers matériaux. La comparaison des résultats obtenus avec les données expérimentales montrent que la sonde en Wollaston est sensible jusqu'à une conductivité thermique de l’ordre de 20 $W.m^{-1}.K^{-1}$. La conductance thermique totale a été aussi évaluée, une valeur de $9.10^{-5}W.K^{-1}$ a été estimée lorsque la sonde est en contact avec un échantillon de cuivre. Cette valeur est du même ordre de grandeur que celle trouvée dans la littérature.

Chapter 2: Heat transfer mechanisms between the probe and the sample

As seen in chapter one, the investigation of materials properties requires a proper interpretation of the heat transfer mechanism between the probe and the sample. This chapter deals with studying closely interactions of probe/sample system which takes into account the whole probe. First we present a simulation approach by developing a model for the i) Wollaston probe and ii) probe/sample system. This modelling allows motion of the surrounding medium between the probe and the sample. Considering this hypothesis, heat transfer mechanisms were investigated while approaching the probe toward a sample. Through this study we highlight on the heat flowing from the thermal probe to air environment. Simulation results were compared to experimental ones for the validation of the model. This simulation results will enable us to determine the contact thermal resistance of the probe and sample in contact.

1. Finite element method base simulation

The study of heat transfer mechanisms between the probe and the sample requires a proper modelling to identify precisely regimes that take place in the system. Therefore, a modelling was developed using COMSOL Multiphysics, a commercial software based on finite element method (FEM). The principle of this method is presented in the coming section.

1.1. Principle of the FEM

Let us consider the case of heat transfer equation within a solid in a three-dimensional domain Ω in steady state regime. The equation governing the heat transfer in this case can be written as [1]:

$$\mathrm{div}(\underline{k}.\overrightarrow{grad}(T)) + \mathrm{Q} = 0 \qquad (1)$$

Where T denotes the temperature, $\underline{k}$represents a symmetric tensor of thermal conductivity and Q is the heat source.

In addition to equation (1) boundary conditions that link the domain Ω with the surrounding medium.

The resolution of such problem can be done from the weak formulation of differential equations based on FEM.

The first step is to integrate equation 1 over the domain Ω:

$$\int_{\Omega} \psi.\left(div(\underline{k}.\overrightarrow{grad}(T)) + \mathrm{Q}\right)dv = 0 \tag{2}$$

ψ denotes the weight functions and dvdefines a differential volume variation. FEM converts the functions to ordinary vectors. The derivative of equation 2 with respect to $dv$is given as:

$$\int_{\Omega} \psi.Q.dv + \int_{\partial\Omega} \psi.\left(\underline{k}\overrightarrow{grad}(T)\right).\vec{n}dS - \int_{\Omega} \overrightarrow{grad}(\psi).\underline{k}.\overrightarrow{grad}(T).dv = 0 \tag{3}$$

Where $\vec{n}$represents the unit normal vector of the boundary surface$\partial\Omega$. The formulation of the problem no longer depends on second derivative of the temperature field. The regularity required on the temperature T to give a meaning to the problem has therefore decreased. A function is regular if it can be locally approximated by a polynomial. Reducing the regularity of the temperature field facilitates its approximation. This fact characterizes the weak integral formulation. On the other hand, the regularity required for the functions ψ(x) has increased.

It is required to incorporate the boundary conditions in the above equation. This step is operated via the surface integral with $\partial\Omega$ which becomes:

$$\int_{\partial\Omega} \psi.\left(\underline{k}\overrightarrow{grad}(T)\right).\vec{n}.dS = \int_{\partial\Omega_T} \psi.(\underline{k}.\overrightarrow{grad(T)}).\vec{n}.ds + \int_{\partial\Omega_q} \psi.(\underline{k}.\overrightarrow{grad(T)}).\vec{n}.ds \tag{4}$$

Conditions of Dirichlet type are imposed on the boundaries $\partial\Omega_T$ and Neumann type on the boundaries of $\partial\Omega_q$. The condition of the second type allows a direct computation of the integrant since it describes the imposed flux at boundaries $\partial\Omega_q$denoted q. Applying a Dirichlet type condition characteristic of an imposed temperature makes the integral on the surface element $\partial\Omega_T$ null. Equation (4) becomes:

$$\int_{\partial\Omega} \psi.\left(\underline{k}\overrightarrow{grad}(T)\right).\vec{n}.dS = \int_{\partial\Omega_q} \psi.q.ds \qquad (5)$$

In the case of Dirichlet condition, the determination of the integrant requires the use of supplementary variable, called Lagrange multiplier and denoted by μ. This Lagrange multiplier enables us to determine accurately the value of the flux on the surface regardless the fineness of the mesh.

FEM relies on the discretization of the problem. The weak integral formulation presented above is valid for a continuous problem. The transition to a discrete problem is done by the application of Galerkin's method [2] and makes the weak form applicable to each elementary domain Ω_e. The weight functions $\psi(\vec{x})$ and temperature functions $T(\vec{x})$can then be defined for each mesh cell by polynomial or linear form.

The division of the whole geometry Ω into m elementary domains Ω_e must verify the two following conditions:

- The union of m elementary domains Ω_e constitute the domain Ω.
- The intersection of two consecutive elementary domains is empty.

Each elementary domain, called mesh cell, is defined by number n^e of characteristics points (nodes). The approximation of finite element method is built from those nodes. These also allow the connection of wanted fields to ensure the continuity of the overall approximation over the domain Ω. Finding values of weight functions$\psi(\vec{x})$and $T(\vec{x})$in these nodes characterizes the nodal approximation.

In order to simplify the approach, we will estimate functions of weight $\psi(\vec{x})$ and temperature fields $T(\vec{x})$ as piecewise linear functions (figure2-1). Whatever the position vector $\vec{x}$ belonging to the elementary domainΩ_e, we can write:

$$\psi(\vec{x}) = \sum_{i=1}^{n^e} \psi_i^e\,.N_i^e(\overrightarrow{x}) \qquad (6)$$

and

$$T(\vec{x}) = \sum_{i=1}^{n^e} N_j^e\,(\overrightarrow{x}).T_j^e \qquad (7)$$

With, in one-dimensional representation, the function:

$$N_i^e(x) = \begin{cases} \dfrac{x - x_{i-1}}{l} & if\ x_{i-1} \le x \le x_i \\ \dfrac{x_{i+1} - x}{l} & if\ x_i \le x \le x_{i+1} \\ 0 & if\ not \end{cases} \tag{8}$$

Where x_i is the abscissa of node i, and *l* is the distance separating two consecutive nodes.

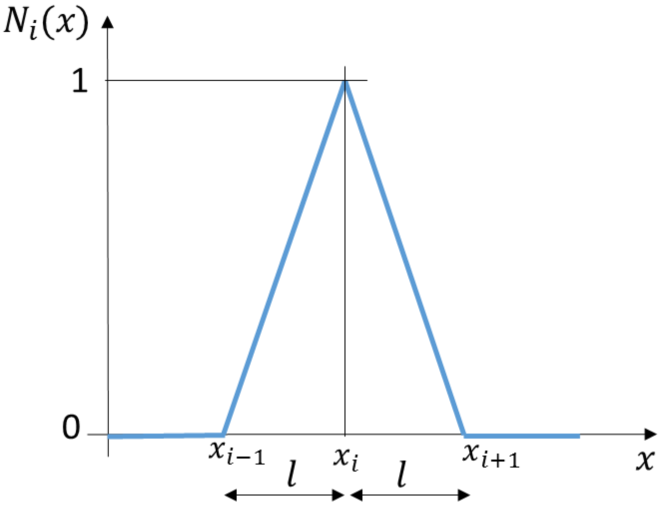

Figure 2- 1: Representation of the piecewise linear function allowing the decomposition of weight function and temperature fields.

These functions can be written in the form of a vector product having as components the different terms of the sum, such as:

$$\psi(\vec{x}) = \langle \psi_1^e, \psi_2^e, \dots, \psi_{n^e}^e \rangle . \begin{Bmatrix} N_1^e(\vec{x}) \\ N_2^e(\vec{x}) \\ \dots \\ N_{n^e}^e(\vec{x}) \end{Bmatrix} = \langle \psi^e \rangle . \{N^e(\vec{x})\} \tag{9}$$

(10)

$$T(\vec{x}) = \langle N_1^e(\vec{x}), N_2^e(\vec{x}), \dots, N_{n^e}^e(\vec{x})\rangle . \begin{Bmatrix} T_1^e \\ T_2^e \\ \dots \\ T_{n^e}^e \end{Bmatrix} = \langle N^e(\vec{x})\rangle . \{T^e\}$$

By incorporating these expressions in the weak integral formulation for a global domain Ω containing m elementary domains Ω_e, equation 3 can be written as:

$$\sum_{e=1}^{m} \langle \psi^e \rangle . \left[\int_{\Omega^e} \{N^e\}. Q. dv + \int_{\partial\Omega^e} \{N^e\}. q. ds - \int_{\Omega^e} \{\overrightarrow{grad}(N^e)\}. \underline{k}. \langle \overrightarrow{grad}(N^e)\rangle . \{T^e\}. dv \right] = 0 \tag{11}$$

The term in parentheses, called elementary residue and denoted by $\{R^e(T)\}$, is a fundamental quantity to which the FEM leads. In the case of a linear problem, the elementary residue can be expressed linearly as a function of temperatures at nodes of the elementary domain Ω_e, thus $\{R^e(T)\}$ is written as:

$$\{R^e(T)\} = \{F^e\} - [\Lambda^e]. \{T^e\} \tag{12}$$

In this last expression, the elementary matrix $[\Lambda^e]$ is a square matrix of dimension $n^e \times n^e$. The vector $\{F^e\}$ is a column vector containing n^e components and called second elementary member.

Solving the whole system becomes possible by the execution of an assembly procedure. This operation consists on transforming the elementary quantities into total ones. It is realized by a matrix noted $[A^e]$ assembling the local node numbering to the global one, such as:

$$\{T^e\} = [A^e]\{T\} \tag{13}$$

And

$$\langle \psi^e \rangle = \langle \psi \rangle^t . [A^e] \tag{14}$$

Therefore, the weak formulation becomes:

$$\begin{aligned}\sum_{e=1}^{m}\langle\psi^e\rangle.\{R^e(T)\} \\ &= \sum_{e=1}^{m}\langle\psi^e\rangle.(\{F^e\}-[\Lambda^e]\{T^e\}) \\ &= \langle\psi\rangle.\sum_{e=1}^{m}{}^{t}[A^e].(\{F^e\}-[\Lambda^e].[A^e].\{T\})=0\end{aligned} \tag{15}$$

So expressions of the second global member $\{F\}$and the global matrix $[\Lambda]$are:

$$\{F\}=\sum_{e=1}^{m}{}^{t}[A^e]\{F^e\} \tag{16}$$

$$[\Lambda]=\sum_{e=1}^{m}{}^{t}[A^e].[\Lambda^e].[A^e] \tag{17}$$

The global residue is written as:

$$\{R(T)\}=\{F\}-[\Lambda].\{T\}=0 \tag{18}$$

Solving this system of equation leads to suppress the global residue. The temperature field is then obtained from the following equation:

$$\{T\}=[\Lambda]^{-1}.\{F\} \tag{19}$$

In the simple case of steady state linear problem, the solution is based on calculation of the inverse matrix$[\Lambda]^{-1}$. Numerical methods allowing this inversion are divided into two classes:

- Direct methods (Gauss, Cholesky, etc.)
- Iterative methods (Jacobi, Gauss-Seidel, etc.)

Depending on the number of unknowns the problem can be solved using direct or iterative methods. When the number of unknowns is small (typically < 10^5), direct method is applicable. When the number of unknowns is large (> 10^5), iterative methods are recommended. COMSOL detects the problem size and the physics being solve and will choose the method accordingly.

The COMSOL based FEM was used to study the thermo-electric coupling for thermoresistive microprobes. The problem is solved by the resolution of two coupled equations: the heat transfer and the electric current equations. They have as unknowns the temperature field and the voltage field. The coupling between these two models is ensured by the dependence of material's electrical resistance on temperature and the power dissipated by Joule effect contributing as internal source of heat Q. This method will be applied to model the whole thermal probe based on Wollaston wire. In the literature, the simulation of this thermal probe was done without considering the modelling of Wollaston wire [3]. Therefore, in this study we decided to take into account the Wollaston wire in its real geometry which will be presented in the next paragraph.

1.2. Wollaston wire modelling

The Wollaston wire contributes to the thermal equilibrium of thermal probe [6]. Its investigation is therefore essential to have a full model. Earlier studies stated that a large part of the heat flowing to the filament is dissipated by conduction via a heat sink. They considered the Wollaston wire as a thermal sink and they simply integrated it in the modelling by applying a heat transfer coefficient through a cylindrical geometry [3, 4].One of these studies stated that the heat flux evacuated through the holder is estimated to 100000 W/m²[3] while Lefevre *et al.* imposed a temperature on the Wollaston surfaces [4]. They estimated the heat flux lost by the platinum wire to the Wollaston to 2.1 mW for a probe mean temperature of 112°C. But no previously published studies developed the real geometry of the Wollaston probe holder.

An experimental approach based on infrared imaging highlighted the presence of a significant temperature gradient within the Wollaston wire [5]. This investigation showed that the Wollaston wire is also heated in ambient air (figure 2-2a). Therefore this should be taken into account for modelling of the probe. The Wollaston wire modelling was based on this previous study [5]. For a well-established modelling a good choice of boundary conditions is required. In the next paragraph we present Wollaston wire simulation and chosen boundary conditions.

1.2.1. Geometry and boundary conditions of Wollaston wire

The Wollaston wire investigation consists on developing a complete model of the probe holder. Therefore the geometry is composed of the Wollaston wire, the glue used to fix wires which is electrically insulating and the mirror used for the topographic performance of the probe.

The choice of boundary conditions influences the pertinence of the results. In this paragraph we define the boundary conditions used for the simulation of the Wollaston wire.

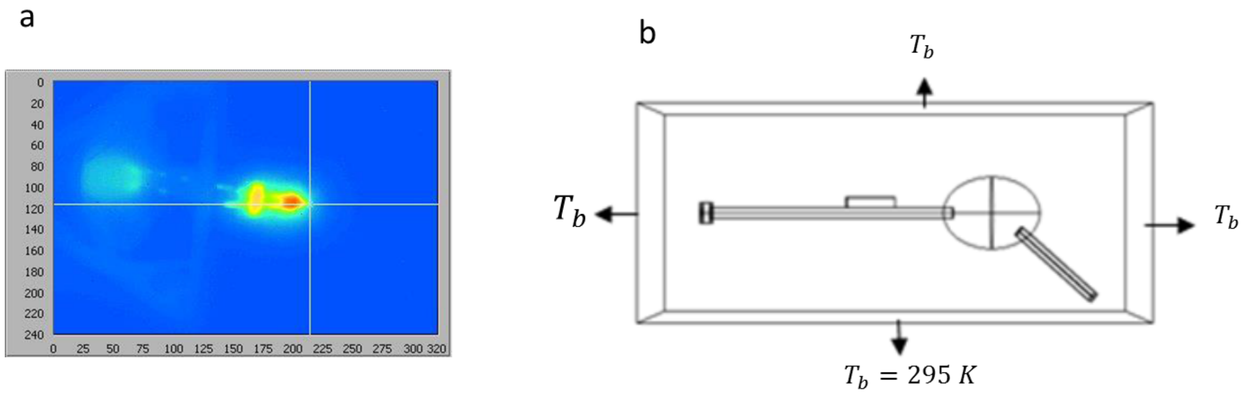

Figure 2- 2: a) Infrared image of the thermal probe at 298°C and b) Schematic representation of the Wollaston wire geometry [3].

Figure 2-2a illustrates the model of Wollaston wire suspended freely in an environment box. The geometry presents all components of the probe holder: the glue, the mirror, the Wollaston wire and electrical wires. The probe holder was modelled with its real size geometry for which dimensions are given in table 2-1. Outer surfaces of the box were set to ambient temperature. The temperature of probe holder was chosen based on experimental data [5]. Figure 2-2a illustrates an infrared image of the thermal probe at 298°C. Subtracting the thermal image of probe at ambient air from the thermal image of heated probe enables us obtaining the temperature rise of Wollaston wire. This temperature was estimated to 40°C and used in the FEM modelling of Wollaston wire.

Materials	Dimensions (mm)		Thermal conductivity ($W.m^{-1}.K^{-1}$)
	Length	width	
Wollaston wire (Silver)	7.5	0.075	429
Glue (Silica)	0.225	0.225	1.35
Mirror (Silver)	0.9	0.25	429

Table 2- 1: Dimensions chosen for the modelling of Wollaston wire [3]

1.2.2. Mesh of the Wollaston wire

The mesh of the system is presented in figure 2-3. It has to be chosen very carefully in order to guarantee a good quality and homogeneity in the decomposition of the geometry from a domain to another. The quality of mesh is ensured by the distance between shapes of elements compared to the regular geometry, it ranges between 0 and 1. In the case of 3D geometry, the algorithm discretizes the global volume to polyhedral forms. In this study a tetrahedral mesh is used. The quality factor which defines whether the mesh is good enough to have pertinent results is then characterized related to a regular tetrahedral. A fine mesh is used for the Wollaston wire with a minimum element size of 10 µm and a maximum element size of 150 µm and a coarse mesh is used for the surrounding air(environment box) with a minimum element size of 120 µm and a maximum of 1200 µm. The choice of those parameters decomposes the whole geometry in 864544 tetrahedral elements. It also ensures the quality of the mesh which is defined by the total elements created with a quality factor > 0.6.

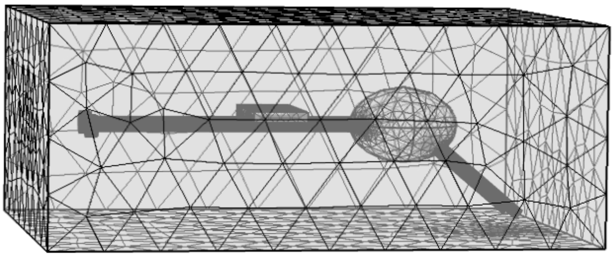

Figure 2- 3: Meshed geometry of the Wollaston wire and the environment box.

1.2.3. Determination of the equivalent heat exchange coefficient to the environment

Since the Wollaston wire is freely suspended in air environment, the heat transfer mechanism accounted in this case is the heat flow to the air environment and thermal radiation. The thermal radiation is neglected due to the temperature chosen for the Wollaston wire. Actually when the temperature is low (40°C) the considered element does not emit enough radiation and this phenomenon can be neglected.

The governing equation in this case is:

$$\rho C_p \frac{\partial T}{\partial t} + \nabla . q = Q \tag{20}$$

With $q = -k\nabla T$

Where T is the temperature of the Wollaston wire, k is thermal conductivity of silver, ∇q is the volumetric heat generation rate, ρ is the density and C_p is heat capacity.Table 2-2 summarizes the thermal properties of silver considered in the model.

Table 2- 2: Thermophysical characteristics of Wollaston thermal probes at 20°C [6].

	Thermal conductivity $W.m^{-1}.K^{-1}$	Heat capacity $J.Kg^{-1}.K^{-1}$	Density $Kg.m^{-3}$	Electrical conductivity $S.m-1$
	k	C_p	ρ	σ
Silver	429	235	10500	$6.13.10^7$
Pt_{90}-Rh_{10}	38	130	19970	$8.9.10^6$

In our modelling natural convection of the surrounding medium is considered. The natural convection consists in solving Navier-Stokes equations for conservation of momentum and the conservation of mass along with heat transfer equation. Those equations are available in the laminar flow physics by:

$$\rho\frac{\partial\vec{u}}{\partial t}+\rho(\vec{u}\nabla)\vec{u}=\nabla[-pI+\mu(\nabla\vec{u}+(\nabla\vec{u})^T)]+\vec{F} \tag{21}$$

$$\nabla(\rho\vec{u})=0 \tag{22}$$

Where µ is the dynamic viscosity, p is the pressure, $\vec{u}$ represents the velocity field.

The dynamic viscosity is that of the air and it is set to be $1.85\ 10^{-5} kg.m^{-1}.s^{-1}$.The lateral surfaces of the box is set as inlets for the air and the upper surface of the box is set as outlet. At the inlets the velocity field is $\vec{u}=-u_{in}.\vec{n}$ with u_{in} is chosen to be 0.001 m/s [7],$\vec{n}$ is the normal unit vector. At the outlets, the pressure is prescribed atmospheric pressure$p=0$. A gravitational force was implemented along z axis with$\overrightarrow{F}=-\vec{g}\times\rho=-18.05\ N/m^3$; where $g$is gravity acceleration and ρ is the density of air.

After solving the full problem, [equations (20)-(22)] a heat transfer coefficient of the Wollaston wire can be determined through the following equation:

$$h=\frac{\varphi}{S\times\Delta T} \tag{23}$$

Where $\varphi$and S are respectively the heat flux dissipated by the Wollaston wire to the environment (W/m^2) and the surface of its whole geometry (m^2). $\Delta T=T_w-T_0$is the difference of temperature between the Wollaston wire and the surrounding medium (K).

The numerical model allows to obtain the heat flux dissipated by the Wollaston wire through the air environment which is$118\ W/m^2$ and the exchange area which is $6.9.10^{-5}\ m^2$. From those values we determined an equivalent heat exchange coefficient of $84000\ W/m^2.K$). This coefficient will be implemented in the modelling of the whole thermal resistive probe in order to be closer to real experimental conditions.

In his thesis Raphael [3] studied a surface convective exchange coefficient equivalent to the thermal sink generated by the Wollaston wire under ambient and vacuum conditions as a function of the frequency. His results showed that this coefficient is independent of the nature of surrounding medium and depending on the frequency. This coefficient tends to a perfect thermal sink with increasing the frequency. The estimated value of the heat exchange coefficient in our study is 20 % less than that found by Raphael which was$100000\ W/m^2.K$.

This is due to the fact that the developed model takes into account real dimensions of Wollaston wire and the temperature gradient applied to the filament.

1.3. Thermal probe modelling

1.3.1. Geometry and boundary conditions

In this paragraph we present a realistic geometry of the Wollaston probe built in COMSOL. The Platinum-Rhodium wire is represented by a V shape with a diameter of 5 µm and a half-length of 125 µm [3].Raphael in his thesis performed scanning electron microscope (SEM) images on different probes to evaluate the length of the Pt-Rh wire. He found that the length of the whole wire is about 250 µm which is about 25 % higher than the value announced by the manufacture (200µm). The curvature radius is fixed to 15 µm. The Wollaston wire is illustrated by a cylindrical geometry with a diameter of 75 µm and a thickness of 5 µm. Figure 2-4 presents the modeled geometry of the resistive probe in a simulation box mimicking the surrounding air.

The thermal equilibrium of the probe is only accessible through the difference of potential at the two extremities of the probe's wire. In fact the direct measurement of probe temperature is found to be inaccurate disruptive from the so-called equilibrium [8]. The modelling of the thermal probe requires a thermo-electrical coupling. Therefore, two sets of boundary conditions are used: the first for the thermal problem, the second for the electrical problem.

For the electrical problem, the boundary conditions were carefully chosen. The external surfaces of the box are electrically isolated. The cantilever is heated by applying a difference of potential between the two ends of the Wollaston wire. This value defines the current flowing through the Wollaston probe which is chosen to be 50 mA in this study. A condition of continuity is considered for all external surfaces of the platinum rhodium wire. No other boundary conditions are used for the probe system. One important parameter for this structure is the electrical conductivity which by its dependence to temperature allows the coupling between electrical and thermal problems.

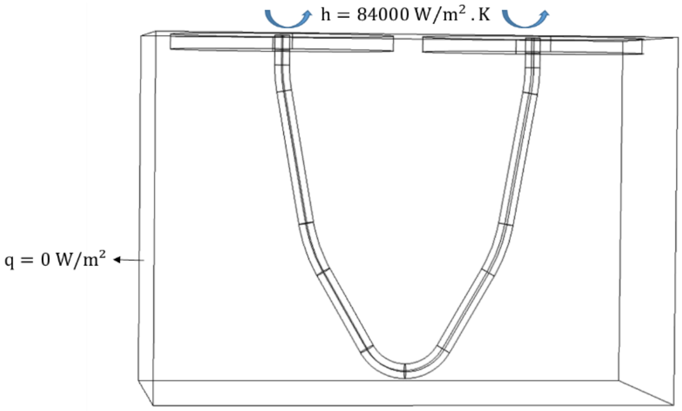

Figure 2- 4: Geometry of the thermal probe in an environment box.

Solving the thermal problem requires more choice of boundary conditions. The modelling of Wollaston wire presented in the previous section allowed determining an equivalent heat transfer coefficient for the Wollaston wire. This value is used as a boundary condition for the Wollaston wire represented by the cylindrical geometry. It is applied on the upper surfaces of the Wollaston wire. A zero null heat flux is applied on all the lateral surfaces of the surrounding box.

1.3.2. Mesh of the Pt-Rh wire

The particularity of the approach using FEM relies on a geometrical approximation of the problem. The relevance of results depends then on the degree of discretization of geometry. The higher the number of nodes, the more accurate the approximation is. However this approach is limited to the capacity of available computer. Therefore, it is necessary to evaluate the suitable number of mesh for the corresponding geometry.

The meshed structure of probe and a zoom of the holder (top view) are presented in figure 2-5a and 5b. The choice of mesh characteristic parameters was done carefully in a way to guarantee the quality of mesh and certain homogeneity in the structure. For the three-dimensional geometry, the algorithm discretizes the global volume into polyhedral forms. For our modelling we chose a tetrahedral mesh. This choice was based on the fact that the platinum-rhodium wire has a curved shape which makes the tetrahedral type of mesh the most adapted to have a well-established mesh structure.

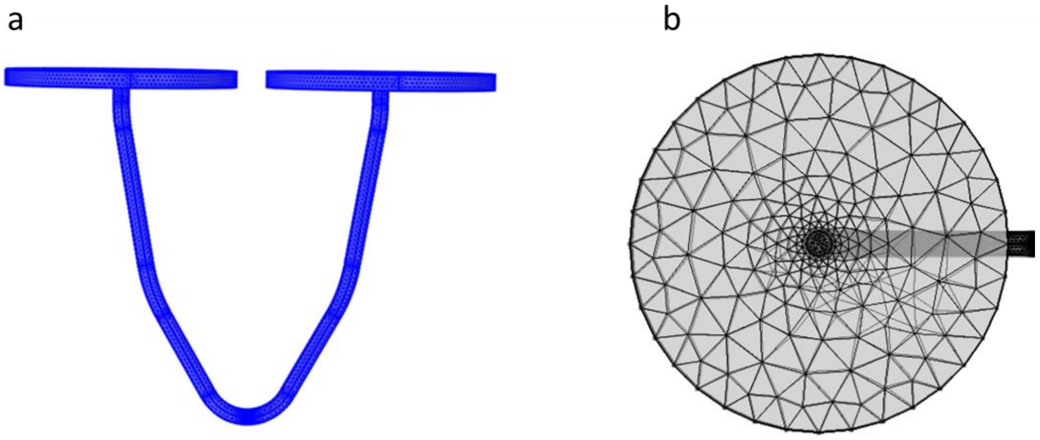

Figure 2- 5: Meshed geometry of a) the Platinum rhodium wire and b) the upper surface.

The mesh dimensions are defined by setting the following characteristic parameters:

- Maximum element size which limits the maximum size of each element, where lower the value, finer the mesh is. It is set to 1.5 µm.
- Minimum element size which limits the minimum size of each mesh element can be. It is set to 0.04 µm.
- Maximum element growth rate defines the size difference of two adjacent mesh elements. It is set to 1.6.
- Curvature factor defines the ratio between the size of a mesh element and curved boundary. It is set to 0.5.
- Resolution of narrow regions controls the size of mesh elements in thin regions. It is set to 0.4.

The use of those parameters decomposes the geometry in 903253 elements presenting a quality factor >0.7. This configuration presents the best compromise between the time of calculation and the accuracy.

1.3.3. Results

In order to solve the electrical and thermal problems for the probe system, we need to use the heat transfer equation (equation 24) and the electrical equation (equation 25). The transient heat conduction equation of the cantilever is:

$$\rho C_p \frac{\partial T}{\partial t} + \nabla . q = \frac{RI^2}{\Delta v} \tag{24}$$

With $q = -k\nabla T$

Where $T$and k are respectively the temperature and the thermal conductivity of the probe (Wollaston or Pt-Rh), ∇q is the volumetric heat transfer rate, ρ is the density and C_p is heat capacity. R is the electrical resistance of the probe and I is the electrical current. The thermal properties considered for the modelling are listed in table 2-2.

And the electric current equation can be written as:

$$J = \sigma E + \frac{\partial D}{\partial t} \tag{25}$$

With $E = -\nabla V$.

Where J is the current density,σ is the electrical conductivity, E is the electric field, D is the dielectric loss and V is the voltage.

Solving equations (24) and (25) by FEM ensure the thermo-electrical coupling needed for the probe response. The solution in steady state allows to obtain the temperature profile behavior of the thermal probe. The probe was modelled in the DC operating mode for a 50 mA current.Figure2-6 illustrates the temperature profile for the heated probe and its surrounding.

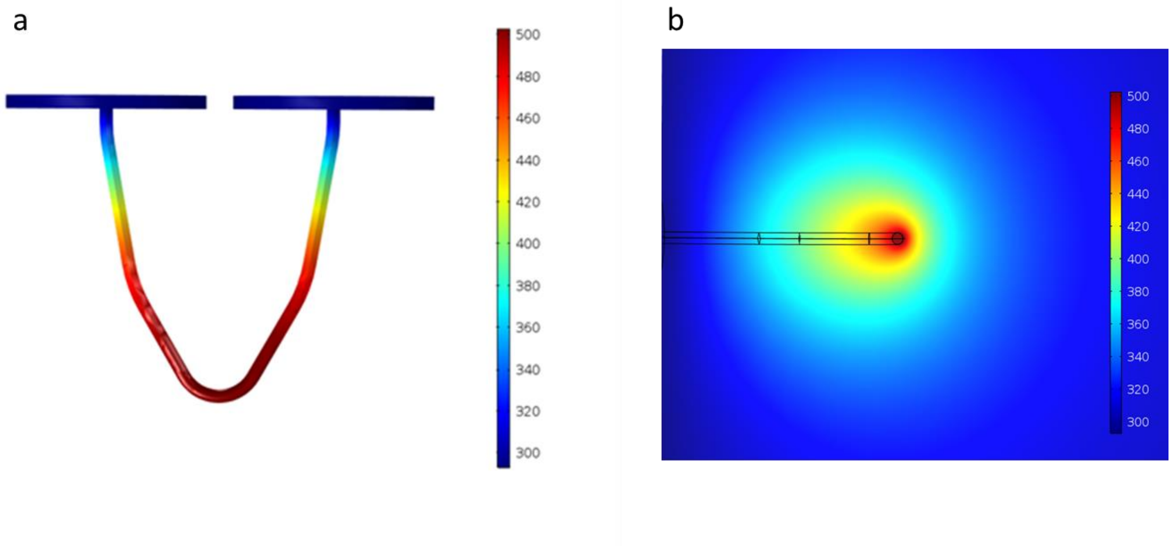

Figure 2- 6:a) The temperature profile in thethermal probe in K, b) an horizontal cut of the Pt-Rh wire showing the heating of surrounding medium.

The temperature field is presented in the symmetry plane in order to provide a detailed representation of heat spread from the probe. The simulation results show that the probe apex has the higher temperature with 416 K, while the mean temperature of the probe is 373 K.

Previous study was done to estimate heat fluxes dissipated by the thermal probe [5]. They used a technique based on experimental data obtained with an infrared thermography system. A model was also developed and was combined with experimental data in order to evaluate the heat flux dissipated by the probe into the sample. Through their approach they also estimated the heat flux dissipated into the Wollaston wire when the probe is out of contact to 13.7 mW for a probe mean temperature of 100°C. Our numerical model gives a direct access for heat fluxes transmitted from the thermal probe. The value of heat flux dissipated into the Wollaston wire for a probe mean temperature of 100°C was estimated to 12.7mW. Our finding is coherent with experimental data reported in the literature.

2. Probe/sample modelling

Herein we present a 3D finite element model of heat transfer between a Wollaston wire probe in contact with a sample and their surroundings. The model of the heated probe in contact with a sample in an environment box is presented in figure 2-7. The aim is to have a geometry close to the realistic set up. Thermal probes are hand based fabrication, thus the tilt of the probe vary from 30 to 80 degrees with respect to the horizontal. Previous studies were done on the influence of probe’s inclination on results [3, 9]. Assy in his thesis have performed measurements showing the variation of probe voltage as a function of the inclination of the probe. No significant variations were observed under ambient conditions while varying the inclination from 0 to 70° with respect to sample surface [10]. Raphael [3] has developed a model that allows to study the influence of different inclinations of the thermal probe on the evolution of the probe’s amplitude (voltage) as a function of probe sample-distance. He showed that increasing the inclination of the probe from 60° with respect to the sample to 90° increases the amplitude of voltage [3]. Massoud in his thesis has studied the case of a straight configuration and a tilted probe of 70° with respect to the normal by developing a model in FEM [9]. He showed that the maximum temperature of probe is higher for the straight configuration since the tip exchanges less heat with the sample thus a decrease of its temperature is obtained [9].Therefore our modelling takes into consideration the inclination of probe with respect to the sample of 60° which is the most observed in experiments.

The contact between the probe and the sample is determined geometrically by a surface of exchange between the platinum-rhodium wire and the sample. The probe is indented in the sample with dozens of nanometer without considering a mechanical stress and strain of the sample surface.

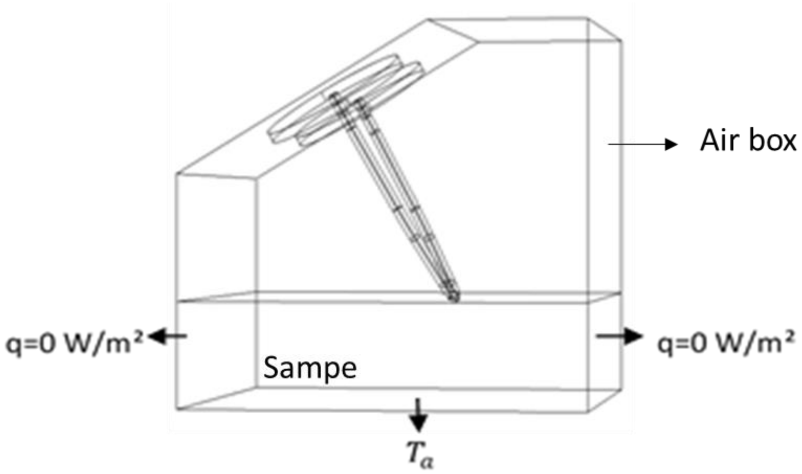

Figure 2- 7: Schematic of the thermal probe in contact with a sample.

The solid that represents the semi-infinite sample is of 800 µm in thickness, 1 mm in width and length. The sample size, therefore the air box sizes, were chosen according to a parametric study that was done in order to define their size which is presented in the next paragraph. The thermal conductivity of the Pt-Rh wire and of the Wollaston wire are the same as used for the modelling of the probe and they are listed in table 2-2.

2.1. Choice of the box size

While performing simulations, results can be influenced by geometrical parameters such as the box size. Therefore a parametrical study was performed in order to estimate the air box size to ensure any influence on results. As a first step, the thermal probe was analyzed without the presence of sample. For this, the length of the bow was considered fixed with a value of 800 µm. The only parameter that was changing is the width of the box. The study was done for different widths starting 500 µm reaching 3000 µm.

The heat flux dissipated from the platinum-rhodium wire was calculated via the numerical model. It decreases while increasing the width and it becomes stable starting 1000 µm. Once this value becomes stable it means that results are no longer affected by the box size which will be the size used for the model. The box size chosen was of 1000 µm since the difference between 1000 and 3000 µm is less than 2% we chose the 1000µm to reduce the duration of simulation which was very high for the case of 3000µm (about 1 day).

In a second step, the probe/sample system is considered. In this step a parametric study was done to define the thickness of sample. The same strategy was used. We varied the thickness of a silicon sample from 300µm to 1000µm. The heat flux dissipated from the platinum rhodium wire into the sample was calculated for each thickness. The results are presented in figure 9. It is observed that the heat flux starts to be stable starting 800 µm which is the value considered for the modelling.

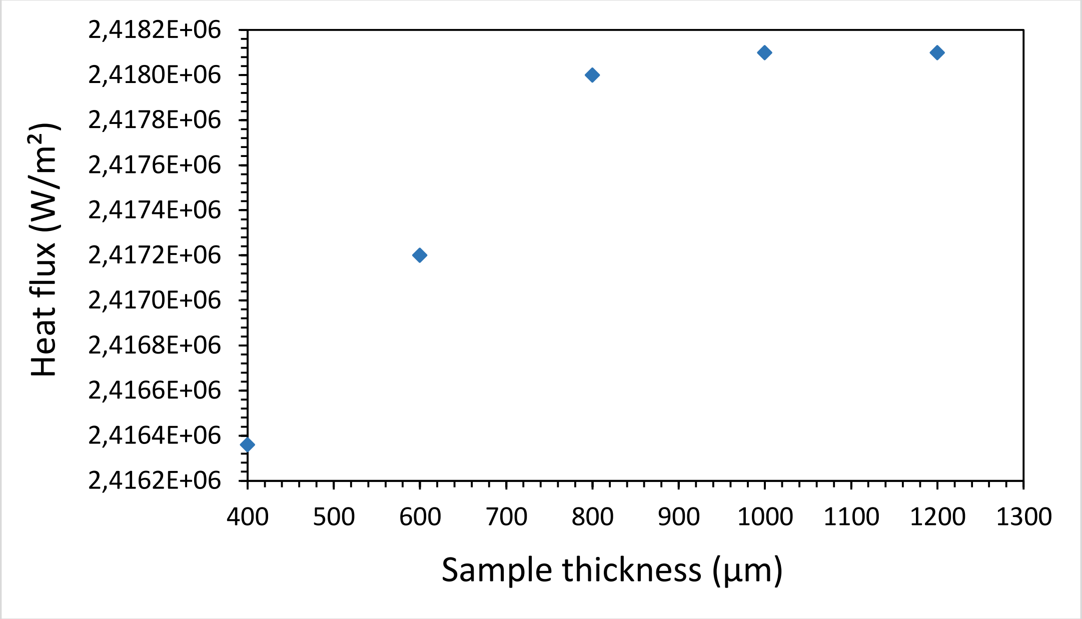

Figure 2- 8: Heat flux of the platinum-rhodium wire versus the silicon sample thickness.

2.2. Hypothesis of air convection considered for the modelling

When the probe is out of contact, the heat transfer mechanism for a heated cantilever by Joule effect in ambient air can be presented by heat losses due to convection, by thermal radiation along the Pt-Rh wire and by thermal conduction through the wire. Previous works showed that the heat transfer through radiation is negligible for the Wollaston probe [11, 12]. We take into account this hypothesis for the usual temperature lower than 200 °C.

Previous studies considered the surrounding medium between the probe and the sample is a motion less and the air surrounding the probe is simply diffusive [3, 11]. Therefore, the environment was represented by a medium having the same thermal properties of air. However Gomes *et al.* showed that the surrounding medium of the probe is heated at large distances which can creates a convective phenomenon of air environment [13]. The heat transfer by natural convection is the description of a fluid movement generated by the gravity forces of due to the variation of the density with respect to the temperature. The change in density creates a movement through Buoyancy forces. The heat transfer by convection is influenced by the thermal conductivity of the surrounding medium.

The particularity of this work relies on the fact that natural convection of the surrounding is considered. Therefore the environment box was filled with air of a thermal conductivity $k_{air} = 0.027\, W.m^{-1}.K^{-1}$ for 295 K. In our modelling we implement in COMSOL the equations of laminar flow that allows the movement in the surrounding medium [equations (21) and (22)]. The movement of air must be defined by choosing the right boundary conditions applied on the geometry. In the next paragraph we will detail the boundary conditions applied to our geometry.

2.3. Boundary conditions

A proper modelling requires a good choice of boundary conditions. The pertinence of the results is related to this choice. For the probe/sample system the boundary conditions are the same as explained in the previous section (1.3.1) with adding the boundary conditions related to the flow.

The lateral surfaces of box that define the sample and the environment are considered as inlets. The upper surfaces of box defining the surrounding medium are considered as outlets. The velocity at normal to the inlets boundaries was set to 1 m/s. The pressure for the outflow is the atmospheric pressure.

2.4. Validation of the model

The developed model can be used to study the probe response as a function of the distance between the probe and the sample. This study will allow to point out the choice of the air convection assumption considered for the probe/sample system. The model is used to evaluate the probe response in DC operation mode. Figure 2-9 represents the evolution of probe response during the approach of probe toward a sample with a current of 50 mA at atmospheric pressure. The inclination of the probe is fixed at 60 degree with respect to the horizontal. The sample is made of copper. The quantity depicted in the graph is a normalized value of the voltage defined as:

$$\frac{V_{3\omega}(d) - V_{3\omega min}}{V_{3\omega max} - V_{3\omega min}} \tag{26}$$

Where $V_{3\omega}(d)$ represents the thermal response as function of distance, $V_{3\omega min}$ is the value just before the contact and $V_{3\omega max}$ represents the response when the probe is far away from the sample where there is no interaction between the probe and the sample. As shown in figure2-9the rise of normalized amplitude is at its maximum between distances of 1 and 100 µm. Three different regimes of heat transfer are observed: (1) for distances ranging between 1 and 20 µm a diffusive regime governs the heat transfer mechanism, (2) an intermediate regime is observed for distances between 0.5 and 1 µm and (3) a linear rise is noticed for distances less than 0.5 µm.

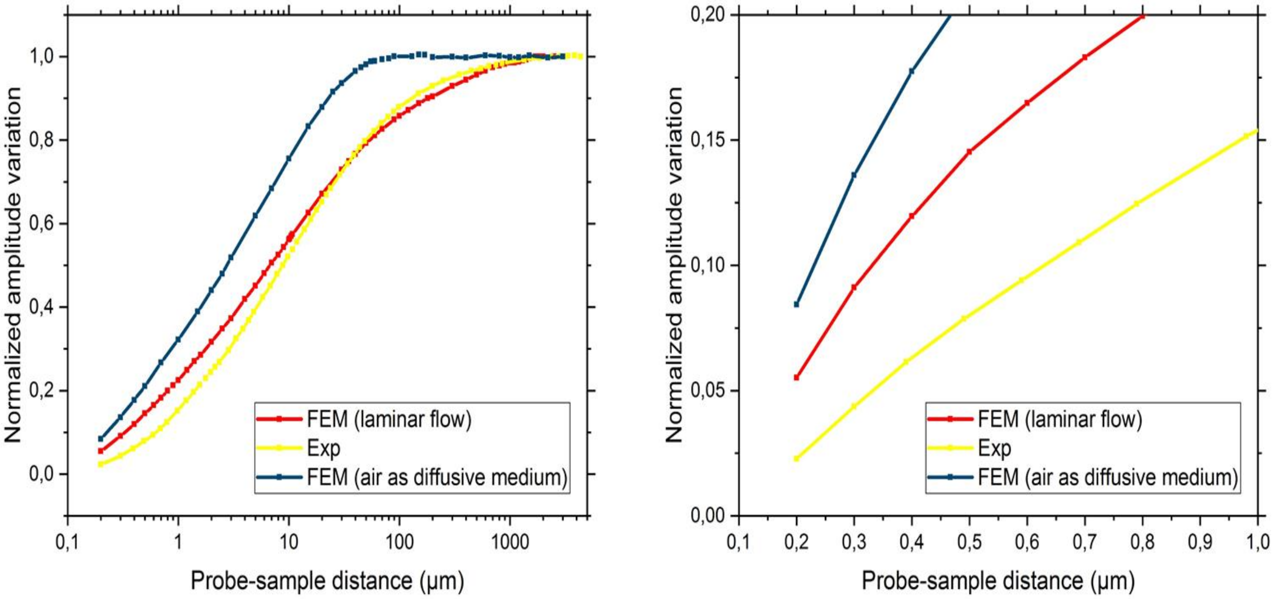

Figure 2- 9: a)Comparison between experimental and FEM results of the normalized amplitude variation versus probe/sample distance while approaching toward a sample of copper and b) zoom for distances below 1 µm.

The normalized amplitude obtained by modelling was compared to data obtained by O. Raphael by FEM where he considered the surrounding medium as diffusive one [3]. Both results were compared to experimental data performed under ambient conditions in the DC operating mode with a current of 50 mA. As observed in figure 2-9a, our FEM results are relatively close to experimental data. For distances lower than 1 µm our FEM gives closer results to experimental one. For distances between 1 and 10 µm our FEM results have the same tendency as experimental ones and they are relatively close, unlike FEM obtained considering air as a diffusive medium. For distances between 10 µm and 100 µm we observe a good agreement with experimental data, while FEM results obtained for diffusive air overestimates experimental results. For distances between 1µm and 0.5 µm an intermediate regime is observed for both FEM results (figure 2-9b) and a linear rise takes place for distances less than 0.5 µm. Several hypotheses can be announced for the interpretation of results. Considering the surrounding medium as moving air is more reliable for distances higher than 10 µm. For lower distances another mechanism tends to oppose the heat exchanged between the probe and the sample as seen in figure 9-2b. It was showed that Raphael's modelling worked well when performing simulations in the AC mode unlike the DC one. In fact when working with DC mode the probe response is more sensitive to boundary conditions and to the surrounding medium. In our modelling, taking into account the medium as moving air improved results of simulations.

3. Approach of measurements in contact for the platinum-rhodium wire

When the probe is in contact with a sample surface, the heat flux dissipated to the sample is ensured through thermal convection and conduction. In this case the total heat flux dissipated by the probe Q_{pc}(W) when the probe is in contact can be written as:

$$Q_{pc} = Q_{conv} + Q_W + Q_s \tag{27}$$

Where:

Q_{conv} is the heat flux dissipated from the Pt-Rh wire by convection when the probe is in contact

Q_W is the heat flux dissipated from the Wollaston wire when the probe is in contact

Q_s is the heat flux dissipated from the probe into the sample

When the probe is out on contact, the total heat flux dissipated from the probe Q_{pa}(W) can be written as:

$$Q_{pa} = Q'_{conv} + Q'_W \tag{28}$$

Where:

Q'_{conv} and Q'_{W} are respectively the heat flux dissipated from the Pt-Rh wire by convection and the heat flux dissipated from the Wollaston wire when the probe is out of contact.

From those equations, the power needed to maintain the temperature of probe constant can be written as:

$$\Delta P = Q_{pc} - Q_{pa} \tag{29}$$

The developed model was used in order to calculate the power dissipated from the thermal probe. When the probe is out of contact, the numerical model gives a direct access to the power dissipated from the Pt-Rh wire into the environment and the power dissipated from the Wollaston wire. Thus the total power $P_a = Q_{pa}$ of probe out of contact can be calculated. When the probe is in contact, the power dissipated from the Pt-Rh wire into the sample, from the Pt-Rh wire by convection and the power dissipated into the Wollaston wire can be also directly evaluated. This enables calculating the total power $P_c = Q_{pc}$when the probe is in contact with the sample. The difference between total heat fluxes dissipated when the probe is in contact and out of contact allows determining ΔP which can be written as:

$$\Delta P = P_c - P_a \tag{30}$$

The expression of $\frac{\Delta P}{P_a} = \frac{P_c - P_a}{P_a}$ will be used for measurement of the effective thermal conductivity of bulk samples which is known as calibration curves. This consists on evaluating the heat flow dissipated in samples with known thermal conductivities to relate the electrical power lost by the probe to thermal conductivity. For this study, seven samples were used: PMMA, Mn, SiO_2, Ti, Ta, Si and Cu. Thermal properties used for these samples are given in table 2-3.

Table 2- 3: Thermal properties of materials used for calibration curves by modelling.

	Thermal conductivity $W.m^{-1}.K^{-1}$	Heat capacity $J.Kg^{-1}.K^{-1}$	Density $Kg.m^{-3}$
Acrylic (PMMA)	0.19	1464	1180
Manganese (Mn)	7	481	7400
Silicon dioxide (SiO_2)	1.46	745	2200
Titanium (Ti)	19	523	4500
Tantalum (Ta)	56	138	16600
Silicon (Si)	147	700	2329
Copper (Cu)	400	385	8960

Figure 2-10 shows the curve of $\Delta P/P_a$ versus sample thermal conductivity for different currents (35 mA and 50 mA).For a probe temperature of 100 °C (50 mA); values of $\Delta P/P_a$ vary from 0 to 0.45. As observed, the normalized power transfer $\Delta P/P_a$ increases with increasing the thermal conductivity of the bulk samples. When the probe temperature decreases to 70°C (35 mA), $\Delta P/P_a$ decreases. Thus the decrease in probe temperature leads to a decrease in heat fluxes exchanged between the probe and the sample therefore $\Delta P/P$ increases. In this case values of $\Delta P/P$ varies between 0and 0.35.

For both curves, the value of $\Delta P/P_a$ tends to a constant value when the sample considered has a thermal conductivity higher than $20W.m^{-1}.K^{-1}$. That means that the thermal probe starts to lose its sensitivity. Thus the Wollaston probe is sensitive to materials having thermal conductivities up to $20W.m^{-1}.K^{-1}$

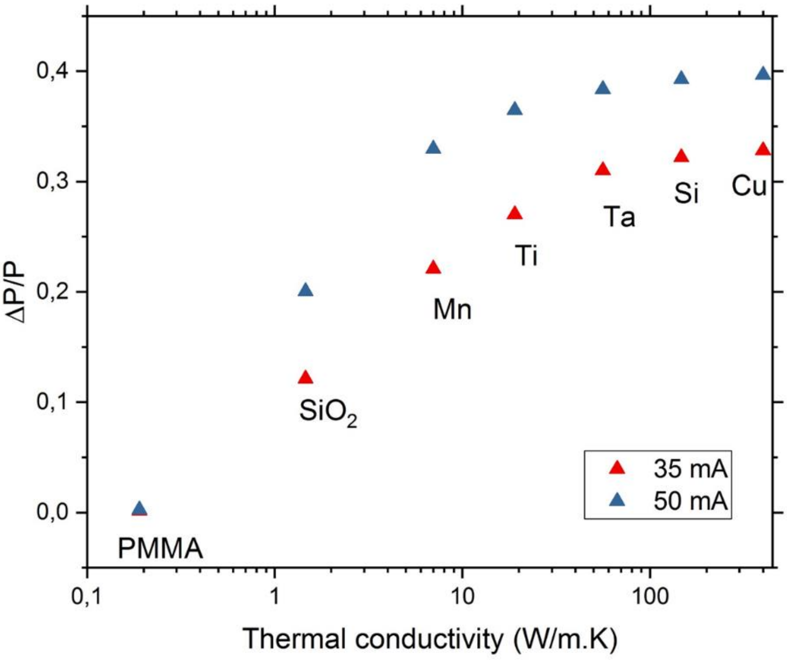

Figure 2- 10: Variation of probe Joule power relative difference predicted by FEM as a function of thermal conduvctivities under ambient conditions for DC operating mode with a current of 35 mA and 50 mA.

Those results were compared to experimental data obtained with a set of samples composed of PMMA, Ceramic, Ti90Al6V4, Ti, Ta and Zn. Table 4 summarizes thermal conductivities considered for those samples which was validated by the ‘Laboratoire national de métrologie et d'essais (LNE). This work was done in the frame of collaborative work between URCA and LNE prior to QuantiHeat project.

Table 2- 4: Thermal conductivities for calibration samples as given and validated by the national laboratory of metrology (LNE).

Samples	PMMA	Ceramic	$Ti_{90}Al_6V_4$	Ti	Ta	Zn
Thermal conductivity $W.m^{-1}.K^{-1}$	0.332	1.61	6.5	19	56.2	115

Figure 2-11 illustrates the curve of $\Delta P/P_a$ obtained experimentally in ambient air for a probe mean temperature of 70°C. The experimental values are slightly lower than modelling values. This can be explained with the fact that a perfect contact was considered between the probe and the sample in FEM simulations which is not the real case for experiments. As seen, the value of $\Delta P/P_a$ increases with the thermal conductivity of the sample and has the same tendency as for the modelling. The values tend to a constant value for thermal conductivities higher than 20 $W.m^{-1}.K^{-1}$ which is in the same order of the platinum-rhodium wire thermal conductivity.

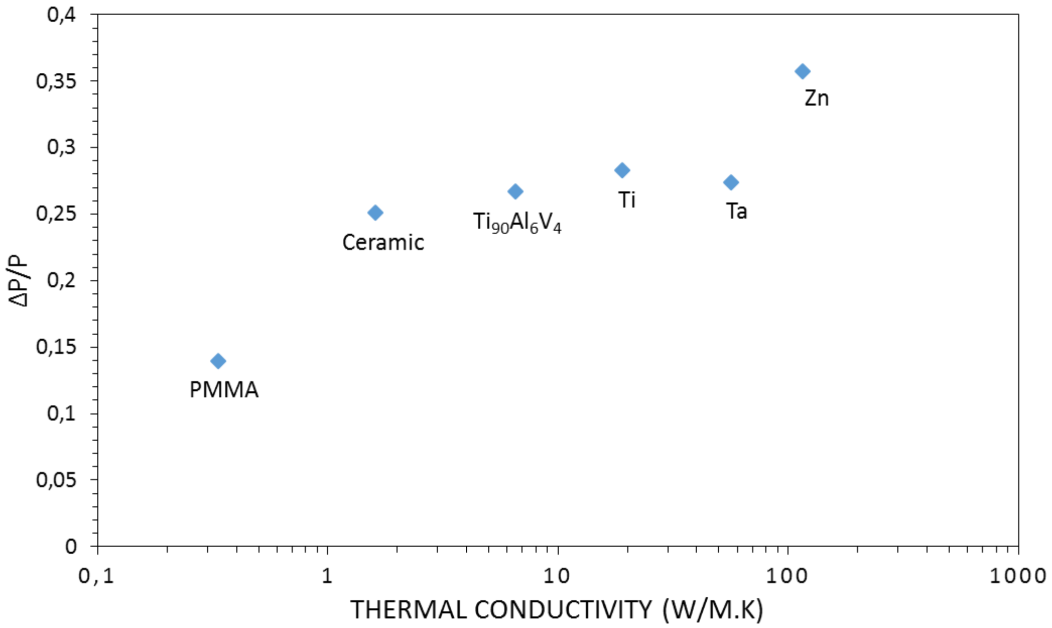

Figure 2- 11: Variation of probe Joule power relative difference experimentally as a function ofsample thermal conductivities under ambient conditions for DC operating mode with a current of 35 mA.

4. Evaluation of total thermal conductance

Mechanisms by which the heat is transferred from the thermal probe to the sample conditions the total thermal conductance. When the probe is out of contact with the sample, under ambient conditions, the heat is ensured by conduction through air. Once the probe gets into contact with the sample, the solid-solid contact and the conduction by water meniscus are added to heat transfer mechanisms between the probe and the sample. According to previous studies, the water meniscus disappears for probe mean temperatures higher than 150°C [14].

Thus the total thermal conductance of water meniscus tends to zero for probe mean temperature higher than 150°C. The total conductance of the probe/sample system $G_{th}$is given by the expression:

$G_{th} = \frac{1}{R_{th}}$with $R_{th} = \frac{\Delta T}{Q}$.

Where R_{th} is the thermal resistance, Q is the total heat flux dissipated by the platinum-rhodium wire into the sample and ΔT is the difference between the temperature of the probe apex at the contact and the sample temperature.

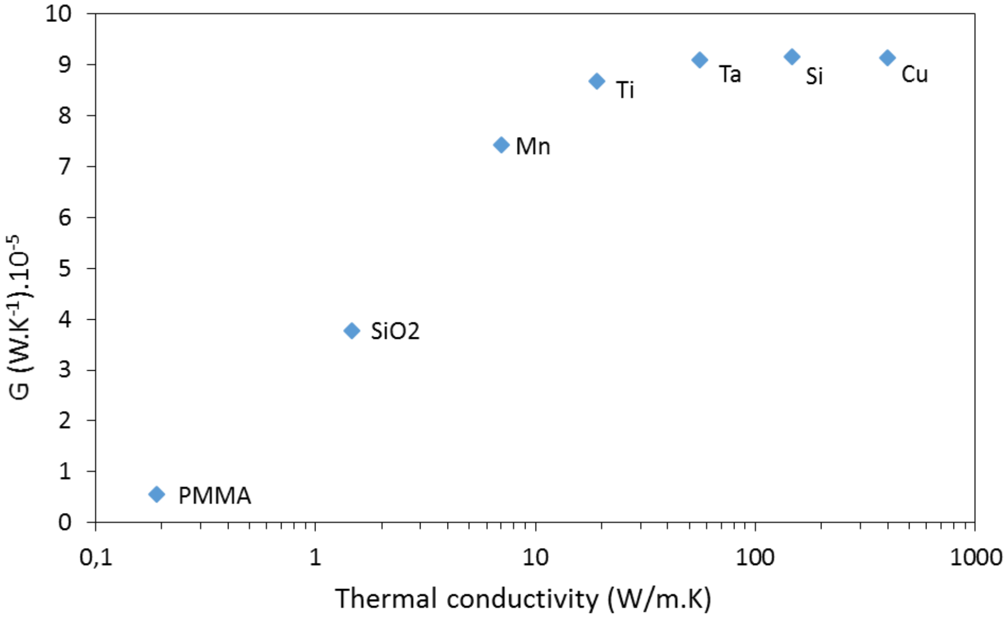

Figure 2- 12: Overall thermal conductance by modelling as a function of material's thermal conductivities.

Figure 2-12 represents results of the total thermal conductance as a function of the thermal conductivity for the samples used in the previous section. The overall thermal conductance increases with increasing the sample thermal conductivity. As observed the curve tends to a constant value for thermal conductivities higher than $50W.m^{-1}.K^{-1}$.This thermal conductivity corresponds to the order of platinum-rhodium wire thermal conductivity. In works done by Mujumdar [15], he proved that the total thermal conductance increases with increasing the thermal conductivity of the material. Many works evaluated the thermal conductance at the contact between the probe and the sample [16, 17, 18, 19].Gostmann *et al.*

performed measurements under vacuum with a silicon tip in contact with a thin film of tetrahedral amorphous carbon over a silicon substrate. They evaluated experimentally and by modelling the thermal contact between the tip and a sample of tetrahedral amorphous carbon over a silicon substrate which is about $10^{-7} W.K^{-1}$ [16]. Nelson et *al.* used a heated silicon micro cantilever in contact with thin film of polystyrene to evaluate experimentally the thermal contact resistance between the probe and sample. They estimated a value to be ~ $10^{7} K.W^{-1}$ which is in the same order of magnitude found in previous works [18]. Wilson *et al.* evaluated the thermal contact resistance by modelling between a Wollaston probe and a bulk sample with a thermal conductivity of $54\, W.K^{-1}.m^{-1}$, they found a value about $4.10^{-4} W.K^{-1}$ [17]. Lefevre *et al.* used an analytical model to evaluate the thermal contact conductance between a Wollaston probe and samples with different samples. He found that values ranged between $4.6 - 6.10^{-6} W.K^{-1}$depending on sample's thermal conductivity.

As noticed in our study the overall thermal conductance evaluated by modelling varies between $0.5 - 9.3\ 10^{-5} W.K^{-1}$depending sample's thermal conductivity. Those values are one order of magnitude less than that found by Lefevre but one order of magnitude higher than the value found by Wilson. This can be explained by the difference in modelling methods and how this quantity is evaluated.

5. Conclusion

In this chapter, we have presented a 3D model of the probe/sample system by COMSOL Multiphysics based on finite element simulation. The probe/sample system was modelled with its surrounding medium in and out of contact with the sample. First, we built a model for the probe holder in order to determine an equivalent heat exchange coefficient to the environment about $84000\, W.m^{-2}.K^{-1}$. This value was used for whole probe modelling. This coefficient was over estimated in previous works ($100000\, W.m^{-2}.K^{-1}$).

We then studied the evolution of the probe's response as a function of probe/sample distance by taking into account the hypothesis of natural air convection of the surrounding environment. Our results show a good agreement with experimental data. Thus the role of convection phenomenon is highlighted in the heat transfer mechanisms between the probe and the sample.

In order to validate our hypothesis we calculated the variation of the probe Joule power relative difference as a function of thermal conduvctivities. This was found to be coherent with experimental data. Moreover the total thermal conductance of the probe/sample system was calculated for materials with known thermal conductivities. The order of magnitude found for the total thermal conductance is in the range as given in the literature.

The following chapter deals with applications of the developed model on nanostructured materials. This will be done in order to present a methodology for the characterization of Wollaston probes.

6. References

[1] J.H Lienhard IV, J.H Lienhard V, A Heat Transfer Textbook, third edition, Cambridge, Massachesettes, U.S.A. (2001).

[2] L. Sainsaulieu, Calcul scientifique, 2nd edition Dunod, Paris (2000)

[3] O. Raphael, Contribution à la microscopie thermique à sonde locale en mode alternative : Caractérisation de la réponse et de l'interaction sonde échantillon. PhD thesis in Reims University, (2008)

[4] S. Lefevre, S. Voltz, J.B Saulnier, C. Fuentes, N. Trannoy, Thermal conductivity calibration for hot wire based dc scanning thermal microscopy, Review of Scientific Instruments 74 , 2418 (2003)

[5] N. Trannoy, J-F Henry, Investigation of thermal resistive probe behaviour used in Scanning Thermal Microscope by infrared imaging system. QIRT Journal (5) 27-44 2(008)

[6] S. Gomes, contribution théorique et expérimentale à la microscopie thermique à sonde locale: calibration d'une pointe thermorésistive, analyse des divers couplages thermiques, PhD thesis in Reims university, (1999)

[7] ISO 7730: 2005, Ergonomie des ambiances thermiques -- Détermination analytique et interprétation du confort thermique par le calcul des indices PMV et PPD et par des critères de confort thermique local, 2005.

[8] S. Gomès, N. Trannoy, P. Grossel, DC thermal microscopy: Study of the thermal exchange between a probe and a sample, Meas. Sci. Technol.(10) 805–811, (1999).

[9] M. Massoud, Experimental characterization of heat transfer in nanostructured silicon based materials, PhD thesis in Lyon University, (2016)

[10] A. Assy, Development of two techniques for thermal characterization of materials: Scanning Thermal Microscopy (SThM) and 2ω method, PhD thesis in Lyon Univesity (2015)

[11]K Kim, W.P. King, Thermal conduction between a heated microcantilever and a surrounding air environment, Applied thermal engineering (29),1631-1641, (2009).

[12] Xu J.B., Läuger K., Möller R., Dransfeld K., Wilson I.H., Heat transfer between two metallic surfaces at small distances, J. Appl. Phys. 76 (11) 7209–7216, (1994)

[13] S.Gomes, N.Trannoy, D.C. scanning thermal microscopy: Characterisation and interpretation of the measurement, Int. J. Therm. Sci. (40), 949–958, (2001).

[14] A.Assy, S. Lefèvre, P.O.Chapuis and S. Gomès,Analysis of heat transfer in the water meniscus atthe tip-sample contact in scanning thermal microscopy, Journal of Applied Physics D, 47, (2014)

[15] Majumdar A., Scanning thermal microscopy, Ann. Rev. Sci. (29), 505–585, (1999).

[16] B. Gotsmann and M. A. Lantz Quantized thermal transport across contacts of rough surfaces, Nature Materials (12), 59–65 (2013).

[17] Wilson AA, Muñoz Rojo M, Abad B, Perez JA, Maiz J, Schomacker J, Martín-Gonzalez M, Borca-Tasciuc DA, Borca-TasciucT.,Thermal conductivity measurements of high and low thermal conductivity films using a scanning hot probe method in the 3ω mode and novel calibration strategies, Nanoscale.(37), (2015).

[18] B. A. Nelson and W. P. KingMeasuring material softening with nanoscale spatial resolution using heated silicon probes, Review of Scientific Instruments, 78 (2007)

[19] Pettes M T, A reexamination of phonon transport through a nanoscale point contact in vacuum J. Heat Transfer (136) 32401, (2014).

[20] Park K, Cross G L, Zhang Z M and King W P, Experimental investigation on the heat transfer between a heated microcantilever and a substrate J. Heat Transfer (130) 102401–9, (2008).

[21] A.Assy and S. Gomès, Heat transfer at nanoscale contacts investigated with scanning thermal microscopy Appl. Phys.Lett. 107 43105, (2015)

Résumé du chapitre 3

Le travail présenté dans le chapitre 3 se situe dans le cadre du projet européen QuantiHeat qui a pour objectif de traiter les problèmes liés à la métrologie thermique aux échelles nanométriques. Notre équipe était impliquée et s'intéressait particulièrement à l'utilisation la microscopie à sonde locale avec la sonde Wollaston pour aborder ce problème. Deux échantillons ont été proposés par l'URCA dans le but d'étudier le signal thermique obtenu par la sonde thermique en Wollaston. L'échantillon a été fabriqué par l'institut VTT de Finlande. Il est composé de structures du silicium ayant une forme pyramidale formée des marches de différentes largeurs (100 nm, 200 nm, 300 nm et 400 nm) sous une couche de dioxyde de silicium déposées sur un substrat de silicium. Des mesures topographiques et thermiques ont été réalisées sur la surface de l'échantillon. Les mesures topographiques ont été réalisées par une sonde KNT et montrent que l'échantillon a une rugosité assez importante qui influence sur les résultats.

Les mesures thermiques ont été réalisées par une sonde en Wollaston sur différentes zones contenant des marches de même largeur. Les résultats montrent que la sonde en Wollaston est sensible aux structures internes de l'échantillon, mais qu'elle n'est pas capable de distinguer les différentes marches. Vue la rugosité de l'échantillon et la difficulté dans l'interprétation des résultats, nous avons proposé une amélioration de la structure de l'échantillon. Un nouvel échantillon a été donc développé par VTT pour la poursuite de l'étude.

Le nouvel échantillon est composé des marches de silicium ayant des largeurs de 600 nm, 1 µm et 2 µm, sous une couche de dioxyde de silicium déposée sur un substrat de silicium. L'avantage de cet échantillon réside dans le fait qu'il permet d'avoir le même contact en balayant sa surface. Des mesures par SThM ont été réalisées. Des images accompagnées des profils thermiques montrent que la sonde est sensible à la structure interne de l'échantillon et permet de distinguer uniquement les marches de 1 µm et 2 µm.

Dans le but d'interpréter plus en détail le signal thermique obtenu par la sonde, un modèle numérique a été développé pour le système sonde/échantillon. Le modèle est basé sur celui de la sonde développé dans le chapitre 2 associé à un modèle 3D pour l'échantillon. Il est composé de 6 marches en Si (260 nm d'épaisseur chacune) sous une couche de SiO_2déposésur un substrat de silicium. L'épaisseur maximale de SiO_2 (qui couvre la dernière marche) est de 2 µm. Deux géométries ont été développées, une pour les marches ayant une largeur de 1 µm et l'autre pour celles de 2 µm. Les mesures ont été effectuées pour différentes positions de la sonde sur la surface de l'échantillon. Les cartographies de température pour une largeur de marche de 2 µm ont été présentées. Elles montrent que la distribution du flux de chaleur est influencée par la présence des marches jusqu'à la 5ème marche. Un modèle formé du film mince de SiO_2 déposé sur un substrat de silicium a été développé afin de comparer le comportement de la sonde en l'absence des structures internes. Le modèle numérique permet de calculer le flux de chaleur dissipée par la sonde dans l'échantillon pour les différentes positions de la sonde (correspondant aux différentes épaisseurs de SiO_2). Ces flux ont été calculés pour les 3 géométries développées. Les résultats montrent que la sonde thermique est sensible à la présence des structures internes jusqu'à une profondeur de SiO_2 de 1,3 µm. Au-delà de cette épaisseur, les flux de chaleur pour les 3 géométries tendent vers la valeur de flux lorsqu'elle est en contact avec un échantillon de SiO_2 massif, ce qui signifie que le silicium n'intervient plus dans la mesure. Le ratio de flux de chaleur dissipée par la sonde thermique vers l'échantillon nanostructuré sur celui dissipé vers l'échantillon du film mince sur substrat a été calculée pour les marches de 1 µm et 2 µm. Les résultats montrent que la sonde n'est pas seulement sensible en profondeur mais qu'elle est aussi sensible à la largeur des marches.

Dans le but de comparer les résultats expérimentaux et issus de la modélisation, le signal thermique obtenu par la sonde a été reproduit par simulation pour la première marche. Pour cela, des simulations ont été faites pour plusieurs positions de la sonde sur la surface de l'échantillon. Les résultats montrent que, lors d'un scan, le signal thermique commence à diminuer avant même que la sonde atteigne le bord de la marche. Ce comportement a été observé expérimentalement et par simulation. Ce qui signifie que le signal thermique ne correspond pas à un profil de géométrie interne mais à un volume sondé. Cet échantillon nanostructuré a été utilisé pour déterminer le rayon d'échange thermique b par simulation. Ce rayon a été évalué pour deux positions différentes de la sonde. Les résultats obtenus donnent une valeur de 890 nm lorsque la sonde est placée au-dessus de la première marche, et une valeur de 2.2 µm lorsque la sonde est placée à la 5eme marche.

Un échantillon nanostructuré formé d'une interface oblique de Si/SiO_2 a été aussi étudié. Des images thermiques et topographiques sont obtenues par SThM sous condition atmosphérique. Un modèle a été développé avec les dimensions réelles de cet échantillon. Le signal thermique de la réponse de la sonde est reproduit par simulation et comparé aux résultats expérimentaux. Les résultats montrent que le signal obtenu par la sonde correspond à un volume contenant la structure interne de l'échantillon.

La dernière partie de ce chapitre consiste à étudier les particules de polymère par SThM dans le but d'évaluer leur conductivité thermique effective. Les polymères sont des particules de 30 µm de diamètre enrobées d'une épaisseur d'argent (60 nm, 100 nm, 150 nm ou 270 nm). Les résultats montrent que les particules de polymère sans une matrice ne sont pas adaptées aux mesures par la méthode de SThM. Par conséquent, nous avons proposé de fixer les particules à l'aide d'une matrice. Le nouvel échantillon est composé des polymères de 30 µm de diamètre enrobés de 150 nm d'argent placé dans une matrice adhésive. Les profils thermiques obtenus par SThM présentent une tendance sphérique qui semble similaire à la forme des polymères. L'interprétation des résultats donnent une conductivité thermique locale qui varie entre 1.5 et $27 W.m^{-1}.K^{-1}$.

Chapter 3: Investigation of nanostructured materials with Wollaston probe

The miniaturization of electronic devices requires a good understanding and management of heat distribution in nanoscale structures. Scanning thermal microscopy (SThM) was proven suitable to this issue for its ability to measure and manipulate local thermal heat. It’s a probing technique that enables mapping simultaneously topographic and thermal images.

As seen in chapter 2, well-defined probe/sample geometry was modeled using software based on finite element method. The validation of this modelling was proven by presenting comparison between experimental and simulation results for i) the probe’s response while approaching toward a sample of copper and ii) calibration curves. In this chapter, we present a methodology to characterize SThM probe using the numerical model developed in chapter 2. This work is in the frame of QuantiHeat project

A good knowledge of SThM requires a full interpretation of the probe thermal signal. To date many methods have been developed in order to calibrate SThM probes [1-3]. But a reliable characterization requires a well-known sample. Therefore, a nanostructured sample composed of silicon buried structures covered with silicon dioxide was proposed and fabricated specifically for this study. A realistic model of the sample was developed and studied while the probe is in contact with the sample. The modelling allowed to evaluate heat fluxes of the probe-sample system which permits to reproduce the probe thermal signal for comparison with experimental results.

1. Thermal investigation of nanostructured materials

1.1. Sample presentation

In the frame of QuantiHeat project, we have proposed a design of a sample dedicated to study the signal obtained by the thermal probe in scanning thermal microscopy. This design was taken into consideration in the frame of QuantiHeat project, fabricated and provided by VTT (Valtion teknillinen tutkimuskeskus) from Finland. The aim of this study is to test STHM's capability to distinguish buried features, to characterize and estimate the effect of probe volume on the thermal measurement, and finally to reveal the change in thermal signal according to the depth of buried features.

The sample is composed of silicon steps with different width buried under silicon dioxide and deposited on a silicon substrate. Since the sample is covered by a silicon dioxide thin film, we suppose that it has the same contact while scanning along its surface. This makes easier the interpretation of thermal measurements between the probe and the sample. In the literature few works studied the capability of the Wollaston probe to perform subsurface imaging [4, 5]. A Hammiche *et al.* performed sub-surface imaging of metallic particles in a polymer matrix; they achieved a depth detection of few microns and a spatial resolution of a micron [4]. But no previous works investigated the signal obtained by the thermal probe when scanning along a sample surface with embedded structures. In the following, we present experimental measurements performed by SThM and AFM for this sample.

1.2. First set of samples

1.2.1. Topography measurements

The first set is composed of 3×3 devices of Silicon with pyramidal shapes spaced by 1020 µm under polished SiO_2. The Si structure has 5 steps with different step length of 100, 200, 300 and 400 nm. Figure 1 illustrates a SEM cross-cut image and an illustration of the sample. Steps have approximatively same heights of 115 nm covered of 100 nm of SiO_2

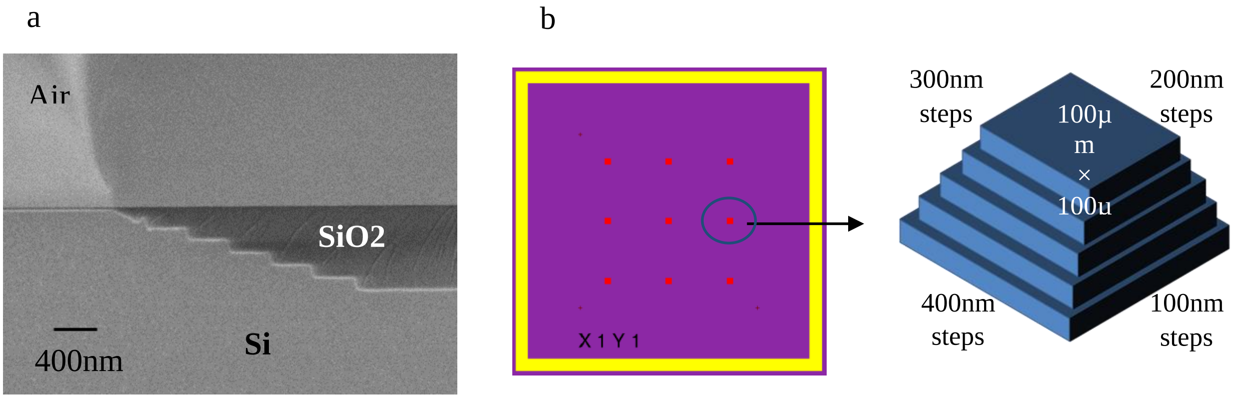

Figure 3- 1:a) SEM cross-cut image of the sample showing Silicon steps buried under Silicon dioxide (from VTT) b) Structure of sample showing nine pyramidal shapes created on a silicon substrate with a zoom of the structure showing different steps.

Atomic force microscopy is a powerful tool to study the sample surface topography. It uses a sharp tip with less than 100 nm in diameter to scan across the sample surface. When the tip approaches to the sample surface, an attractive force between the tip and the sample cause the deflection of the cantilever towards the surface. When the cantilever is brought very close to the surface, a huge repulsive force takes place and causes the deflection of cantilever away from the surface. This technique gives an image of 3D surface profile with a resolution depending on the used probe. Those kinds of images provide nanoscale information on sample surface including defects and roughness [6]. When scanning along the sample surface, the presence of dust or manufacturing defects is revealed on the topographic image.

Topography measurements were done for different step widths using palladium probes in order to obtain topography profiles. Those kinds of probes have a spatial resolution in the order of few nanometers [3]. The measurements were performed on different squares of the X1Y1 area as represented in figure 1b. Topography image and profile obtained for a side of 400 nm step width of a specific square are presented in figure 3-2.

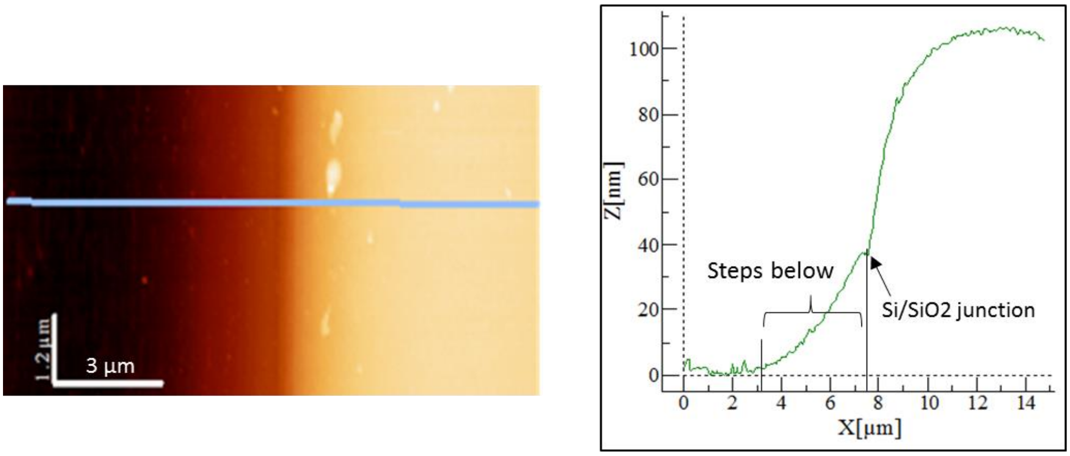

Figure 3- 2: 15×15 µm Topography image and its corresponding line profile obtained for a side of 400 nm step width.

A clear contrast is observed on the topographic image showing that the surface is not plane. The darkest part corresponds to Silicon and the brightest part to Silicon dioxide. The topography variation observed in the topographic profile is of 105 nm along 8 µm, where a variation of 37 nm is seen for the silicon over 4.5 µm and for silicon dioxide a variation of 68 nm is detected on 2.5 µm. Since steps are of 400 nm width, than 5 steps should be over a distance of 2µm which is seen on the topographic profile. Measurements were done for all sides of the square which means for the step width of 100, 200 and 300 nm. They showed that steps correspond probably to the variation of the signal when the probe scans over SiO_2.Measurements of roughness were done for different squares of the sample and for different step width. They showed that depending on the measured area, the sample has a root mean square average (RMS) roughness higher than 70 nm. This value is considered quiet high and doesn't allow a good interpretation of measurements. Table 3-1 summarizes the roughness obtained for this specific square. The RMS of silicon for 200 nm step width is 58 nm which is considered high and can influence measurements while performing scans over the sample surface. For the 400 nm and 100 nm the roughness is respectively 30 nm and 37 nm which are lower than for the case of 200 nm but those values are still considered high and may have their influence when performing thermal measurements with SThM. The following section presents SThM imaging performed for this square.

Table 3- 1: RMS (root mean square average) and the Ra (arithmetic average) of the sample surface on a specific square for different step width: the silicon substrate (Si), the silicon dioxide (SiO_2) and the Si/SiO_2 junction.

Steps	**RMS (nm)**			**Ra (nm)**		
	Si	**SiO_2**	**Si/SiO_2**	**Si**	**SiO_2**	**Si/SiO_2**
400	30.79	36.26	33.32	27.67	34.76	30.82
200	58.65	31.01	38.8	55.42	25.53	32.23
100	37.05	67.92	46.66	31.76	66.02	40.14
300			20.34			15.98

1.2.2. Thermal measurements with Wollaston probe

Several measurements were made on the square of low roughness that was chosen to be studied. In the following we will present thermal images with their corresponding study of thermal profiles. Note that all measurements are done with active mode where the probe is simultaneously the heater and the sensor. Measurements were done using TopoMetrix commercially available microscope with Wollaston probes commercialized by Bruker. A corner of the square with step width of 100, 200, 300 and 400 nm was studied more specifically in the X1Y1 zone (figure 3-1b).

Figure 3-3 shows thermal images with their corresponding thermal and topographic profiles obtained under ambient conditions. The bright part of thermal image corresponds to more heat exchange and the dark one means that less heat in absorbed. The signal in z axis for the thermal profile corresponds to the thermal signal in Volt. As observed on the thermal profile the signal remains stable above Silicon steps and it suddenly drops when the probe scans above Si/SiO_2 junction, then the signal stabilizes when scanning above the SiO_2.

As discussed in the previous section, the 200 nm sides of the square have the highest roughness with a value of RMS equal to 58.65 nm. Figure 3-3b shows topographic and thermal line profiles obtained for the 200 nm step width. When comparing both profiles a correlation is observed between them, this may be linked to the high roughness obtained for this area. In the same image the topographic profile of 100 nm step width which has a roughness of 37 nm doesn’t seems to be correlated with the thermal profile. Figure 3-3c shows that topographic and thermal images seem to be correlated for 400 nm but not for 300 nm.

Our results showed that the thermal signal is sensitive to the presence of internal structures, but as seen steps are not distinguished on the thermal profile. This is probably due to the fact that step widths are too small and cannot be distinguished with this kind of probe. To aboard this issue, we proposed an improvement in the sample design with larger step widths and highest steps thickness. A new set of samples was developed for the pursuit of the study.

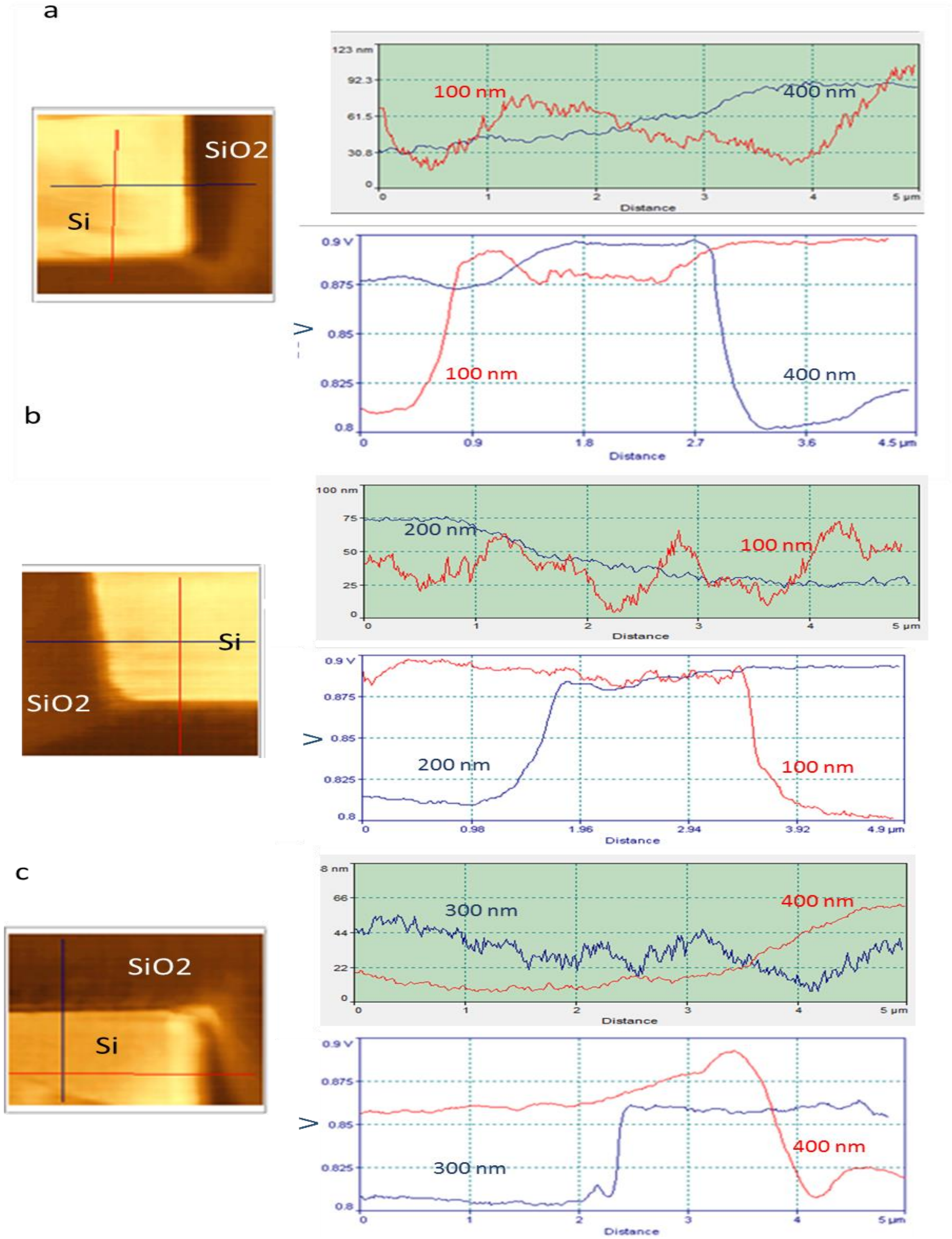

Figure 3- 3: a) 5×5 µm thermal (top left), topographic (top right) and thermal profiles (bottom) obtained for a corner of a square having steps of 100 nm (red curve) and 400 nm (blue curve) b) 5×5 µm thermal (top left), topographic (top right) and thermal profiles (bottom) obtained for a corner of a square having steps of 100 nm (red curve) and 200 nm (blue curve) c)) 5×5 µm thermal (top left), topographic (top right) and thermal profiles (bottom) obtained for a corner of a square having steps of 400 nm (red curve) and 300 nm (blue curve).

Measurements obtained with thermal conductivity contrast by SThM produce an image that is linked to the thermal transport properties while scanning across the sample surface. But the presence of artifacts (dust or fabrication defects) on the sample surface and surface roughness creates changing in the heat flux from the probe into the sample [7]. As seen in this section, the sample roughness influences SThM measurements.

During measurements it was hard to identify a square having low roughness. This sample suffers from practically high roughness (RMS 20 nm – 67 nm) which is induced in the data obtained for thermal and topographic image. To carefully interpret results obtained by SThM it is essential to eliminate these artifacts [8-10]. Therefore to aboard this issue a new fabrication procedure should be considered. In the coming section the new sample design will be presented.

1.3. Second set of samples

1.3.1. Sample fabrication

The second set of sample is composed of Silicon steps with 260 nm thicknesses covered with 200 nm of Silicon dioxide. Figure3-4 illustrates a deflection (DFL) image of the developed sample used in the present study. The sample is fabricated from a commercially available 150 mm bulk silicon wafer.

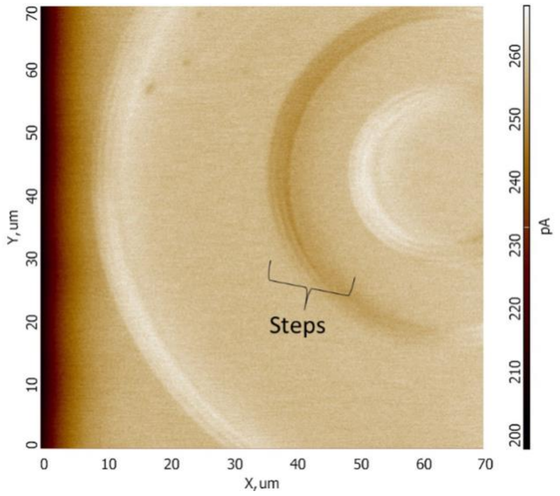

Figure 3- 4:DFL image of the sample displaying steps structure.

Fabrication protocol from information given by VTT:

In the first step of fabrication, 1 µm deep alignment marks were created on the wafer using contact photolithography and dry plasma etching in order to align the following lithography steps between them with high accuracy. Then, topological steps are realized in silicon. Each step is done with the same process with slightly modified mask. The first step mask is created by electron beam lithography. After that, the silicon is etched 260 nm in depth with chlorine based plasma and the resist is removed. This process is repeated 3 times with the same steps except for the electron beam lithography where with each following step the mask is reduced in different areas by different sizes with 300 nm, 600 nm, 1µm and 2µm step width with different step length. The step height was set to 260 nm. Once the steps are etched, a 2 µm thick LTO type silicon oxide is deposited in a furnace for low pressure chemical vapor deposition (LPCVD). Finally the sample surface is pressed by chemical physical planarization (CMP) in order to obtain a flat and smooth surface.

1.3.2. SThM thermal investigation

SThM imaging for micrometric measurements was performed under ambient conditions. Due to a breakdown in the AFM Explorer microscope, a new microscope commercialized by NT-MDT was used for measurements. We should note that the thermal control unit of the AFM Explorer was linked to the new microscope to allow comparison between measurements. Probes used for the first set of sample were manufactured by Bruker who stopped to fabricate them. Therefore we used probes manufactured by Czech metrology institute (CMI).All measurements were done in active mode for thermal conductivity mapping. The probe mean temperature during measurements is about 100°C in this study in order to avoid water meniscus [11].

Measurements were performed for steps width of 600 nm, 1µm and 2µm. Figures 3-5a and 5b represents respectively topographic image and profile of a region showing internal steps of 2µm step width. Figure 3-5c and 5d illustrates the corresponding thermal image and profile. The topographic profile shows a low surface roughness of 5 nm. The presence of steps is not detected on the topographic profile but they are clearly seen on the thermal one. Therefore this analysis shows that the thermal signal is not correlated with the topographic image. The thermal image reveals a clear contrast between the Silicon and the silicon dioxide (figure 3-5).The thermal conductivity of silicon steps are considerably higher than the silicon dioxide. This explains the change in the thermal signal when the probe scans over steps area. Thus the thermal signal decreases when the probe approaches to the silicon dioxide steps. Figures 3-5e and 5f represents respectively thermal image and profile for 1µm step width. As observed for steps of 2µm, the thermal probe is also sensitive to steps. We will show in the following that the thermal signal obtained corresponds to a scanned volume containing the steps.

Figure 3-5g and 5h illustrate the thermal image and its corresponding line profile for 600 nm step width. The thermal signal reveals a change when the probe scans over the steps but it is difficult to identify them on the thermal profile unlike the case of 1 µm and 2 µm step widths. The obtained thermal profile looks like the previous ones presented in figure 3-3.Hence, the probe seems too big to distinguish features of 600 nm. In this case, the thermal signal was only sensitive to presence of steps but couldn’t be distinguished on the thermal signal. Results showed that the probe is sensitive to the internal features down to 1µm. Therefore this kind of probe provides a lateral resolution above 600 nm and below 1 µm.

In order to investigate further the thermal signal obtained by the Wollaston probe, a 3D realistic model for the probe in contact with the sample was developed. The sample is modeled with its realistic geometry. The modelling is presented in the next section.

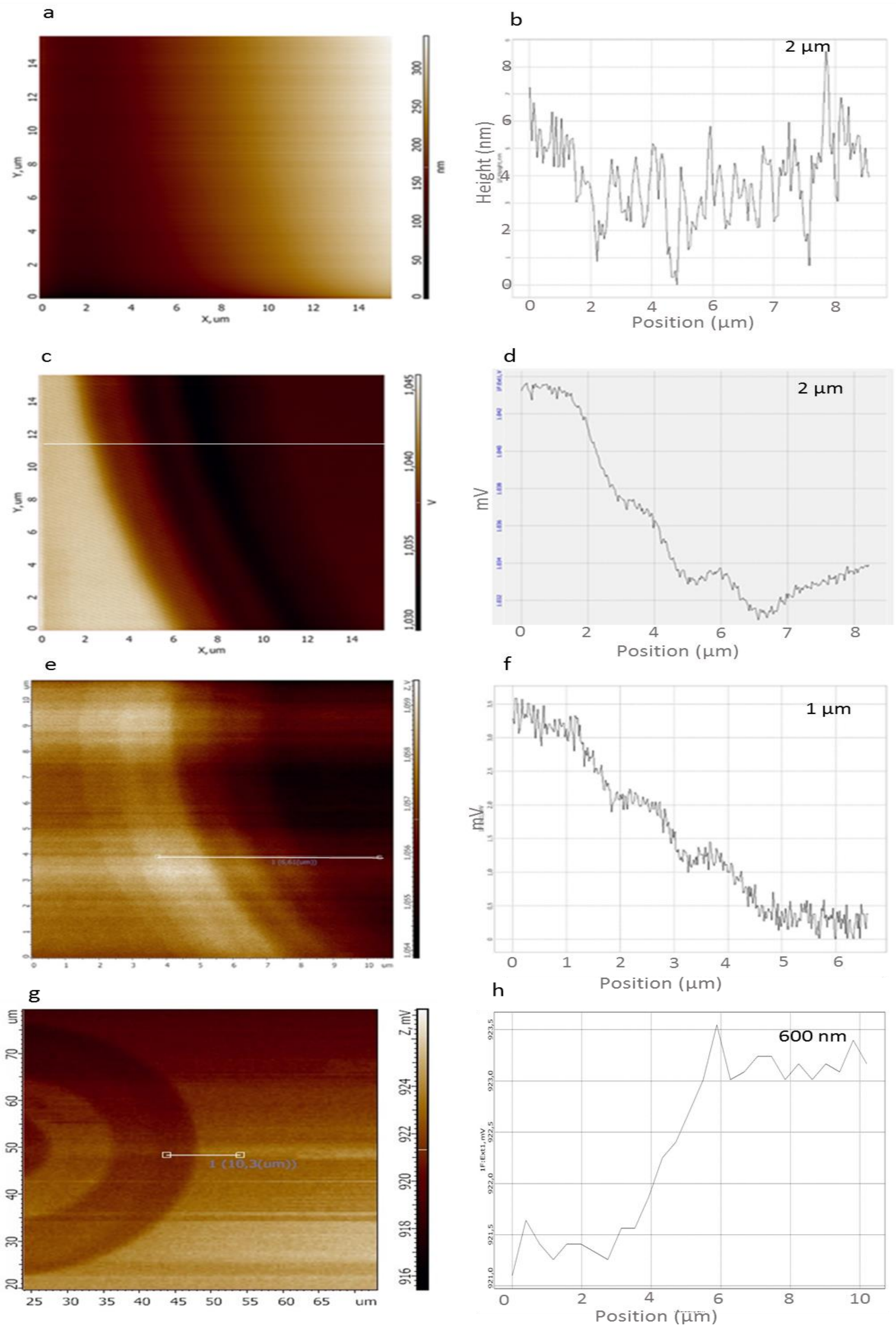

Figure 3- 5: 15 ×15 µm a) topography scan b) line profile and their corresponding thermal c) image b) line profile analysis for 2 µm step width e) thermal scan f) line profile analysis for 1 µm step width g) thermal scan h) line profile for 600 nm step width performed by SThM under ambient conditions for I= 50 mA.

1.4. Numerical analysis of nanostructured sample

The goal of this study is to develop a methodology so that the sample studied can be used for exploring SThM probe in a simple way. Therefore, a 3D realistic geometry of the Wollaston probe and the sample was developed which allows to calculate the heat flux between the probe and the sample. The 3D modelling was done using COMSOL Multiphysics based on finite element method (FEM).

1.4.1. Geometry and boundary conditions

The thermal probe was modelled with a realistic geometry as shown in figure 2-6. The modelling of probe in this chapter has the same dimensions and the same boundary conditions as seen in chapter 2. Therefore, an equivalent heat transfer coefficient of 84000 $W.m^{-2}.K^{-1}$which was estimated in chapter 2 from the simulation of the holder was applied on the upper surfaces of the Wollaston wire. For the platinum-rhodium wire, the heat losses to the environment are presented by the coefficient h which is 2500 $W.m^{-2}.K^{-1}$[12]. This coefficient was chosen instead of considering air convection for the environment medium to allow the comparison of results with partners of QuantiHeat project and to save calculation costs in time (each calculation point needs more than 1 day when considering air convection). A null flux was considered for the lateral surfaces of the sample. And the

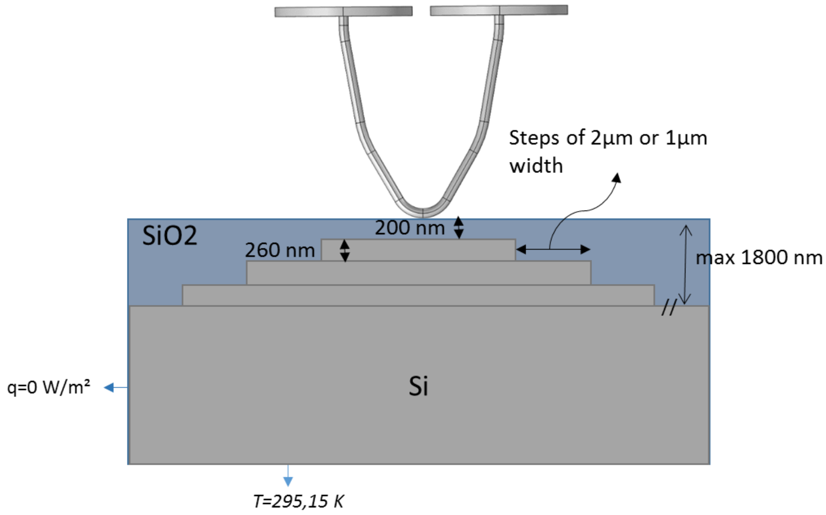

Figure 3- 6: Schematic representation of the sample with realistic dimensions used for the modelling.

temperature at the bottom of sample was set to ambient temperatureT_a.

The sample is composed of six steps with a thickness of 260 nm each, the whole is covered with silicon dioxide thin film of 200 nm. Two geometries were modelled having different steps width respectively for 1µm and 2 µm (figure 3-6). Thermal conductivities used in the modelling of the sample are represented in table 1 [13, 14, 15].

Table 3- 2: Thermal conductivities used in FEM modelisation

Materials	Thermal conductivity W.m^{-1}.K^{-1}
Si thin film (260 nm) [13]	50
SiO_2(2 µm) [14]	1.1
Si substrate	130

1.4.2. Mesh of nanostructured sample

The pertinence of results relies on the discretization of the geometry. Creating a mesh consists on building a sequence of nodes which are considered as operations. The size of the mesh used is very important and it conditions the accuracy of results. The mesh of the Wollaston probe is the same as the one used in chapter 2. Since the sample is composed of nanostructured elements, the mesh should be built carefully. Tetrahedral elements were used to mesh the structure. An extremely fine mesh was used for the internal structures composed of six steps. Where the minimum element size was set to 0.01 µm and the maximum element size to 8 µm. Figure 3-7 illustrates the meshed structure of steps with a top and side view. The substrate is of 500 µm in thickness, width and length therefore a fine mesh with maximum element size was set to 33 µm and the minimum element set was 2.5 µm. The choice of element size allowed to have a homogeneous distribution of elements for the whole geometry. In this case the overall mesh of the whole geometry has a quality factor of 0.9.

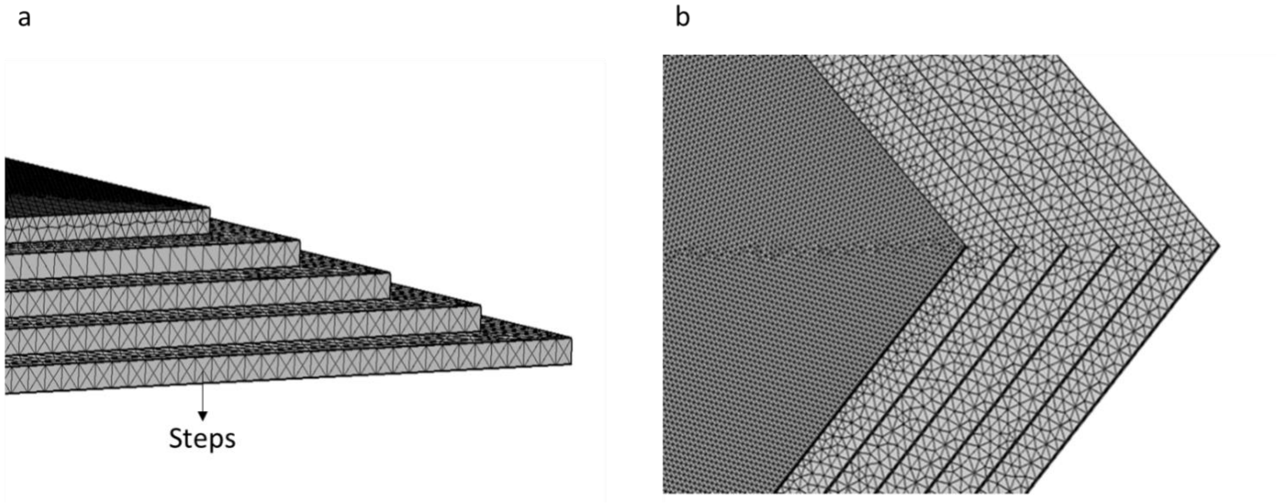

Figure 3- 7:a) Side view of silicon steps (without SiO_2 coating) b) top view of silicon steps meshed structure.

1.4.3. Results

Solving heat transfer and electrical current equations [(24) and (25) from chapter 2] for the probe/sample system allows to obtain the temperature distributions. The thermal probe was modelled in direct operation mode.

The model was run for several positions of the probe above the sample surface as presented in figure 3-8a. The temperature distribution of the Wollaston probe in contact with the sample is presented in figure3-8b, c and d for three different cases. Each case represents the position of probe on the sample surface above internal steps. The first position is considered 3 µm away from the edge of the first step it corresponds to the distance 0 in figure 3-8a. Its temperature distribution is presented in figure 3-8b. The fourth position presented in figure 8c is 8 µm away from the first position. The fifth position is presented in figure 8d and it is 10µm away from the first position. The temperature field differs according to the probe position above the sample surface. When the probe is located at the first position its mean temperature (T_m=429 K) is lower than when it's located in the fourth position (T_m= 450 K).This is due to the difference in the composition of materials under the probe (from a position to another). As observed even at the fifth position, which is represented in the last image of figure 3-8d, the heat distribution is influenced by the presence of steps.

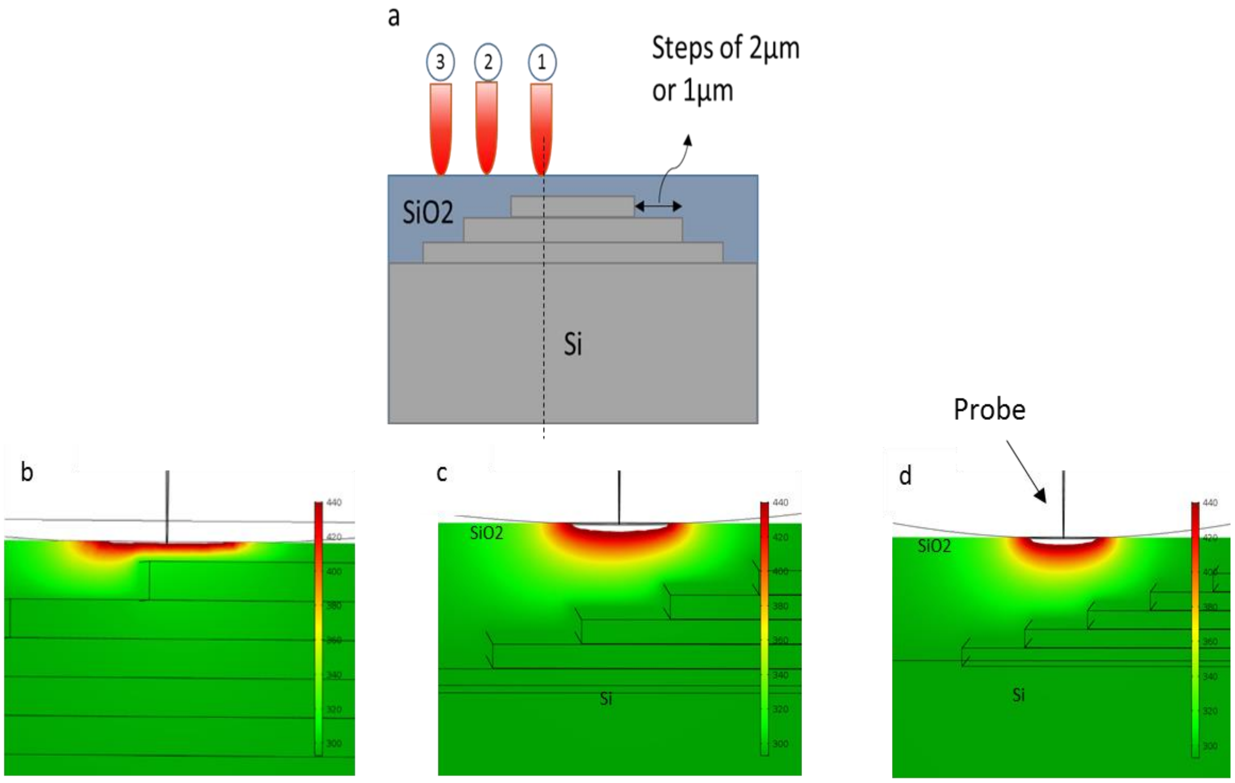

Position 1 (0) Position 4 (8 µm) Position 5 (10 µm)

Figure 3-8: a) Schematic of the sample and probe positions b) Cross section temperature distribution of the Wollaston probe in contact with the sample for different probe positions.

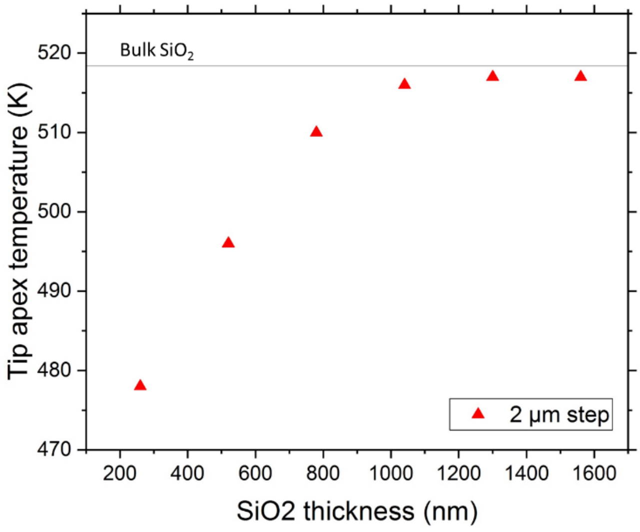

Figure 3-9: Tip apex temperature as a function of Silicon dioxide thickness for 2 µm step width.

The tip apex temperature of 2 µm step width is given in figure 3-9 as a function of SiO_2 thickness. As observed the temperature increases with increasing the thickness of SiO_2. It becomes stable when reaching the fifth position which is also seen in temperature distribution of figure 3-8d. Starting the fifth position the tip apex temperature tends to when the probe is in contact with a sample of bulk Silicon dioxide.

Besides the modelling of structured sample, geometry was built for a sample composed of silicon dioxide thin film over a silicon substrate for purpose of comparison with the nanostructured sample. The modelling was developed with several thicknesses of SiO_2 reaching the total thickness of the steps as illustrated in figure 3-10.Thermal conductivities used in the modelling are taken from the literature and corresponds to the equivalent of silicon dioxide thin film [14, 15]. Table 3 summarizes thermal conductivities used for SiO_2 thin films. The comparison of each thickness from this structure with the corresponding thicknesses of SiO_2 in the nanostructured sample allows observing the behavior of thermal probe according to the depth of internal structure.

Table 3- 3: The corresponding thermal conductivity of silicon dioxide to each thickness taken from the literature [8, 10].

SiO_2 thickness (nm)	260	520	780	1040	1300	1560	1820
Thermal conductivity ($W.m^{-1}.K^{-1}$)	0.95	0.95	1	1	1.1	1.1	1.1

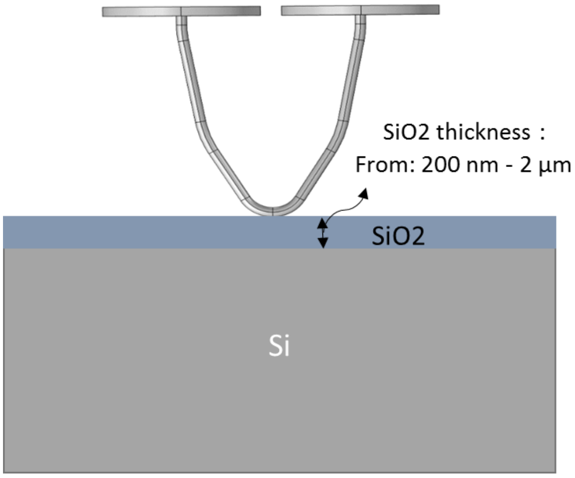

Figure 3- 10: Schematic representation of the modelling of silicon dioxide thin on a silicon substrate.

The numerical model allows to calculate the heat flux dissipated from the thermal probe into the sample$\emptyset_{steps}$. Figure 3-11a illustrates the heat flux transmitted from the tip into the sample as a function of SiO_2 thickness. It was evaluated for three models: the step width of 1µm, 2µm and the thin film over the substrate.

As observed in figure 3-11a, the heat flowing from the thermal probe into the sample decreases with increasing the thickness of silicon dioxide for three geometries. The 2 µm step width has heat flux lower than the case of 1 µm step, while for SiO_2 thin film over substrate $\emptyset_{Thin\ film}$ is the lowest. As noticed for the first point which corresponds to a thickness of 260 nm a big difference is observed between the values obtained for the structured sample and the thin film on a substrate sample. In this case, the probe is placed at the first position as represented by the dashed line in figure 3-8a which is about 3 µm away from the edge of the first step. For both geometries 1µm and 2 µm step width, the value is almost the same. This is due to the fact that the thermal probe is not yet sensitive to steps widths. When the probe is located at the second position, $\emptyset_{steps}$ for the 2 µm step width is closer to the heat flux obtained for the thin film geometry. This shows that the probe is influenced by the internal structure but it's getting closer to the probe behavior when it's in contact with SiO_2 thin film. When the probe is at the fifth position, $\emptyset_{steps}$ for 1µm and 2 µm steps widths and $\emptyset_{Thin\ film}$ has approximatively the same value. This indicates that the probe is no longer influenced by the presence of the steps. Therefore the heat flux tends to the same value of the heat flux dissipated from the probe in contact with a bulk silicon dioxide whit thermal conductivity of $1.1\ W.m^{-1}.K^{-1}$.

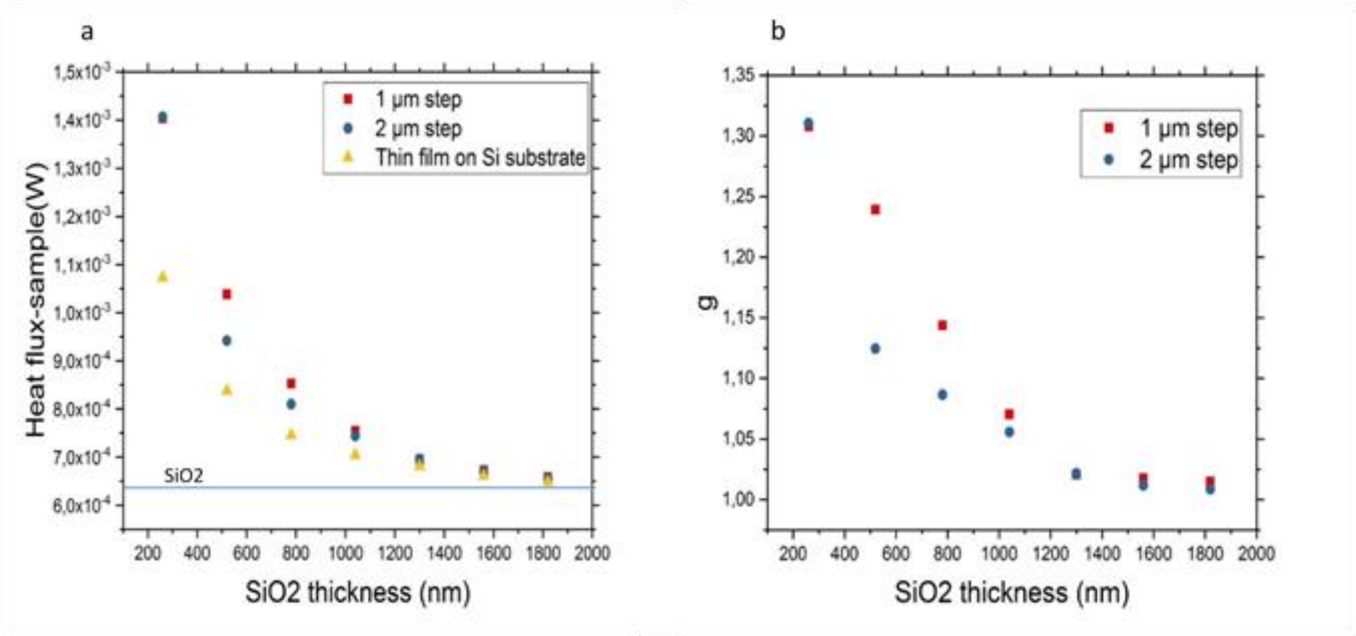

Figure 3- 11:a) Heat flux dissipated from the probe into the sample as a function of SiO2 thickness b) Ratio of heat flux dissipated by the thermal probe into the nanostructured sample/heat flux dissipated by the probe into thin film on a substrate as a function of SiO2 thickness.

In order to highlight the thermal probe behavior according to the step width, we calculated the ratio of heat flux dissipated from the resistive probe into the sample versus the thicknesses of SiO_2 $g = \frac{\emptyset_{Steps}}{\emptyset_{Thinfilm}}$(figure 3-11b). This ratio represents the heat flowing from the steps over the heat of the thin film on the substrate. The first position of the probe doesn’t show any difference in the ratio which means that the probe have the same behavior since it is positioned 3 µm away from the edge of the first step therefore it is not influenced by the near-by step. This means that the signal obtained by the probe is only due to the presence of Silicon. When the probe is located above the second step, 4 µm away from the first position, the total thickness of SiO2 is about 460 nm. The thermal signal is influenced by the depth and as shown it is influenced by the step width. The heat is transferred from the probe to an asymmetrical sample due to its structure thus at the second step the thermal signal is more influenced by the silicon steps than by the silicon dioxide which explains the difference in the ratio between the step width of 1 µm and 2µm. When the probe is located above the third step, the ratio of 1 µm and 2µm step width decreases. As the probe is moved above the fourth step, we observe that the ratio of 1 µm step width is closer to the ratio of 2 µm step width. The ratio becomes stable when the probe is located 10 µm away from the first position which corresponds to silicon dioxide depth of 1.3 µm.

The thermal signal is sensitive to internal structures of the sample and has sensitivity up to 1.3 µm thickness of silicon dioxide. In earlier studies a group of researchers studied the depth detection of Wollaston probe using a polymer sample with buried copper particles at different depth [4]. They developed a theoretical model to simulate the probe's response for different depths. They stated that the Wollaston probe is sensitive to internal features down to 2 µm in depth. The modelling developed in this study is based on realistic geometry and dimensions of the probe/sample system which makes results more reliable.

1.5. Comparison of simulation with experimental results

The comparison between experimental data and simulation results allows to validate the modelling. As seen in the previous section, the 2 µm step width are more revealed in the thermal signal than that of the 1 µm step width. Therefore the model of 2 µm step width was taken into account for the comparison with experimental results.

Figure 3-12a shows an experimental thermal image obtained with a Wollaston probe for 2 µm step width. The presented area contains three steps of silicon under silicon dioxide. The thermal profile illustrated in figure 3-12b corresponds to the line profile presented in figure 3-12a (white line). As observed, the thermal signal is stable when the probe scans the silicon area. It starts decreasing once the tip approaches to silicon dioxide steps.

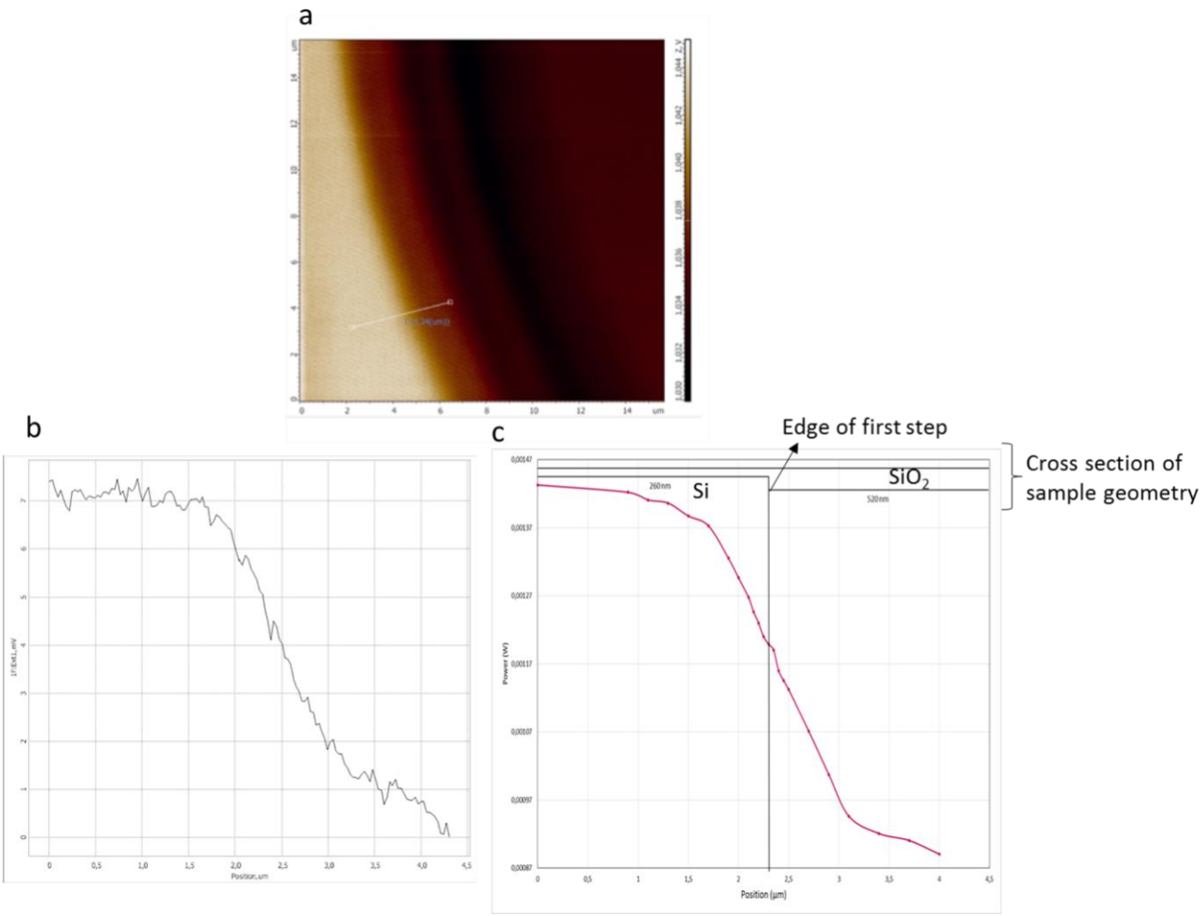

Figure 3- 12: Thermal a) image and b) experimental profile analysis obtained with Wollaston probe for 2µm step width compared with c) numerical thermal profile.

The thermal signal obtained with Wollaston probe was modelled in FEM and presented in figure 3-12c. As observed finite element method is in good agreement with experimental results. The modelling was done over a distance of 4.5 µm which covers the first step. Each point of the curve was calculated successively for different positions of probe above the sample surface. The sample geometry has been added above the numerical profile to show the position of the step edge comparatively to the thermal profile. Once the thermal probe feels a change in thermal properties of the volume containing the information, its thermal behavior will change. While scanning line by line across the sample surface, the thermal signal starts decreasing before reaching the edge of the nearby step. It seems to show the geometrical shape of steps but in fact it doesn’t correspond geometrically to steps which mean that the thermal signal obtained corresponds to a scanned volume. Thus the thermal signal gives volume information not a surface one.

1.6. Discussion

In this section we discussed a methodology to investigate the thermal signal obtained by the Wollaston probe. SThM was shown to be a persistent tool to study nanostructured materials and perform sub-surface imaging on materials with different thermal conductivities. The sample was designed with different steps width to allow the determination of the effective resolution of the used probe. The measurements showed that the thermal probe is sensitive to the steps having width from 1µm. These kinds of probes provide then a micrometric lateral resolution and they are sensitive the information at nanometric scale. Numerical model was developed in FEM to validate the probe performance. Experimental measurements were also performed in the thermal conductivity mode, which was shown to be in good agreement with numerical data. This technique can be applied for other probes to study in detail particular aspects of the internal structure influence on the heat transfer between the probe and sample.

2. Determination of the thermal exchange radius

When the probe is in contact with the sample, the interpretation of results becomes more complex. As known modes of heat transfer depends on the sample’s thermal conductivity, surface chemistry, humidity and room temperature. The assessment of sample’s thermal conductivity requires a determination of the thermal exchange radius b which allows providing more accurate results. Previous studies have assumed that the value of b defined in chapter 1 is constant [16]. In this study a methodology was developed in order to calculate b.

The developed model allows obtaining the values of heat flux transmitted from the thermal probe to the environment and into the sample. From these quantities several thermal properties can be extracted. In this section the main interest is determining the thermal exchange radius b. When the contact occurs between the Wollaston probe and a sample, the heat source is considered as a circular one. Yovanovich [17] defined the spreading resistance of the sample for a circular source as $R_s = \frac{1}{4kb}$ where k is the sample thermal conductivity and b is the thermal exchange radius. This expression is valid when the sample is a bulk one.

When the sample is a thin film over substrate the thermal spreading resistance of the sample can be written as [17]:

$$R_s = \frac{1}{4k_{sub}b} + \frac{\ell}{\pi k_{film}b^2} \tag{26}$$

Where, k_{sub} is the thermal conductivity of the substrate, $k_{film}$is the thermal conductivity of thin film andℓ denotes the thickness of thin film.

The determination of b is done by determining R_s in equation 26 since thermal conductivities are known. The heat transfer rate between the probe and the sample Q_s can be determined by modelling. Its equation is given by:

$$Q_s = \frac{\Delta T_p}{R_c + R_s} \tag{27}$$

Where $\Delta T_p = T_p - T_0$ represents the temperature rise of probe and R_c is the thermal contact resistance between probe and sample. The thermal contact resistance can be calculated using the following equation:

$$R_c = \frac{\Delta T_c}{Q_s} = \frac{T_c - T_0}{Q_s} \tag{28}$$

Where T_c represents the temperature at the contact point with the sample.

The unknown quantities in equations (26) and (27) can be calculated via the numerical model in order to obtain R_s. The value of R_s will be then implemented in equation (27) in order to obtain the thermal exchange radius b.

Let's consider the situation where the probe is located on the fifth position (10 µm away from the first step and 1.3µm depth of silicon dioxide) in this location the probe signal is not influenced by the presence of the step. Which means the case studied is similar to a silicon dioxide thin film over silicon substrate. For this configuration, using equations (27), (28) and (29) the value of the thermal exchange radius b can be determined. Table 3-4 represents the values of Q_s, T_c, T_p and R_c obtained for this configuration. From these values, the thermal exchange radius b was found to be 2.2µm. Wilson *et al.* [18] determined the thermal exchange radius for low conductivities bulk samples and for thin film on a substrate. They stated that the value of b evaluated to 2.8 µm remains constant for low thermal conductivity samples (0.12 $W.m^{-1}.K^{-1}$ – 1.22 $W.m^{-1}.K^{-1}$). Thus our results are in the same order of magnitude as in the literature.

Table 3- 4: Values of the heat flux dissipated into the sample, the probe temperature at the contact with the sample, the probe mean temperature and the thermal contact resistance obtained from our modelling.

	Q_s (W)	T_c(K)	T_p(K)	R_c (K.W^{-1})
1st position	$13.636.10^{-4}$	478	430	$0.9.10^5$
5th position	$7.7301.10^{-4}$	516	450	$1.875.10^5$

When the probe is located in the middle of the first step, the thickness of silicon dioxide is 200 nm. This case is similar to a configuration of SiO_2 thin film over silicon substrate. Table 3-4 summarizes the values calculated from the numerical model for this case. Using equations 27, 28 and 29 the thermal exchange radius was calculated for this geometry. The computed value was found to be890 nm. Previous studies showed that for high thermal conductivity sample, the value of b is in the range of few hundreds of nanometers which is coherent with our result. Table 4 summarizes the value of b obtained by different group of researcher [5, 19, 18]. The values of the thermal exchange radius obtained by Zhang *et al.* and Wilson *et al.* were evaluated by modelling. We note that none of them used a modelling with the realistic dimensions of the Wollaston probe/sample system. This may be the reason of the difference obtained in the values of b.

Table 3- 5: Comparison between values of effective thermal exchange radius b evaluated in this study to values from the literature.

	b	Sample
Our method	2.2µm	SiO_2 thin film (1.3 µm) on Silicon substrate
Our method	890nm	SiO_2 thin film (200 nm) on Silicon substrate
Wilson *et al.* [18]	2.8 µm	SiGe film (1.8 µm) on glass substrate
Puyoo *et al.* [5]	820 nm	SiO_2 thin film (200 nm) on Silicon substrate
Zhang *et al.* [19]	2.45 µm	Bi_2Te_3 on glass substrate

3. Modelling of free topography materials

In the frame of QuantiHeat project, a sample composed of nanostructured features with silicon and silicon dioxide was fabricated by VTT. The sample is composed of 4 rectangular shapes of 10 µm in length and width respectively 4.3 µm, 1 µm, 0.6 µm and 0.3 µm having each a slope with an angle of 10° with silicon dioxide and on silicon substrate. The investigation of this sample aims to support the methodology developed previously for the characterization of the Wollaston probe. And to characterize the effect of probed volume by revealing the change in thermal signal according to the depth of buried feature. Figure 3-13 illustrates the sample structure and a SEM image of the slope formed into sample.

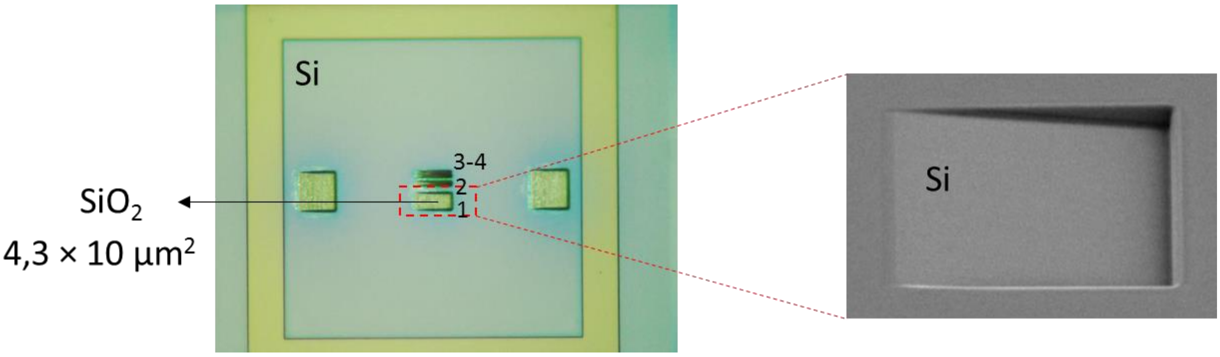

Figure 3- 13: The sample structure showing features (1, 2, 3 and 4) presented on the sample and a SEM image of the slope on the chip without SiO2 coating (as given by VTT).

Topographic and thermal measurements were performed using a NTMDT microscope with the same control unit of topometrix microscope in the DC mode. We used standard Wollaston probes manufactured by CMI.

3.1. Experimental and numerical measurements

Figure 3-14a and 3-14b represent the topography scan and line profile analysis performed on the sample surface. On topographic image, two features are observed which corresponds zone 1 and 2 of figure 3-13. The line profile shows an average roughness of 2.5 nm for the sample surface. Figure 3-14c and 3-14d represents respectively the thermal image and line profile of the same area on sample surface. On the thermal image, three features are clearly identified which corresponds to the area underneath the oblique interface Si/SiO_2 with a slope buried into the chip.

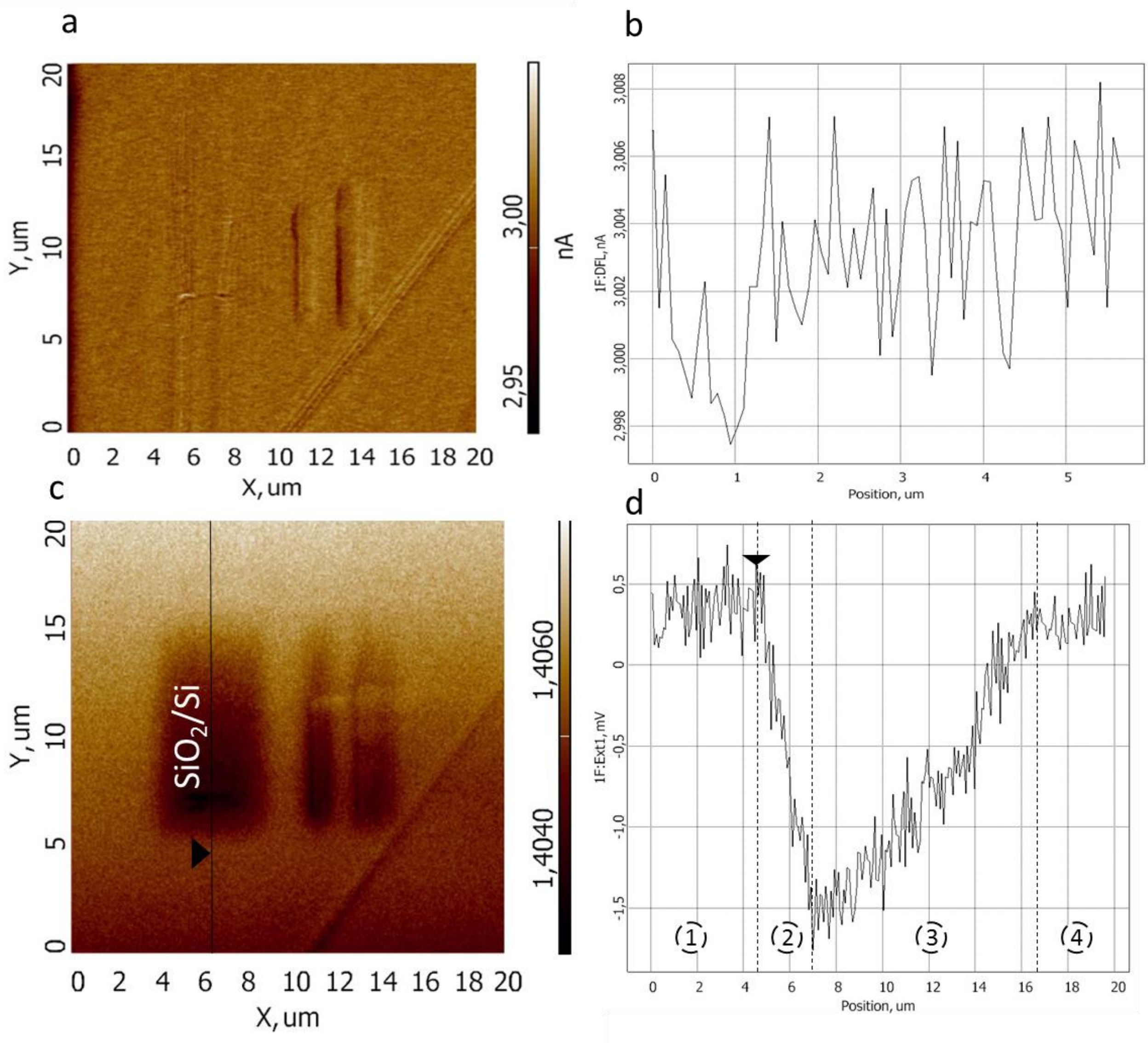

Figure 3- 14: 20×20 µm topographic a) image and b) line profile analysis and their corresponding thermal c) image and d) line profile analysis performed by SThM on the structured sample under ambient conditions.

As observed on the thermal line profile, in zone 1 the signal remains stable when the probe scans over the silicon substrate. The black triangle (figure 3-14c) indicates the place where the thermal signal starts decreasing which is before reaching the edge of the Si/SiO$_2$ interface. This means that it decreases when the probe is influenced by the thermal conductivity of near-by material. At the edge of the interface, the silicon dioxide have the highest thickness. Therefore, a sharp drop of the signal occurs forming an inclined line (zone 2). The thermal profile starts increasing again when the thickness of silicon dioxide increases (zone 3) forming the shape of the Si/SiO$_2$oblique interface. The thermal signal becomes stable again (zone 4) when the probe scans over the Silicon substrate. In order to more understand the behavior of this signal, a model was developed with a realistic geometry of the sample.

Figure 3-15 represents the geometrical dimensions of sample used for the modelling. The sample is composed of Silicon substrate represented by a solid with 400 µm in thickness, width and length. It is coated with a thin film of silicon dioxide with 400 nm in thickness. The slope is formed in the middle of sample with a right angled triangular shape. It is composed of Silicon dioxide with 1.75µm in depth and 10 µm in width and an angle of 10°.

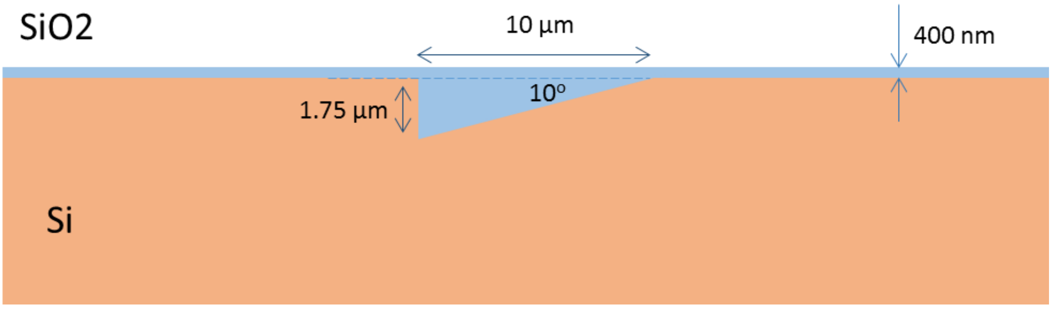

Figure 3- 15: Schematic of the sample geometry and dimensions used in the modelling.

Once the geometry is built, a mesh should be created. The choice of mesh for this structure should be chosen carefully especially for the slope and the contact area between the probe and the sample. The slope has an angle of 10° and it must be correctly defined since it will be the factor that plays a major role in the accuracy of results. For the slope we chose an extremely fine mesh with a4.3µm maximum size of elements and a minimum size of

0.013µm. A representation of the mesh is shown in figure 3-16. In this case the quality factor of the geometry is 0.8 which is considered good for solving the discretized geometry.

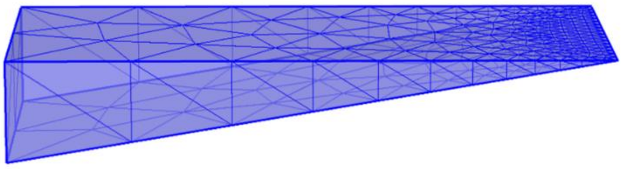

Figure 3- 16: The meshed structure of the interface as built in the modelling.

3.2. Results

Solving the heat transfer equation in COMSOL allows us to obtain the heat distribution in the system. Figure 3-17 represents the temperature distribution of the probe/sample system for DC operating mode with a current of 50 mA. The mean temperature of the probe in contact can be evaluated from the modelling, it is about 460 K when the probe is placed at the level of the slope's edge.

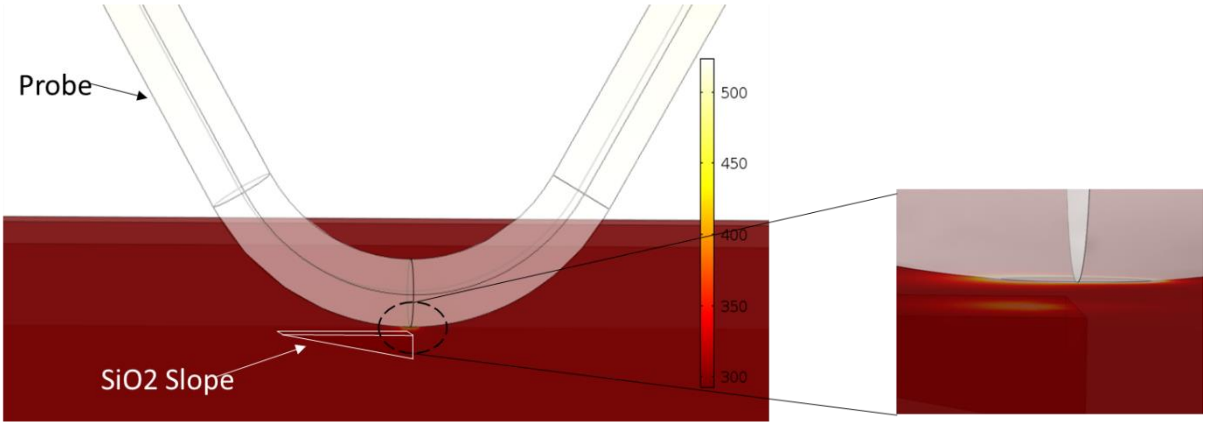

Figure 3- 17 : Temperature distribution of the probe/sample system obtained by modelling in DC operating mode under ambient conditions for a current of 50 mA.

The modelling was done for several positions of the probe over the sample surface in order to cover the overall surface of the slope. The heat flux transmitted from the thermal probe into the sample was calculated via the numerical model and presented in figure 3-18. Each point of the curve represents a probe position.

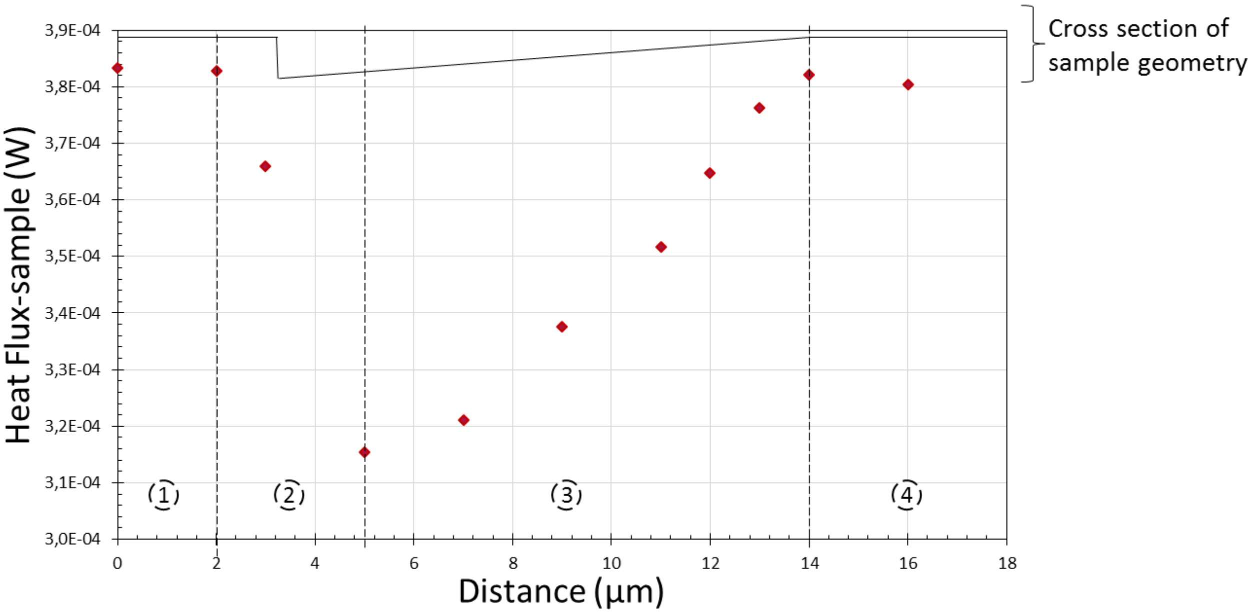

Figure 3- 18: Heat flux dissipated by the thermal probe into the nanostructured sample as a function of the probe position.

The distance 'zero' of the axis corresponds to the position where the probe is 3 µm away from the edge of the Si/SiO$_2$ interface. As illustrated in the curve the heat flux remains stable when the probe scans over the silicon substrate (zone 1). Once the probe approaches to the edge of the triangle, the heat flux transmitted into the sample decreases sharply which is linked to the increased thickness in SiO$_2$ (zone 2).The drop in the signal forms a linear curve between zone 1 and 2 which is also seen for experimental results. By moving the tip along the surface the heat flux increases again since the thickness of silicon dioxide decreases (zone 3). The tendency of the curve obtained by simulation follows well the shape of the structure. The curve part (zone 3) does not show a straight linearity as the real geometry created on the sample. The thermal signal becomes stable again once the probe scans over Silicon substrate (zone 4). The behavior of the probe thermal signal obtained by modelling is the same as experimental results. The experimental profile obtained by SThM was rebuilt by modelling. It showed that despite the size of the probe (5 µm in diameter) it is sensitive to Nano internal features. The probe thermal signal is influenced by the presence of internal structures and corresponds to a scanned volume which takes into account material's thermal properties. The dependency of thermal signal on material's thermal properties allows to assess material's thermal conductivity. In a further study this can be done using inverse methods. This sample can be a powerful tool for characterizing other thermal probes.

The tip apex temperature was also evaluated as a function of the probe position above the sample surface (figure 3-19). As illustrated in the curve probe temperature remains stable when it scans over the silicon substrate (zone 1). Once the probe approaches to the edge of the triangle, the temperature increases sharply which is linked to the increased thickness in SiO_2 (zone 2). The drop in the temperature forms a linear curve between zone 1 and 2 also seen for experimental results. By moving the tip along the surface the tip apex temperature increases again since the thickness of silicon dioxide decreases (zone 3). The temperature becomes stable again once the probe scans over Silicon substrate (zone 4).

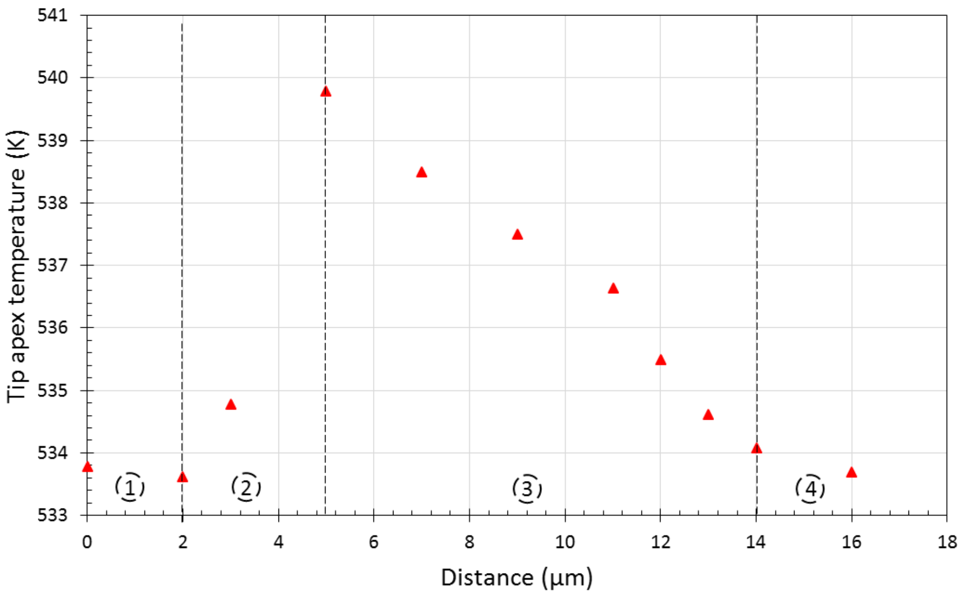

Figure 3- 19: Tip apex temperature as a function of the probe position above the sample surface.

4. Thermal characterization of polymer particles

In the frame of the European project, the industrial company 'Compart' aims to investigate the thermal properties of single particles polymers. Compart develops and supplies materials for the electronics industry based on unique manufacturing process. They focuses on polymer particles of micrometric size coated with nano films of metals and aim to provide particles of thermal conductivity higher than 2 $W.m^{-1}.K^{-1}$with high electrical conductivity (> $3300 S.m^{-1}$). Polymer particles with various thicknesses of silver coating were provided to QuantiHeat partners in order to characterize and measure their thermal conductivities. Several methods were used such as: i) indirect method which is based on measurements of the thermal diffusivity, density and specific heat, ii) scanning thermal microscopy. URCA have used SThM for the thermal characterization of these particles.

4.1. Polymer particles

The first set of sample received was composed of 30 µm in diameter polymer particles coated with different thicknesses of silver: 60 nm, 100 nm, 150 nm and 270 nm. The sample preparation was done in our laboratory following Compart instructions:

In a first step, the polymer particles of each coating were immersed in 96 % of ethanol. The mixture was exposed to high frequency ultrasonic vibration for 15 minutes to de-agglomerate the particle clusters. Then droplets of ethanol/particle solution were placed on a silicon chip. The specimens were left to dry in a clean environment for 12 hours in order to remove any ethanol left in particles. Four samples were obtained: A, B, C and D with silver thicknesses respectively 60 nm, 100 nm, 150 nm and 270 nm.

Once the preparation was done, all samples were investigated using scanning thermal microscopy in the active mode under ambient conditions. The microscope used in this study is AFM explorer commercialized by Topometrix. The aim of this study is to assess the thermal conductivity value of nanoparticles by SThM imaging. Figure 3-20 represents thermal images and their corresponding thermal profiles for the different samples studied.On the thermal profile of sample A, the highest value of the thermal signal is about 0.73 V which seems corresponds to the silicon substrate and the lowest value of about 0.6 V seems to represents the polymer particles.

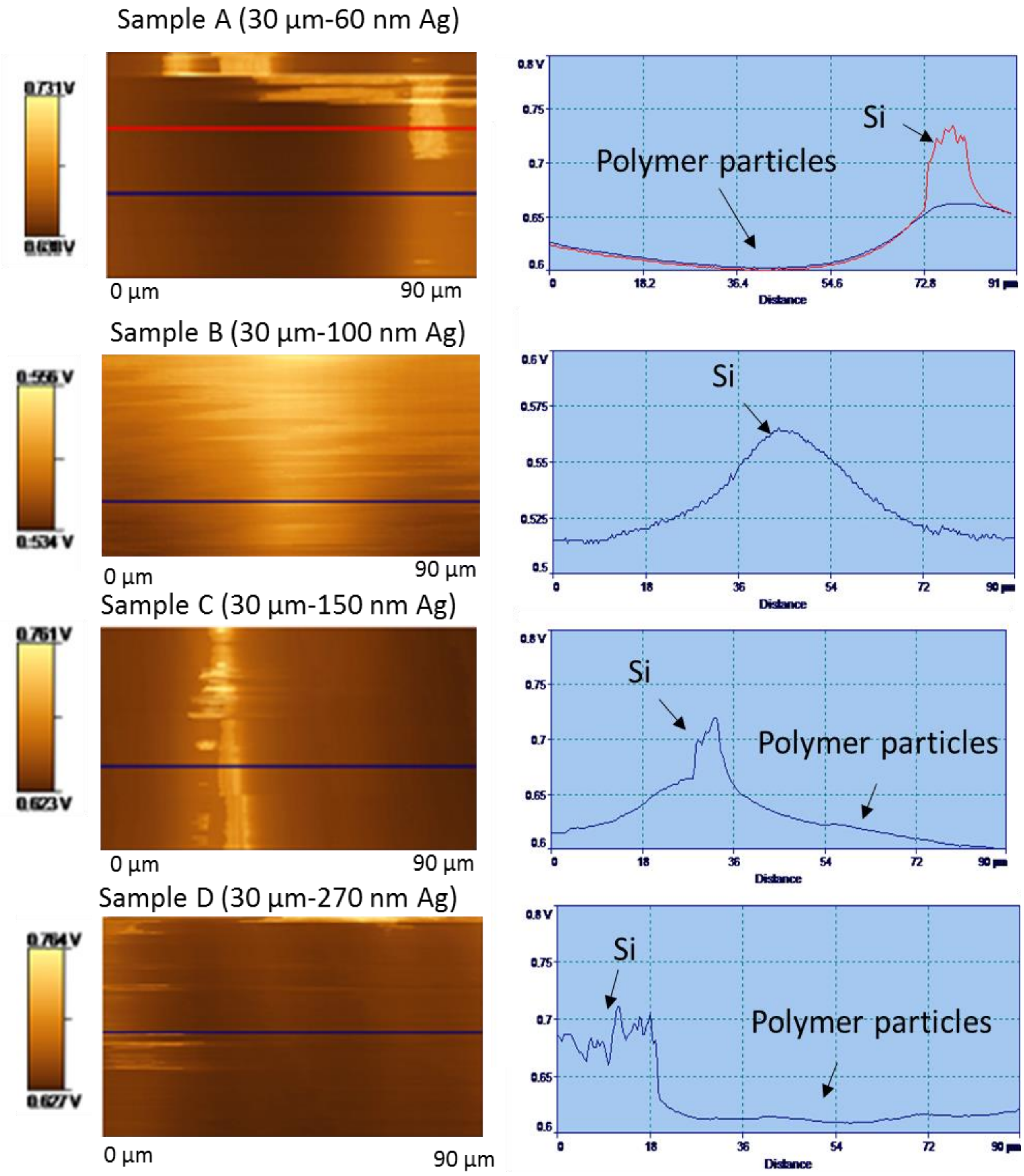

Figure 3- 20: Thermal images and their corresponding thermal profiles performed by SThM using a Wollaston probe for four samples (A, B, C and D).

Thermal images were made on a zone of 90µm × 90µm corresponding to 3 particles. Those images show that the silicon substrate and particles are smoothed. While scanning above the sample surface, the polymer particles are removed by the thermal probe due to the lack of nanoparticles adhesion on the silicon substrate. Therefore it was very difficult to obtain thermal images with this kind of sample. Several measurements were performed on those samples but none of them was presented satisfying thermal images and profiles.

This study shows that single particles on silicon substrate are not adapted to be investigated with SThM's technique due to inappropriate sample preparation. Therefore, we suggested a development in the sample preparation that consists on adding particles to an adhesive matrix. This suggestion was taken into consideration, thus a new sample was prepared by Compart to continue the investigations of their specific polymer particles.

4.2. Polymer particles in an adhesive matrix

The new sample fabricated by Compart is composed of 30 µm polymer particles coated with 150 nm of silver in an adhesive matrix. The investigation of this sample has presented some difficulties due to its dimension (≈ 5 mm*1cm*2mm) and to the position of interest area. Due to the high roughness of the sample, only a small polished area could be investigated as presented in figure 3-21. Therefore, a holder was fabricated that allows placing the sample below the microscope head.

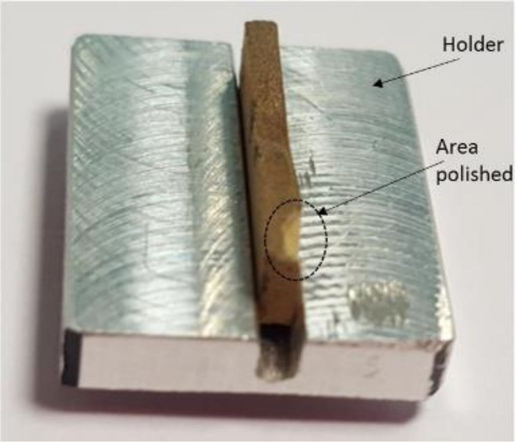

Figure 3- 21: The sample provided by Conpart and its holder with the polished area to be investigated.

All measurements were performed under ambient conditions in the DC mode. Figure 3-22 represents the thermal image and line profile analysis for an area of 80×80 µm. The thermal profile in figure 3-22b represents a spherical tendency which seems to be similar to the shape of polymer particle. We should note that a specific attention was given in the interpretation of these measurements due to a breakdown in our microscope scanner. Actually the scan was performed in one direction, thus the obtained image represent the same line repeated 150 times. Peaks presented in the thermal signal corresponds to the Silver coating whereas the value of thermal conductivity obtained does not correspond to that of Silver. As discussed previously the thermal signal obtained corresponds to a probed volume which in this case contains the polymer particles.

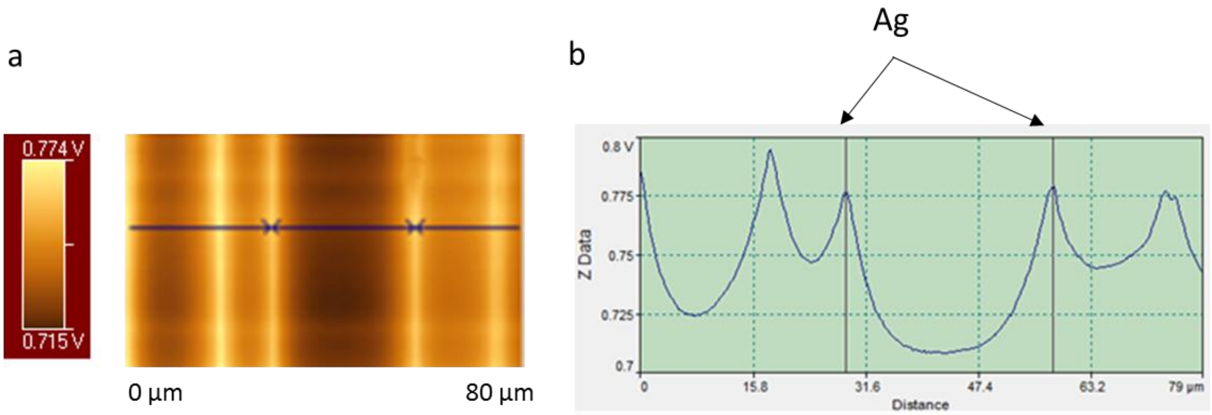

Figure 3- 22: a) Thermal image of polymer in matrix sample and b) thermal profile analysis.

The probe used in the analysis of polymers particles was calibrated in order to estimate the thermal conductivity of polymer particles sample. Six different calibration's samples (Zn, Ta, Ti, TiAlV, Vitro ceramic, black acetal) having known thermal conductivity were measured using the same Wollaston probe. For each calibration sample the value of voltage $V_{\text{out-air}}$ (when the tip is out of contact) and V_{out} (when the tip is in contact) were noted and used in the calculation procedure in order to obtain ΔP of each sample. The voltage is linked to probe Joule power with the equation $P = \frac{V^2}{R_p}$, where V is the voltage across the probe tip and R_p is the probe resistance at the operating temperature. The calibration curve was done with a probe mean temperature of 70°C.

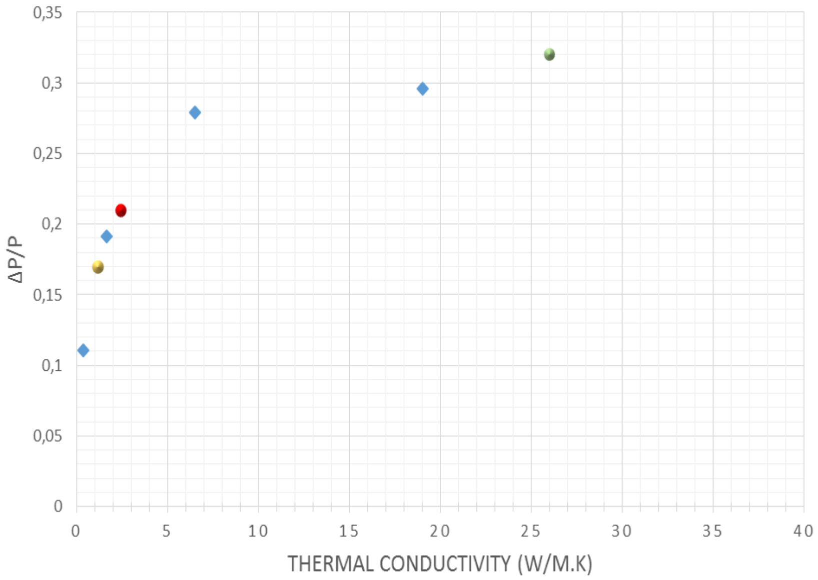

Figure 3- 23: Variation of ΔP/P as a function of sample the thermal conductivity where the yellow, red and green dots represent respectively the minimum value, average value, highest value of sample thermal conductivity.

Figure 3-23 represents the thermal signal variation ΔP/P as a function of samples thermal conductivities. Several thermal measurements were performed on the sample surface with different area. The voltage average was calculated from the obtained thermal profiles which allow to calculate the probe Joule power. The red dot corresponds to the average thermal conductivity which is approximatively 3 $W.m^{-1}.K^{-1}$deduced from these profiles. Yellow dots corresponds the minimum value of thermal conductivity obtained from the minimum value of thermal profile (1.5 $W.m^{-1}.K^{-1}$). The green dot signifies the highest value of thermal conductivity which is larger than 20 $W.m^{-1}.K^{-1}$. This value is linked to the presence of silver coating in the scanned volume.

In this section we aimed to assess by imaging the local thermal conductivity of polymer particles in adhesive matrix. The interpretation of results was complicated due to the breakdown that occurred in the microscope scanner. The local thermal conductivity varies between 1.5 and larger than 20 $W.m^{-1}.K^{-1}$ due to the silver coating. Thermal profiles obtained for this sample revealed its internal geometry (spherical shapes in this case).

These polymer particles can be investigated through developing a 3D model in order to evaluate the thermal behavior of polymer particles. The modelling allows to assess several thermal quantities that can lead to material’s effective thermal conductivity. Therefore this work should be completed in an upcoming study to investigate deeply these polymer particles.

5. Conclusion

In this chapter, a methodology of probe/sample characterization was developed. In the frame of QuantiHeat we proposed a sample composed of internal steps with 100, 200, 300 and 400 nm steps length to study the probe thermal signal behavior. This sample was fabricated and provided by VTT. Topographic and thermal measurements were performed using Wollaston probe. Results showed that the thermal signal is sensitive to the internal structures but cannot distinguish between the features. Therefore, we proposed another design of the sample with wider steps widths of respectively 600 nm, 1µm and 2µm. Performing SThM imaging on this sample allowed to point out on the probe spatial resolution which was evaluated to 1µm. A 3D modelling was developed in FEM with a real geometry of the sample to investigate deeply the probe thermal behavior. Our results showed that the probe is sensitive to sample internal structures and has sensitivity up to 1.3 µm depth. With our modelling, we were able to rebuild the experimental profile obtained by our SThM. Our results showed that the thermal signal is not only sensitive to internal structures but also gives volume information which takes into account material’s thermal properties at nanoscale.

A nanostructured sample composed of Si/SiO$_2$ interface with a slope of 10° provided by VTT was investigated in order to confirm our results obtained with the previously discussed sample. Realistic sample geometry was developed in FEM that allowed to reproduce the experimental thermal profile. Our results showed once again that the probe is sensitive to the internal structure and gives a probed volume depending on material’s thermal properties. This study can be followed up by using inverse method to assess material’s thermal conductivities.

In the frame of QuantiHeat, the industrial company ‘Compart’ aims to characterize polymer particles coated with Nano films of Silver having thermal conductivities higher than $2\ W.m^{-1}.K^{-1}$with electrical resistivity (> 3300 S/cm). For this purpose we used scanning thermal microscopy to asses these particles thermal conductivity. A first set of polymer particles with different thicknesses of Silver coating was sent to be studied. The sample preparation was done in our laboratory following Compart instructions. SThM measurements showed that the probe washed away polymer particles while scanning along the sample surface which made very difficult to obtain thermal images. Our results showed that this kind of sample is not adapted to be investigated by SThM. Therefore we have proposed a development in the sample preparation that consists on adding particles to an adhesive matrix. It was composed of 30 µm polymer particles coated with 150 nm of silver in an adhesive matrix. This sample was also investigated using scanning thermal microscopy, due to a breakdown in our microscope the interpretation of thermal images was very difficult but the thermal profile is linked to internal geometry. Our results showed that the local thermal conductivity varies between 1.5 and 27 $W.m^{-1}.K^{-1}$due to the silver coating. It is very interesting to precede the investigation of this sample by developing a model in order to evaluate polymers thermal behavior. Due to a lack in time this couldn't be done in this work but it should be achieved in an upcoming study.

The thermal exchange radius b was calculated using the steps sample provided by VTT. When scanning along the sample surface, the material's thermal properties changes (depending of the depth of SiO_2). Therefore we decided to calculate the thermal exchange radius for two different positions of the probe. The first one corresponds to 200 nm Silicon dioxide thickness over Silicon substrate where b was evaluated to 890nm. The second position corresponds to 1.3 µm Silicon dioxide thickness over Silicon substrate where b was evaluated to 2.2 µm. It should be noted that the thermal contact resistance of the sample is supposed to be the same along the sample surface since it is covered with 200 nm of Silicon dioxide. Therefore it seems that b depends on the effective thermal conductivity, on the conductance of the sample and on subsurface structures and it varies depending on material's thermal properties.

6. References

[1] Gomès S, Trannoy N, Grossel P, Depassa F, Bainier C, Charraut D, D.C. Scanning thermal microscopy: characterization and interpretation of the measurement, Int. J. Therm.Sci. (40) 949–958, (2001).

[2] Wielgoszewski G, Babij M, Szeloch R, Gotszalk T, Standard-based direct calibration method for scanning thermal microscopy nanoprobes, Sensors and Actuators A: Physical 1-6, (2014).

[3] Tovee P, Kolosov O, Mapping nanoscale thermal transfer in-liquid environment immersion scanning thermal microscopy, Nanotechnology 24 (2013).

[4] A. Hammiche, H. M. Pollock, M. Song, D. J. Hourston, Sub-surface imaging by scanning thermal microscopy, Meas. Sci. Technol. (7) 142-150 (1996).

[5] E. Puyoo, S. Grauby, J. Rampnoux, E. Rouvière and S. Dilhaire, Thermal exchange radius measurement: Application to nanowire thermal imaging, Review of Scientific Instruments 81, 073701 (2010).

[6] P. klapetek, J. M%artinek, P. Grolich, M. Valtr, Graphic cards based topography artefacts simulations in Scanning Thermal Microccopy, Int. J. of Heat and Mass Transfer (108) 841-850, (2017)

[7] Cretin B, Gomès S, Trannoy N, Vairac P, Scanning Thermal Microscopy, Microscale and Nanoscale Heat Transfer 181-238, (2007).

[8] Yunfei Ge, Yuan Zhang, Jonathan M. R. Weaver, Haiping Zhou, and Phillip S. Dobson Topography-free sample for thermal spatial response measurement of scanning thermal microscopy, Journal of Vacuum Science & Technology B (33), 06FA03 (2015).

[9] A. Soudi, R. D. Dawson, and Y. Gu, Quantitative heat dissipation characteristics *in* current-carrying GaN nanowires probed by combining, Nano 5, 255 (2011).

[10] S. Somnath and W. P. King, An investigation of heat transfer between a microcantilever and a substrate for improved thermal topography imaging, Nanotechnology 25, 365501 (2014).

[11] A. Assy, S. Gomez, Heat transfer at nanoscale contacts investigated with scanning thermal microscopy, Applied Physics Letters 107 (2015).

[12] O. Raphael O, N Trannoy, P.Grossel, Thermal resonance at the microscale in AC scanning thermal microscopy with a thermal resistive probe, Int. J. Thermophysics (33), 1259-1269, (2012).

[13] D. Baillis, J. Randrianalisoa, Prediction of thermal conductivity of nanostructures: Influence of phonon dispersion approximation, Journal of Heat and Mass Transfer (52), 2516-2527, (2009).

[14] H.C. Chien, D.J.Yao, M.J. Huang, T.Y. Chang, Thermal conductivity measurement and interface thermal resistance estimation using SiO2 thin film, Rev. Sci. Instrum.79 (5), 054902, (2008).

[15] T. Yamane, N. Nagai, S.I. Katayama, M. Todoki,, Measurement of thermal conductivity of silicon dioxide thin films using a 3ω method, J. Appl. Phys. 91(2002) 9772–9776

[16] K. Kim, W. Jeong, W. Lee, S. Sadat, D. Thompson, E. Meyhofer and P. Reddy, Appl. Phys. Lett. , 105, 20, (2014).

[17] Yovanovich, M. and E. Marotta, Thermal spreading and contact resistances. Heat Transfer Handbook, (1), 261-394, (2003).

[18] Wilson AA[1], Muñoz Rojo M, Abad B, Perez JA, Maiz J, Schomacker J, Martín-Gonzalez M, Borca-Tasciuc DA, Borca-TasciucT.,Thermal conductivity measurements of high and low thermal conductivity films using a scanning hot probe method in the 3ω mode and novel calibration strategies, Nanoscale.(37), (2015).

[19] Yanliang Zhang[1], Eduardo E. Castillo[1], Rutvik J. Mehta[2], Ganpati Ramanath[2], *and* Theodorian Borca-Tasciuc[1,], noncontact thermal microprobe for local thermal conductivity measurement, Review of Scientific Instruments (82), 024902 (2011).

Résumé du chapitre 4

Le chapitre 4 porte dans une première partie sur l'étude du signal thermique obtenu par la sonde nanométrique en Palladium. Un dispositif expérimental a été développé pour étudier la réponse de la sonde Palladium en fréquence lors de son approche vers un échantillon dans le régime alternatif sous pression atmosphérique. Le dispositif est composé d'un pont de Wheatstone et d'une détection synchrone. Le pont de Wheatstone a été développé au sein de notre laboratoire. Il permet d'avoir une résistance variable avec des incréments de 0.01 **Ω**. La détection synchrone permet d'extraire les composantes en amplitude et en phase de la réponse de la sonde en 3ω. Le dispositif expérimental est composé d'un porte-échantillon qui permet le déplacement de l'échantillon vers la sonde avec une résolution de 20 nm, d'une caméra de haute résolution permettant la surveillance visuelle du déplacement de l'échantillon vers la sonde. La sonde est fixée sur un support au-dessus de l'échantillon. L'ensemble sonde/porte échantillon et camera sont placés dans une enceinte de protection qui limite l'influence des mouvements d'air extérieurs.

Ce dispositif est utilisé pour réaliser des courbes d'approches de la sonde Palladium vers des échantillons de cuivre et de verre. L'étude est faite pour 4 fréquences : 400 Hz, 800 Hz, 1500 Hz et 3000 Hz. Les résultats montrent que le transfert de la chaleur vers l'air joue un rôle important dans les mécanismes du transfert thermique entre la sonde et l'échantillon sous condition atmosphérique. L'évolution de ces courbes montre une diminution de l'amplitude lorsque la sonde se rapproche vers l'échantillon. La diminution de cette amplitude est plus importante pour les faibles fréquences alors que la variation du déphasage est maximale pour les hautes fréquences. Ces variations se traduisent par l'augmentation des échanges de chaleur entre l'échantillon et la sonde à travers l'air environnant.

Les variations en amplitude et en phase ont été normalisées par rapport à la réponse de la sonde loin de l'échantillon c'est-à-dire en l'absence de toutes interactions. Cette étude a mis en évidence la présence d'un phénomène irrégulier dans les évolutions de la réponse de la sonde. Une augmentation de la température de la sonde lors de son approchement vers l'échantillon a été observée. Cette élévation atteint un maximum pour une distance caractéristique à chaque fréquence. Ces distances caractéristiques ont été comparées à la longueur de diffusion thermique dans l'air. Les résultats montrent une dépendance du phénomène aux propriétés thermiques de l'air environnant. Ce phénomène a été traduit par une résonnance d'ondes thermiques pour le système sonde/air/échantillon. Les variations en amplitude et en phase pour une fréquence de 3000 Hz ont été comparées pour les échantillons de cuivre et du verre afin d’étudier le rôle de l’échantillon dans ce phénomène. Les résultats montrent une indépendance des propriétés thermiques du matériau sur l’établissement de ce phénomène.

Dans le cadre du projet Européen QuantiHeat, une étude a été menée afin d’étudier le domaine de validité des modèles numériques. Ils comprennent des modèles sub-continuum comme la balistique et des modèles continuum comme les méthodes par éléments finis ou différences finis. Pour ce faire, des modèles ont été développés pour la nanosonde en Silicium lors de son rapprochement vers un échantillon de silicium. La comparaison des résultats nécessitait un développement d’une géométrie commune pour le système sonde échantillon. La sonde est composée d’un hémisphère en silicium avec 50 nm de diamètre qui est autour de la limite de la conduction balistique. La sonde est placée au-dessus d’un échantillon de silicium semi-infini avec 150 nm en longueur et largeur et 100 nm d’épaisseur. Le milieu environnant entre la sonde et l’échantillon est considéré diffusif. Nous avons réalisés des simulations par FEM pour des distances de 1nmjusqu'à15 nm entre la sonde et l’échantillon. Le modèle numérique permet d’évaluer le flux de chaleur dissipée par la sonde en silicium vers l’air environnent. Les résultats montrent une diminution de ce flux de chaleur en s’éloignant de la surface de l’échantillon. La comparaison de nos résultats avec les résultats obtenus pour la méthode de différence finie réalisé par CMI montrent que les deux méthodes numériques utilisées sont adaptées pour simuler des sondes des dimensions nanométriques. Mais les résultats de simulation doivent être comparés avec des résultats expérimentaux afin de vérifier le domaine de validité des modèles numériques.

La troisième partie de ce chapitre se situe également dans le cadre du projet QuantiHeat, elle consiste à développer des outils de modélisation permettant aux utilisateurs de SThM d’avoir une idée sur le comportement thermique du matériau lors de la réalisation de mesures par SThM. Les matériaux étudiés sont des matériaux massifs en silicium et dioxyde de silicium, des films suspendus et des polymères. La modélisation a été faite en utilisant COMSOL. Elle consiste à placer une source chaude à la surface des matériaux.

Pour les matériaux massifs, la conductivité thermique du silicium et du dioxyde de silicium ont été tracée en fonction de la température. Les données des conductivités thermiques des matériaux sont issues de la littérature. Elles sont implémentées dans les modèles sous la forme de fonctions polynomiales. Les polymères amorphes et les polymères à inclusions cristallines sont également étudiés dans cette section. Ces types de matériaux ont une conductivité thermique anisotrope. Les conductivités thermiques dans les directions x, y et z ont été tracées en fonction du pourcentage en volume de cristallinité. A partir de ces courbes, une fonction polynôme d'ajustement a été obtenue pour chaque direction. Les conductivités thermiques ainsi obtenues ont été implémentés dans le modèle numérique.

La même méthode a été appliquée aux films minces suspendus. Ils sont considères comme des matériaux bidimensionnels, ou le transfert de chaleur dépend de la direction. Par conséquent, les conductivités thermiques dans le plan et hors plan pour les couches minces de silicium sont nécessaires pour la modélisation. La conductivité thermique des couches minces de silicium dans le plan et hors plan de 20 nm, 100 nm et 420 nm sont issus de la littérature [4]. Puis tracées en fonction de la température. A partir des courbes, une fonction polynomiale d'ajustement est obtenue pour chaque conductivité thermique (dans le plan et hors du plan). Puis également programmé dans le modèle 2D.

Tous les modèles développés permettaient de calculer le flux de chaleur dissipée par la source de chaleur placée à la surface de l’échantillon. Les flux de chaleur sont tracés en fonction de la variation du diamètre de la source de chaleur. Ces modèles ont été transmis à l’université de Lancaster qui gère leur diffusion sur une ‘plateforme’ accessible aux groupes des chercheurs intéressés. Ces chercheurs n'auront qu'à modifier les paramètres de simulation tels que la température ambiante, l'épaisseur des matériaux et de nombreux autres paramètres.

Chapter 4: Scanning thermal microscopy with Nano Probes

This chapter is dedicated to the study of probe/sample system using probes with nanoscale curvature radius and to the development of materials library in COMSOL.

The first part consists on the investigation of heat transfer mechanisms between Palladium probe and a sample as a function of distance between them in AC mode. For this, a homemade electronic dispositive was created in our laboratory to study the probe's response at the third harmonic. From experimental results, we studied interactions at high distances for the probe while approaching toward different samples. The investigation of probe's response highlights on a resonance phenomenon associated to the temperature field of probe/air/sample system in the AC operating mode.

The second part of this chapter is in the frame of QuantiHeat project. It consisted on evaluating the validity domain of numerical models using Silicon nanoprobes. For this purpose, a model of Silicon probe while approaching toward a Silicon sample was developed using different simulation methods such as finite element or finite difference. Our part of the work consisted of using the finite element method. From the modelling we investigated the heat flux dissipated from the probe and compared results with different simulations performed by other partners.

The third part which is in the frame of QuantiHeat project consists developing a modelling tool that allows having a prediction about material's thermal properties. We study the case of a heat source placed on the upper surface of bulk materials and free standing films. A library of materials was developed in COMSOL using thermal properties based on the literature. We evaluate thermal conductivities from polynomial functions using fitting procedure which will be implemented in the modelling. This allows investigating material's thermal behavior.

1. Study of the probe-sample system with the Palladium probe

A previous study by Raphael et *al.* investigated the Wollaston probe thermal response while approaching toward a sample of copper using 3ω method in the AC operating mode [3]. Their study pointed out on a resonance phenomenon that takes place between the probe and the sample, which was shown to be dependent to the used frequency. It was interesting to verify whether this phenomenon is also observed with nanometric probes such as Palladium probe. To this end an electronic and experimental set up were developed to investigate the 3ω signal of Palladium probe while approaching a sample. It consists of a lock in amplifier and a homemade Wheatstone bridge. The bridge was specially developed in our laboratory in order to make easier the interpretation of measurements.

1.1. Electronic set up

1.1.1. Wheatstone bridge

The electronic set up used for measurements is presented in figure 4-1. It is composed of a homemade Wheatstone bridge and a lock in detection (refer to Appendix A).

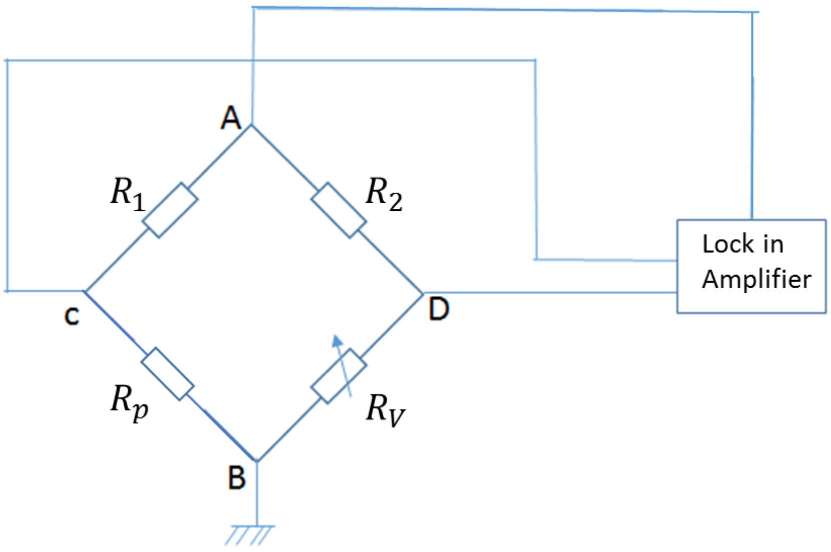

Figure 4- 1: Schematic representation of the electronic set up used for measurements in AC operating mode. It's composed of a Wheatstone bridge, a lock in amplifier.

The Wheatstone bridge was developed in a way to ensure a high protection for the probe and to simplify the measurements. Therefore, a switch was set up in order to short-circuit the probe to ensure its protection while connecting the wires of the probe to the bridge. Another switch was placed to short-circuit the bridge allowing the measurement of the control resistance.

The choice of resistances in the bridge must be done considering the sensitivity to variations in the probe resistance and the type of available power supply. For reasons of stability we preferred to limit as much as possible the power applied to the bridge. Therefore, values of $R_1$and R_2 were chosen to be respectively 2 KΩ and 10 KΩ. Those two resistances define the ratio of the bridge which is 5 in this one. The control resistance R_V is selected by the user using three buttons allowing to work with a defined range of control resistance. The control resistance can be incremented with steps of 0.01 Ω which is more secure when working with probes that can be easily damaged if the current flowing exceeds 1 mA. This set up allows to know at each moment the current flowing in the probe.

1.2. Experimental set up

Figure 4-2 represents the experimental set up used in this study. It is composed of:

- Sample holder
- Protection air box
- High resolution camera

The probe holder is used to maintain the probe position stable. The sample holder is used to ensure the approach between the probe and the sample. A high resolution camerais placed to allow an optical supervision of the probe while the sample is approaching. A detailed description about those devices will be presented in the next paragraphs.

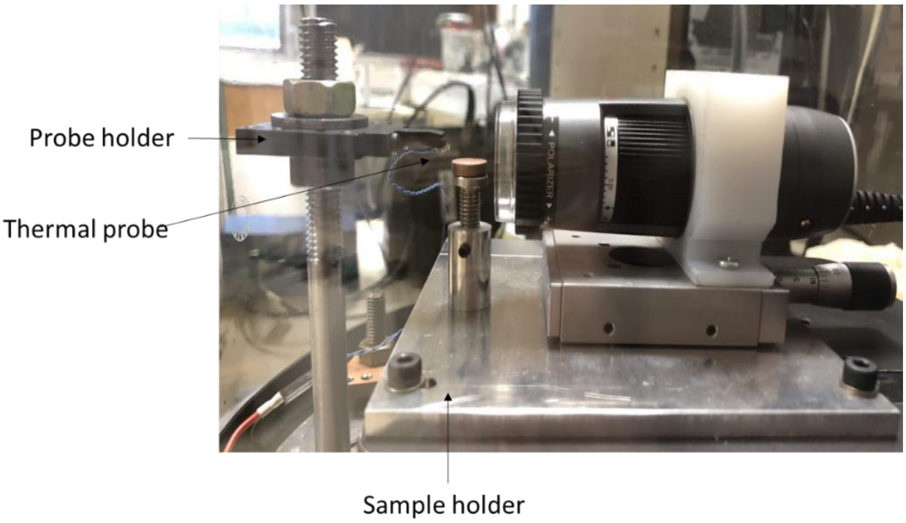

Figure 4- 2: Schematic representation of the experimental set up composed of the probe holder, a camera and the sample holder with a motorized stage.

1.2.1. Sample holder

To perform a stable approach of the probe toward the sample with high precision, a sample holder was developed in our laboratory during the thesis of O. Raphael. A motorized movement stage marketed by Newport was used. This ultra-compact stage allows vertical displacements with nanometric precision due to the presence of a linear optical ruler which eliminates the errors due to mechanical positioning. This device provides a vertical displacement of 4.8 mm in steps of 20 nm. This board is associated with control electronics that manages the power supply, the measurement and the respect of the sample position. It also manages the adjustment of speed and steps, and the displacement by steps.

This sample holder is controlled by a computer that allows through a software to program the approach and withdrawal cycles. The software allows control the steps during the approach in order to ensure large displacement when the probe is at large distances and small ones at small distances from the sample. It also control the time of displacement needed between each step. Lateral displacements of sample are ensured by two manual plates. These plates are composed of steel for high rigidity and stability. They are composed of a double row ball bearing linear stage providing a great stability along a 25 mm travel distance. These plates have micrometric stops that offer a sensitivity of 1µm. All stages are settled under a massive solid. This large block has been excavated to provide the necessary space for the sample holder. The choice of a massive block is justified by the inertial gain needed to ensure the stability of the microscope.

1.2.2. Protection air box

As stated in previous studies [1] nanoprobes are very sensitive to external ambient conditions. Thus the thermal probe response depends on the different heat transfer mechanisms between the probe and the surrounding environment. In this study a protection air box was used to prevent any distortion of the air movement. Therefore measurements are done in an environment which is perfectly stable.

1.2.3. High resolution camera

The palladium probes have a tip apex with radius smaller than 100 nm. When performing approach curves, a camera was placedto observe the probe optically in order to monitor the tip/sample contact. Therefore we used a camera commercialized by Dino-lite universal. The camera has a resolution of 1.3 Megapixels and a magnification of 200. It was placed face to the tip/sample system. This camera has a USB connection which is linked directly to the computer and can be motored using specific software. The camera is equipped with a built-in polarizer to reduce reflections in order to ensure a better visibility.

1.3. Experimental results

In this section, approach and withdrawal curves were performed using the 3ω method. In this experiment the probe is fixed and the sample is moved toward the probe until the contact point. Once the signal is stabilized, the sample was moved again away from the probe. Figure 4-3 shows the recorder output voltage of the probe for approach-retract curves for a sample of copper (400 $W.m^{-1}.K^{-1}$) with the Palladium probe. E. Puyoo in his thesis studied the cut-off frequency of the Palladium probe, this value was evaluated to 2fc=2750Hz [2]. Therefore the frequency used in this study was set to 1500 Hz. The current flowing into the probe was set to 530 µA. Using equation 9 from chapter 1 the probe temperature is calculated to $T_{pd/SiO2} = 105°C$in this study.

The approach was done with large steps for distances away from the sample and with steps of 30 nm for distances close to sample. The red and blue curves correspond to the approach and retract curves. The positions from 1 to 5 will allow us to further detail steps constituting the approach and retract phases of the probe from the sample surface.

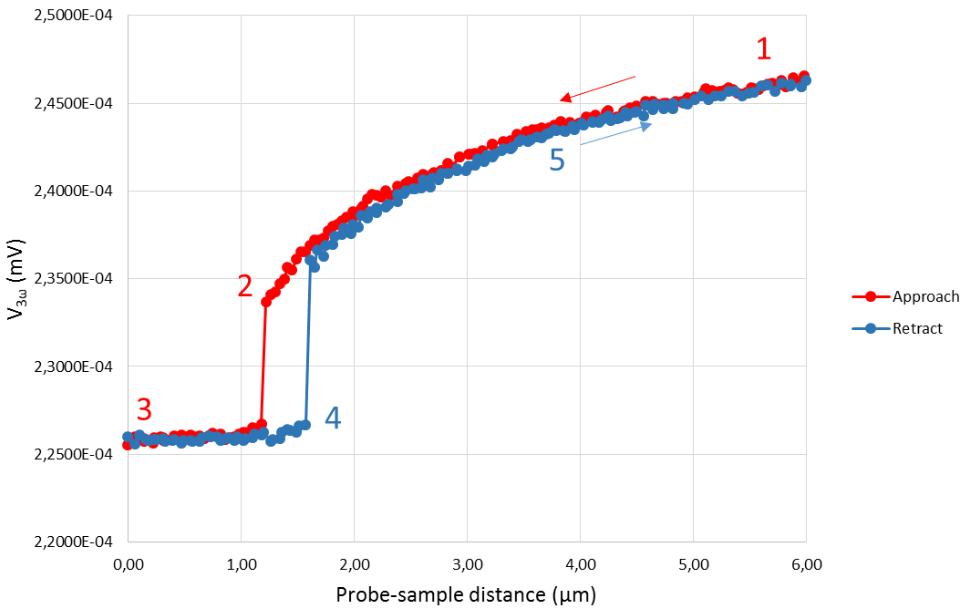

Figure 4- 3: Evolution of the probe response while approaching and retracting toward a sample of copper under ambient conditions for a frequency of 1500 Hz with a current of 530 µA.

In position 1, the probe is out of contact, at a distance of few microns away from the surface. The probe is then moved toward the sample to position 2 where it precisely enters in contact with the sample. As observed, a quantity of heat is transferred from the probe into the sample well before the contact. As the probe approaches to position 2, the amount of heat transmitted to the sample increases. Indeed, a significant decrease in the probe temperature is observed. Although this kind of probe has a nanometric tip radius, the tip is sensitive to the presence of sample surface even for distances higher than 6 µm separating the probe from the sample.

In position 2, the probe comes into contact with the sample. The 3ω signal drops sharply because a large amount of heat is transferred from the probe into the sample. In fact, two additional transfer mechanisms are added: the solid-solid contact and the water meniscus. From position 2 to 3 the probe is mechanically pressed against the sample. Between these two positions, the 3ω signal is constant regardless the contact force.

From position 3, the probe is progressively removed from the surface of the sample to position 4 where it is ripped from the contact. The probe response at 3ω signal exhibit a hysteresis due to the presence of adhesion forces from the probe to the sample. In position 5, the probe is out of contact. The curves of approach and retract superimpose once again.

Previous works performed approach and retract curves with the palladium probe under vacuum conditions (figure 4-4) [2]. When retracting the probe from the sample, the 3ω signal remains stable unlike what happens in our study. The comparison of results showed that while working under vacuum, the heat transfer mechanism occurs mainly through the solid-solid contact [1, 2]. The curves of approach and withdrawal in this study allowed verifying that under ambient conditions the conduction through air plays an important part in the heat transfer mechanisms between the probe and the sample.

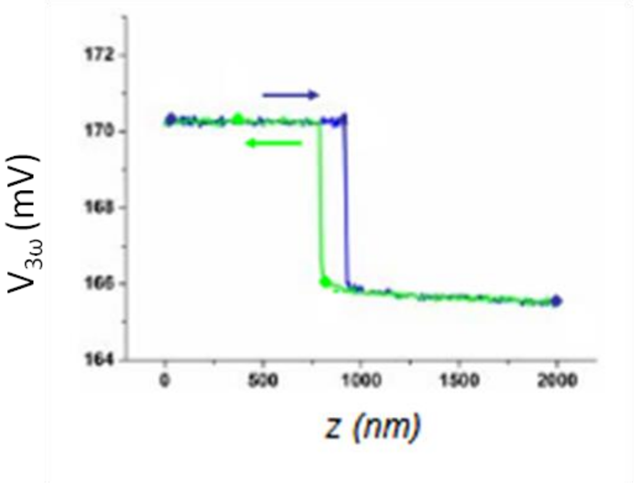

Figure 4- 4: Approach (blue line) and retracting (green line) curves of the palladium probe while approaching toward a sample of Silicon in AC operating mode with a current of 308 µA [2].

1.4. Highlighting thermal wave resonance phenomenon

In a previous study, Raphael *et al.* used the Wollaston probe to study the evolution in amplitude and phase of the probe response at the third harmonic as a function of the probe/sample distance for a sample of copper with different frequencies [3]. Their study highlighted on the presence of a resonance phenomenon that occurs between the probe and the sample. This phenomenon depends on the thermal frequency and a characteristic distance separating the probe from the sample which is linked to the thermal diffusion length. In this study we performed measurements using the Palladium probe in order to determine whether this phenomenon is observed with nanoscale probes.

Figure 4-5 represents the amplitude and phase evolution of the probe response at the third harmonic, as a function of the distance between the Palladium probe and a sample of copper for four frequencies. The distance ‘zero’ characterizes the contact point with the sample. The contact is defined when a sudden drop in the voltage signal is observed. This study is performed starting a distance of 2 mm away from the sample surface. As observed in figure 4-5, the probe’s response presents a noise when working at low frequency (400 Hz) it becomes more stable once the frequency increases. The 3000 Hz the probe’s response presents the most stable measurements. Regardless the frequency studied, the presence of sample does not influence significantly the probe response, and therefore its temperature for distances higher than 100 µm. For lower distances, the decrease in amplitude is more relevant for lower frequencies. While for the phase the variation is at its maximum for a frequency of 3000 Hz. The phase is therefore more sensitive to the presence of the sample for higher frequencies.

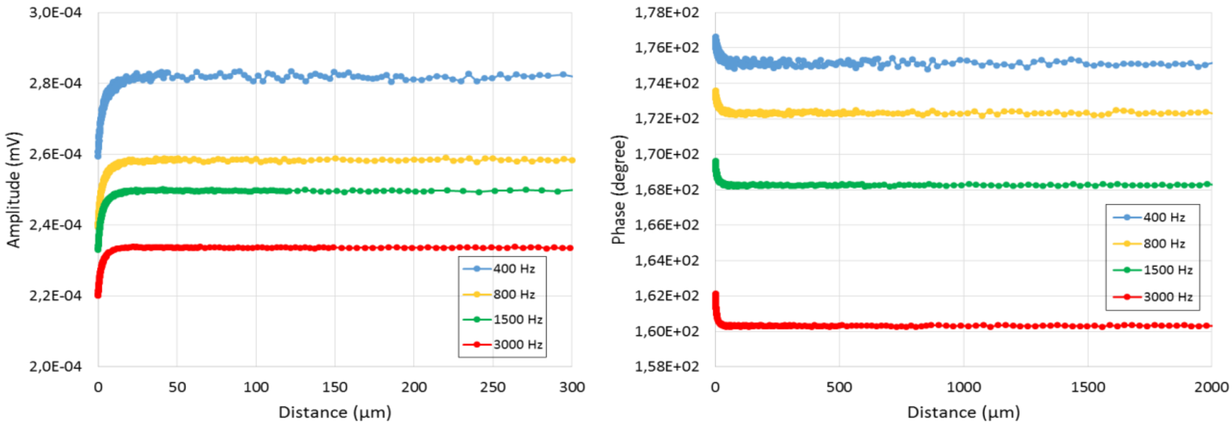

Figure 4- 5: Evolution in amplitude and phase of the probe response at the third harmonic as a function of the distance between the probe and a sample of copper for four different frequencies. The measurements were performed under ambient conditions for a current of 530 µA.

In order to compare more precisely the probe response for different frequencies, the temperature behavior for amplitude and phase is magnified by normalization. Results were normalized by the signal obtained when the probe is far from the sample which means when no interaction is observed between the probe and the sample. Figure 4-6 represents the normalized evolution of amplitude as a function of probe-sample distance (chapter 2-equation 28). As observed, with increasing the frequency, the probe response becomes more stable.

The study of the probe response highlights on an irregularity observed in the signal while approaching toward the sample. It is characterized by a rise in the amplitude and a decrease in the phase. This phenomenon is more marked on the amplitude (figure 4-6). This rise of temperature reaches a maximum for a characteristic distance dR depending on the frequency, this distance decreases with increasing the frequency. As observed, by increasing the frequency, the phenomenon becomes more localized. This study shows that the maximum amplitude is for 800 Hz and 1500 Hz for both amplitude and phase.

The comparison of the characteristic distance of each frequency to the thermal diffusion length of ambient air allows linking the dependence of this phenomenon on the thermal properties of the surrounding medium. The thermal diffusion length is defined as:

$$\mu_{th} = (\sqrt{a_a/\pi f_{th}}) \tag{29}$$

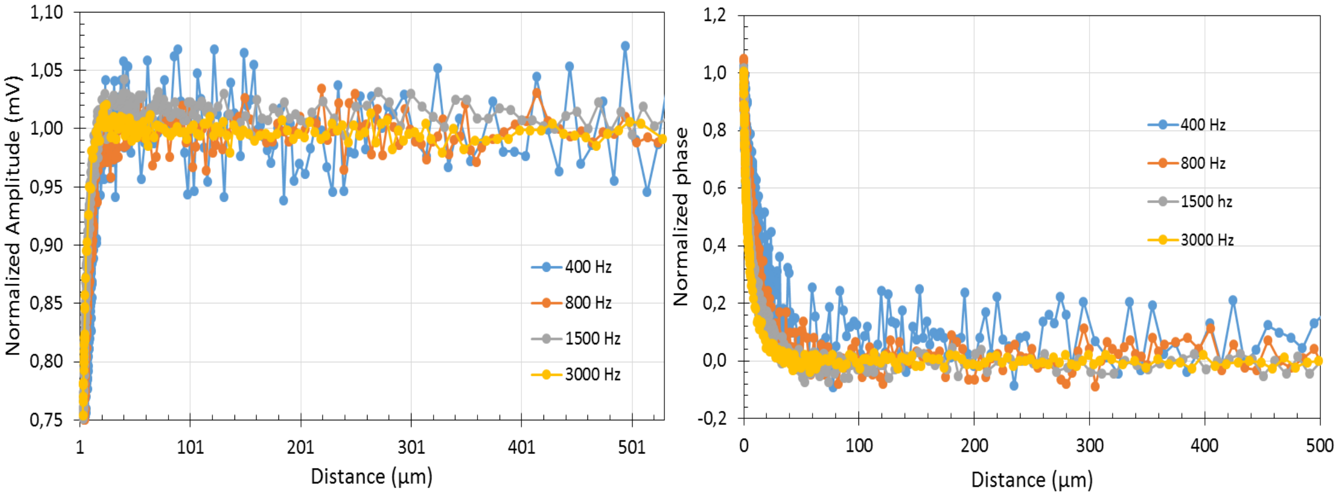

Figure 4- 6: Normalized evolution of amplitude and phase of the probe response at the third harmonic as a function of the distance between the probe and a sample of copper for 4 different frequencies. Measurements were done under ambient conditions with a current of 530 µA.

Where a_a represents the thermal diffusivity of air ($a_a = 2.21.10^{-5} m^2 s^{-1}$) and f_{th} if the thermal frequency. Figure 4-7 represents the comparison between the characteristic distance and the thermal diffusion length, these results are approximatively close. Thus they reveal a correlation between the resonance phenomenon and the thermal properties of the surrounding environment (air).

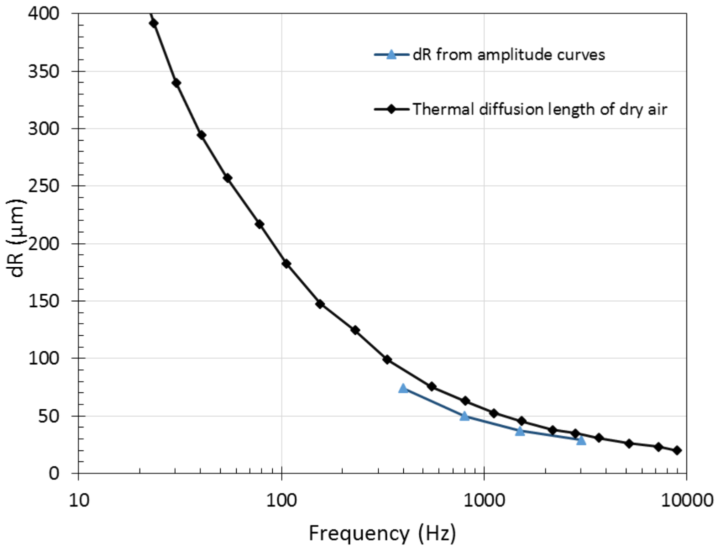

Figure 4- 7: Comparison of characteristic distances dR from the amplitude curve to the thermal diffusion length of dry air as a function of excitation frequency.

The local rise in amplitude is linked to a resonance phenomenon in the propagation of thermal diffusive waves. In fact, in the AC operating mode, the probe temperature oscillates periodically. In conductive medium, it is the whole system of probe, surrounding air, and the sample that is affected by the alternating field and can be assimilated to a thermal diffusion wave field.

The influence of the sample material on the establishment of this phenomenon was also studied. To do this, the evolution of the probe response at the third harmonic was also studied for a sample of glass ($1.4\,W.m^{-1}.K^{-1}$) and compared to copper sample. Figure 4-8 represents the comparison of the probe response evolution for a frequency of 3000 Hz. We observe that evolutions in amplitude and phase are practically superimposed. The observed phenomenon seems independent of thermal properties of the studied sample.

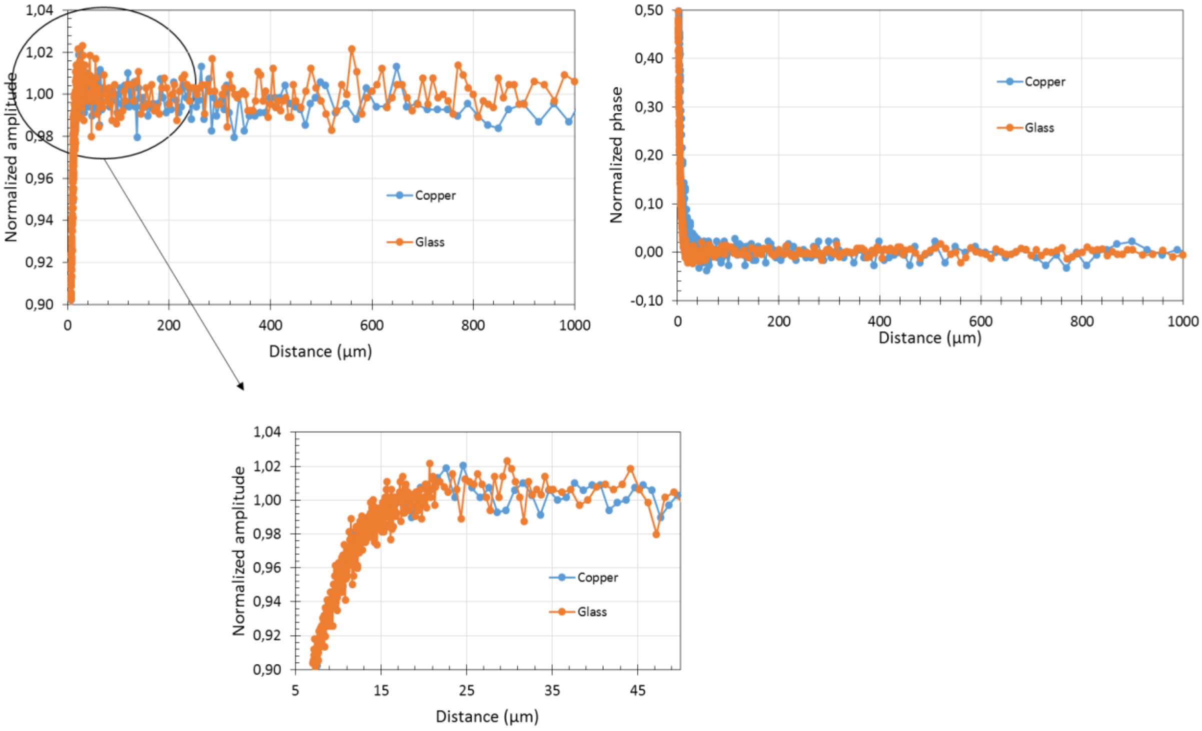

Figure 4- 8: Comparison of the probe response evolution in amplitude and phase at the third harmonic as a function of the distance for two samples with different thermal conductivities (copper, glass) for a frequency of 3000 Hz under ambient conditions with a current of 530 µA.

We performed the same experiment at Glasgow University. Professor Jonathon Weaver has developed an experimental system to perform preliminary measurements in the AC operating mode at the third harmonic for the Palladium probe. This team has developed a Wheatstone bridge with the particularity that the equilibrium of this bridge was adapted to each probe resistance used in measurements. This allowed having stability of probe signal. The experiments were done for different frequencies ranging from 800 Hz to 15 KHz. The increase in the AC probe temperature when attending a characteristic distance was observed for all frequencies. But the increase was more observed for the lowest frequencies. Those experiments allowed having an idea about the phenomenon that we wanted to interpret. Note that the electronic circuit we used in our measurements did not allow the change in resistances of the bridge. This may be the origin of the noise observed in our measurements.

Through these experiments we showed that the resonance phenomenon of the probe/air/sample system takes place when working with micrometric and nanometric probes. This phenomenon is more revealed when working with Wollaston probes. This is due to the fact that the probe signal obtained for Wollaston probes is much higher than for Palladium probes.

2. Numerical analysis of probe-sample system with silicon nanoprobes

In the aim of evaluating the validity domain of numerical modelling, a study was established in the frame of European project QuantiHeat using a model nano probe. Partners involved in this work should develop models by different methods. They include sub-continuum models such as ballistics and continuum models such as finite element, finite difference. The comparison of results required the development of a common geometry for the probe-sample system while approaching toward a sample of Silicon. For this purpose we developed a model using finite element method while CMI partners used finite difference method (FDM). The length scale of the model of the probe in Silicon is 50 nm in diameter, and was chosen around the ballistic heat conduction limit. Therefore it is important to treat carefully boundary conditions between the probe and the sample.

2.1. Geometry and boundary conditions

The geometry used for this modelling is described in figure 4-9. It consists of a 3D model with cylindrical symmetry, formed by a silicon hemisphere of 25 nm radius placed above a semi-infinite layer of Silicon. The geometry was intentionally chosen simple and it presents basically the probe/sample system in SThM. The probe/ sample system is placed in an environmental box. The sample is of 150 nm in length and width and it has a thickness of 100 nm. The temperature on the bottom surface of Silicon film is set to 300 K. The upper surface of the sphere and the bottom layer is set to 350 K. A diffusive medium is considered for the surrounding environment where the air is initially at 300 K. A heat flux of 'zero' is applied to the boundaries of the sample. The thermal conductivity of Silicon layer was set to 40 $W.m^{-1}.K^{-1}$[4].

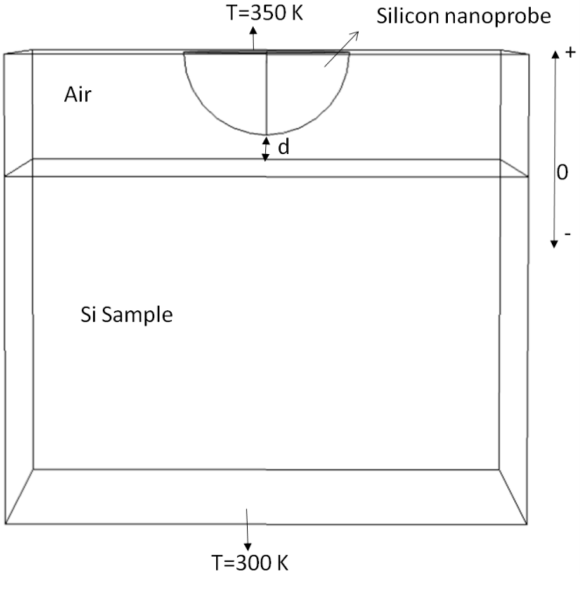

Figure 4- 9: Schematic representation of the silicon nanoprobe above a silicon sample.

2.2. Mesh of the probe/sample system

The choice of mesh is essential for the pertinence of results. In order to define the best compromise between the precision of results and the cost of calculation, a parametrical study was performed with different size of mesh. For that we used a free tetrahedral mesh and we changed the mesh size in the geometry for a fixed distance between of probe-sample system.

The most adaptive mesh in our case was a personalized fine mesh with a maximum size of element of 2 nm and a minimum size of element of 0.7 nm.

2.3. Results

Solving the heat transfer equations presented in chapter 2 (equation 24) allows to determine the temperature distribution of the geometry. Figure 4-10depicts the temperature distribution of the probe/sample system. The given configuration is for the contact point with the silicon layer. At the contact point, the probe dissipates the heat into the sample and a diminution in its temperature occurs.

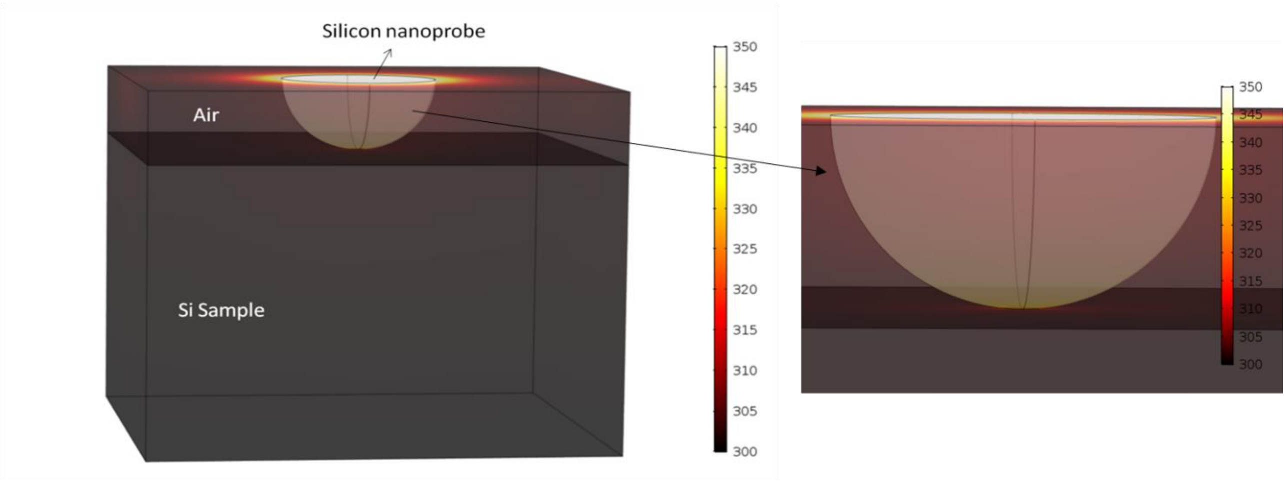

Figure 4- 10: Temperature distribution of the silicon probe when in contact with Silicon sample and a zoom of the probe.

The model allows obtaining the heat flow rate dissipated by the probe into the environment for several probe-sample distances between 1 and 15 nm away from the sample surface. Results of this heat flux as a function of probe-sample distance are given in figure 4-11. They were compared to FEM modelling from the literature obtained by P. Klapetek *et al.* (CMI partner) (redline) [5]. The ‘zero’ distance in this curve corresponds to the contact point between the probe and the sample. The heat flux dissipated from the silicon nanoprobe decreases rapidly as the distance from the sample surface increases then it smoothly decreases for distances higher than 6 nm between the probe and the sample. As observed results of FEM obtained by our modelling are relatively close to those of CMI partners. The difference between both models is probably due to the mesh used by each research group.

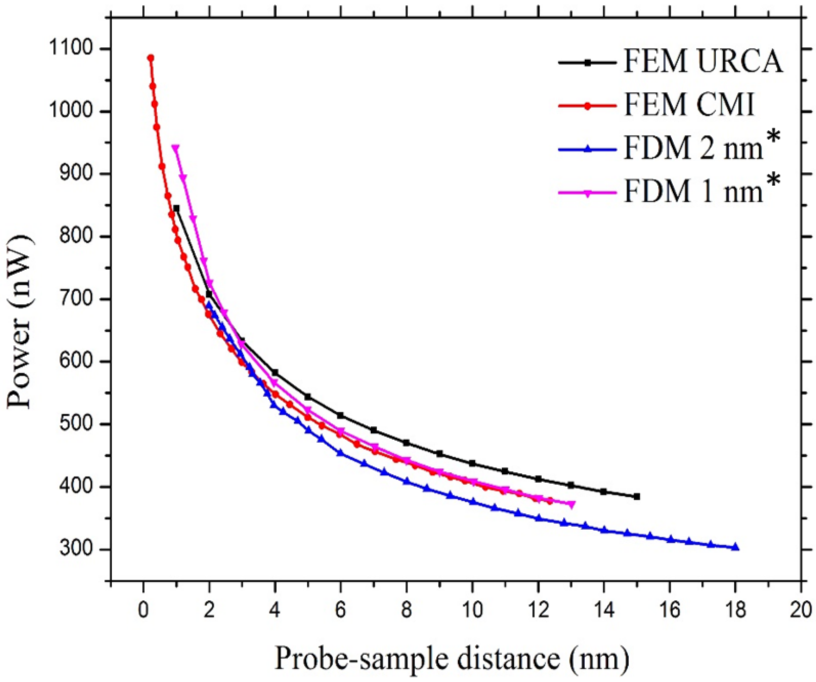

Figure 4- 11: Comparison of our FEM results with FEM and FDM (1 nm and 2 nm mesh size) obtained by CMI partner for the heat flux dissipated from the half sphere as a function of the probe/sample distance.

FEM results were also compared to finite difference method (FDM) given by CMI. The Finite different method allows to obtain numerical solutions by solving differential equations. It consists on discretization a physical domain into finite number of elements. CMI partners built a code based on FDM and they used rectangular mesh with respectively 1 nm and 2 nm mesh size. The comparison of results for different methods shows the same tendency for all curves where the heat flux transmitted from the probe decreases as the probe-sample distance increases. FDM with 2 nm mesh size seems to underestimate results while FDM 1 nm has relatively same results as FEM. It should be noted that the present model cannot be assumed completed. Therefore part of heat losses by the probe cannot be presented in this model such as the heat transferred from the cantilever through air. Thus this model allows having a simplified and fast numerical tool for the interpretation of data when the continuum regime is applicable. To determine the most reliable method, those results should be compared directly to experimental SThM measurements. Therefore experimental measurements should be performed in a further study to allow the determination of numerical methods validity domain.

3. Prediction of material’s effective thermal properties

SThM users need to have a prediction about the material’s thermal behavior and effective thermal properties when performing SThM measurements. For this in the frame of QuantiHeat modelling tools were essential to be developed, it consists on bulk materials such as silicon and silicon dioxide, free standing films and polymers. This study is a collaboration work with D. PRATAP, postdoctoral who works in our team. The modelling was done using FEM. The main idea is to allow SThM users to have previously built models having properties established from materials library so they will only have to change the simulation parameters such as ambient temperature, thickness of the materials and many other parameters.

3.1. Modelling of 3D materials

The geometry used for the modelling of bulk material is presented in figure 4-12. It consists of a heat source of a circular shape of diameter varying between 30 nm and 3000 nm. The heat source is placed on the upper surface of a bulk sample having a length, width and thickness of 100 µm. For the heat source a temperature of 350 K is imposed. The top surface of the sample has a zero heat flux. While side walls and the sample bottom is set to ambient temperature with $T_{amb} = 293\ K$.

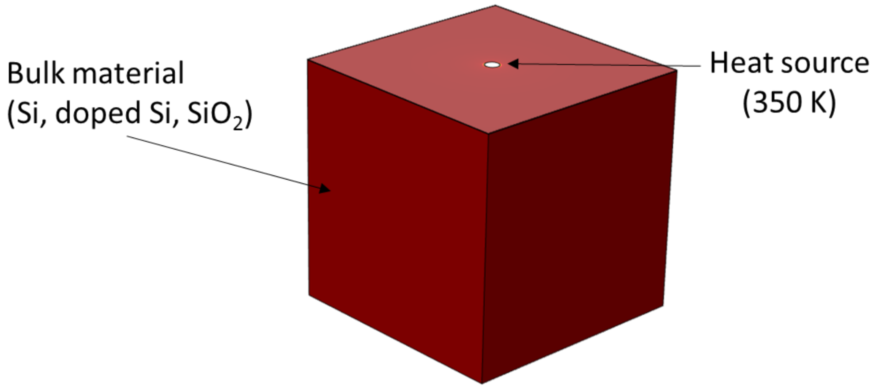

Figure 4- 12: Schematic representation of a bulk material with a heat source place at the sample surface.

For this geometry, four simulations were done for the Silicon, Silicon dioxide, B-doped Siof different densities and polymers with inclusions of various densities. Thermal conductivities of these materials are obtained from polynomial functions using fitting procedure. The data of thermal conductivities where obtained from previous studies [6, 7, 8 et 9] and plotted as a function of different temperature (figure 4-13).

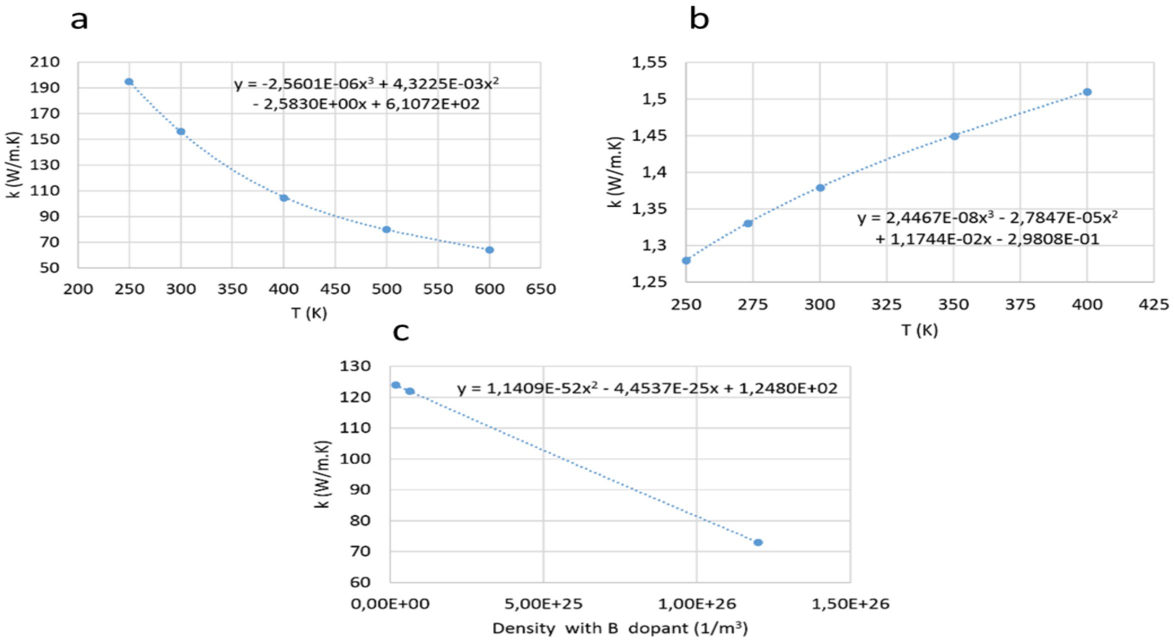

Figure 4- 13: Thermal conductivity of bulk a) silicon and b) bulk silicon dioxide as a function of the temperature. Thermal conductivity of doped silicon with Boron as a function of density at a temperature of 300 K.

For Silicon, Silicon dioxide, the polynomial function used is of third order and it is given in the following equation:

$$k = a_0 + a_1 T + a_2 T^2 + a_3 T^3 \tag{30}$$

Where T is the absolute temperature in Kelvin

For the B-doped silicon the equation is given by:

$$k = a_0 + a_1 \eta + a_2 \eta^2 + a_3 \eta^3 \tag{31}$$

Where ηdenotes the doping density of Bore. Table 1 summarizes the polynomials coefficients for the listed above equations. Those values were implemented in COMSOL as model variables. The B-doped Si were calculated for two densities with $\eta = 0$ and$\eta = 1.10^{25}$.

Table 4- 1: Coefficients of 3rd order polynomial for thermal conductivity of Si, SiO_2 and Si (B). Coefficients of Si and SiO_2 provide thermal conductivity versus temperature while coefficients for B-doped Si provide thermal conductivity versus doping density at 300 K

Sample	a_0	a_1	a_2	a_3
Si	6,1072E+02	- 2,5830E+00	4,3225E-03	-2,5601E-06
SiO_2	- 2,9808E-01	1,1744E-02	- 2,7847E-05	2,4467E-08
Si (B)	1,2480E+02	- 4,4537E-25	1,1409E-52	0

The numerical model allows evaluating the total heat flux dissipated from the heat source. Results obtained for the bulk silicon, SiO_2, doped silicon (ρ=0), and doped silicon (ρ=1.10^{25}) are given in figure 4-14 as a function of the heat source diameter. For all cases, the dissipated heat flux decreases with increasing the diameter of the heat source. The heat flux decreases sharply for a diameter ranging between 30 nm and 200 nm. When the diameter of the heat source reaches a distance higher than 1000 nm, the rate of the heat flux remains constant and tends to zero for all the cases. As observed for the doped silicon with a density of zero, the total heat flux is higher than that of density 1.10^{25}.

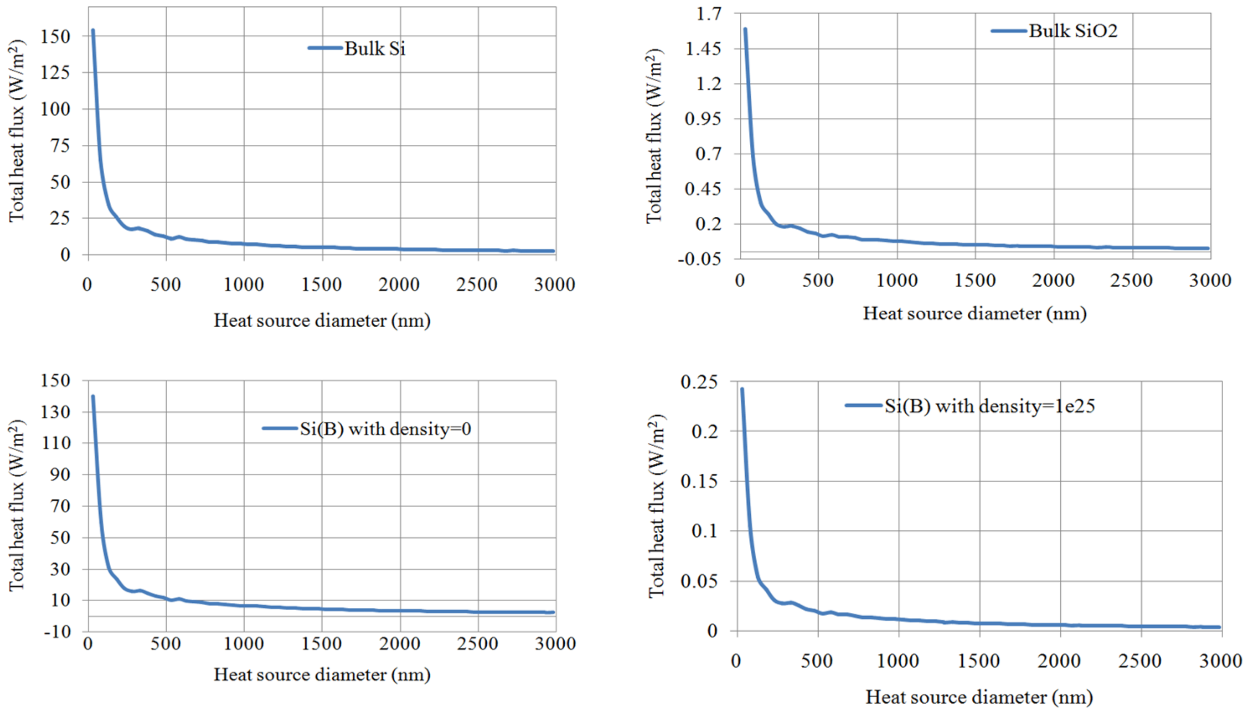

Figure 4- 14: The total heat flux of the heat source as a function of its diameter variation for a) bulk silicon b) bulk SiO2, c) B-doped silicon with a density of zero, d) B-doped silicon with a density of 1e^{25}.

The amorphous polymers and polymers with crystalline inclusions are also studied in this section. These kinds of materials have anisotropic thermal conductivity. Thermal conductivities used for the fitting were taken from previous study [10] in which thermal conductivities in x, y and z directions were plotted as a function of volume percent crystallinity as presented in figure 4-15.

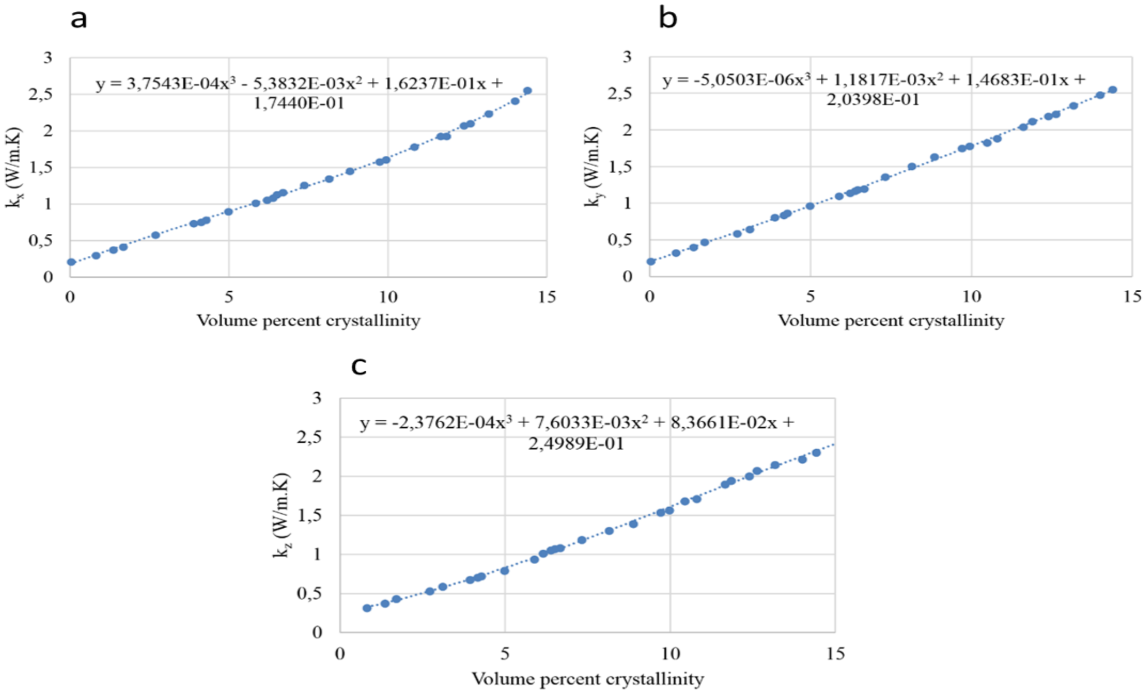

Figure 4- 15: Thermal conductivity (a) k_x, (b) k_y and (c) k_z of bulk polymer as a function of volume percent crystallinity.

From these curves a fitting polynomial was obtained for each direction. The equation of fitting polynomial function for polymers is given in the equation:

$$k_{pol} = d_0 + d_1\eta + d_2\eta^2 + d_3\eta^3 \tag{32}$$

Where η represents the inclusion density. Table 2 summarizes coefficients of the third order polynomial thermal conductivities in x, y and z directions.

Table 4- 2: Coefficients of 3rd order polynomial for thermal conductivities k_x, k_y, k_z of polymer with volume percent crystallinity.

Directional thermal conductivity	***d₀***	***d₁***	***d₂***	***d₃***
k_x	1,7440E-01	1,6237E-01	- 5,3832E-03	3,7543E-04
k_y	2,0398E-01	1,4683E-01	1,1817E-03	-5,0503E-06
k_z	2,4989E-01	8,3661E-02	7,6033E-03	-2,3762E-04

Figure 4-16 represents the total heat flux dissipated from the heat source for different diameters. Simulations were performed for three densities of inclusions (0%, 5% and 10%). As observed, the rate of the heat flux increases with increasing the density of inclusions (figure 4-16). For all cases the heat flux decreases with increasing the diameter of the heat source with a drastic drop for low diameters. The total heat flux tends to zero for diameters higher than 1000 nm.

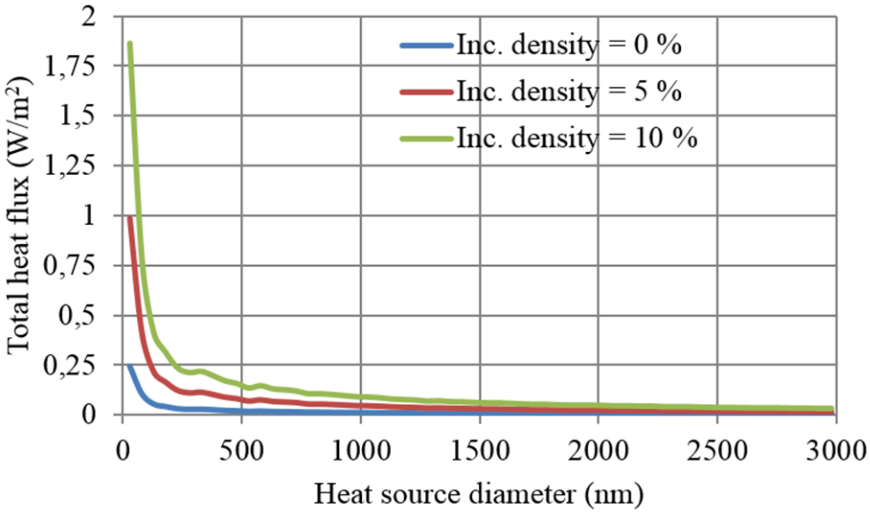

Figure 4- 16: The total heat flux of the heat source as a function of its diameter variation with three different inclusion densities in polymers.

3.2. Modelling of 2D materials

The modelling of 2D materials is represented by the investigation of free standing films where the thin film is studied without any substrate. It was essential to consider this geometry since thin films are highly used in modern devices.

The geometry consists on a silicon thin film having a heat source on its upper surface. Therefore a thin film of 100 µm in length and width is considered. The heat source has a circular shape with a diameter ranging from 30 nm to 300 nm. Figure 4-17 illustrates the schematic representation of the modelled geometry.

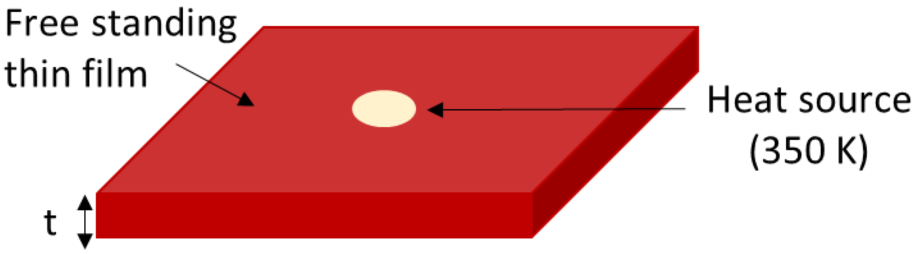

Figure 4- 17: Schematic representation of the free standing thin film used in the modelling with a heat source placed on its surface.

A zero heat flux was applied on the upper surface of the free standing film. The side walls and the bottom surface were set to ambient temperature $T_{amb} = 293\ K$. The temperature of the heat source was set to 350 K. Simulations were performed for three thicknesses (t) of the free standing (20 nm, 100 nm and 420 nm).

When working with two dimensional materials, the heat transfer depends on the direction. Therefore, the in-plane and out-of-plane thermal conductivities for silicon thin films are required for the modelling. The thermal conductivity of the in-plane and out-of-plane silicon thin films of 20 nm, 100 nm and 420 nm were taken from previous study [4]. Those thermal conductivities were plotted as a function of temperature as presented in figure 4-18.

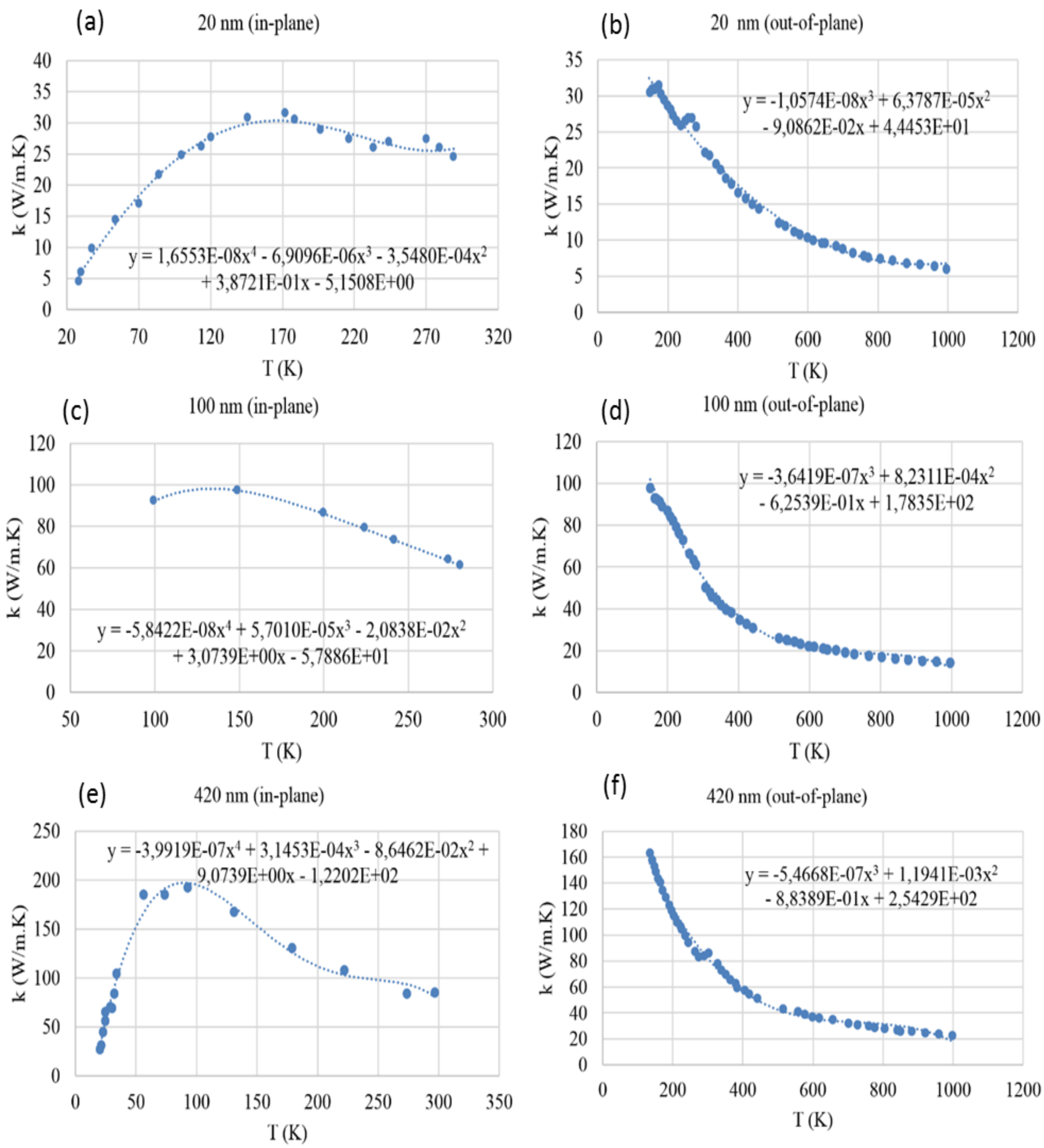

Figure 4- 18: In plane thermal conductivity of a) 20 nm c) 100 nm and e) 420 nm of silicon thin film as a function of the temperature. Out-of-plane thermal conductivity of b) 20 nm, d) 100 nm and f) 420 nm of silicon thin film as a function of temperature.

A fitting polynomial function is obtained for the in-plane and out-of-plane thermal conductivity. A polynomial expression of fourth order is obtained for the in-plane thermal conductivity and it is written as:

$$k_{in} = b_0 + b_1T + b_2T^2 + b_3T^3 + b_4T^4 \tag{33}$$

Where T is the initial temperature. The coefficients b are function of thickness of considered thin films. Curves fitting the b coefficients as function of thickness t are given by the following expressions:

b_0 = -3,8273E+01ln(t) + 1,1235E+02

b_1 = -3,7084E-05t^2 + 3,8034E-02t - 3,5863E-01

b_2 = 1,2741E-07t^2 - 2,7133E-04t + 5,0208E-03

b_3 = 8,0393E-07t - 2,3164E-05

b_4 = -3,1928E-13t^2 - 8,9887E-10t + 3,4658E-08

Table 4-3 presents the coefficients of fourth order polynomial of in-plane thermal conductivity of silicon thin films with respect to the temperature.

Table 4- 3: Coefficients of 4th order polynomial of in-plane thermal conductivity of silicon thin films with respect to the temperature.

Si film thickness (nm)	b_0	b_1	b_2	b_3	b_4
20	- 5,1508E+00	3,8721E-01	- 3,5480E-04	- 6,9096E-06	1,6553E-08
100	- 5,7886E+01	3,0739E+00	- 2,0838E-02	5,7010E-05	-5,8422E-08
420	- 1,2202E+02	9,0739E+00	- 8,6462E-02	3,1453E-04	-3,9919E-07

The fitted polynomial for the out-of-plane thermal conductivity is given in the following equation:

$$k_{out} = c_0 + c_1T + c_2T^2 + c_3T^3 \tag{34}$$

Curves fitting the c coefficients as function of thickness t are given by the following expressions:

c_0 = 6,9211E+01ln(t) - 1,5567E+02

c_1 = -2,6192E-01ln(t) + 6,5759E-01

c_2 = 3,7329E-04ln(t) - 1,0037E-03

c_3 = -1,7697E-07ln(t) + 4,9754E-07

Table 4-4 summarizes coefficients of third order polynomial of out-of-plane thermal conductivity of silicon thin films with respect to the temperature.

Table 4- 4: Coefficients of 3rd order polynomial of out-of-plane thermal conductivity of silicon thin films with respect to the temperature.

Si film thickness (nm)	c_0	c_1	c_2	c_3
20	4,4453E+01	- 9,0862E-02	6,3787E-05	-1,0574E-08
100	1,7835E+02	- 6,2539E-01	8,2311E-04	-3,6419E-07
420	2,5429E+02	- 8,8389E-01	1,1941E-03	-5,4668E-07

The in-plane and out-of-plane thermal conductivities evaluated from fitting parameters where implemented in the modelling. The total heat flux dissipated from the heat source was evaluated as a function of the variation of its diameter. Figure 4-19 represents results for silicon thin films of 20 nm, 100 nm and 420 nm.

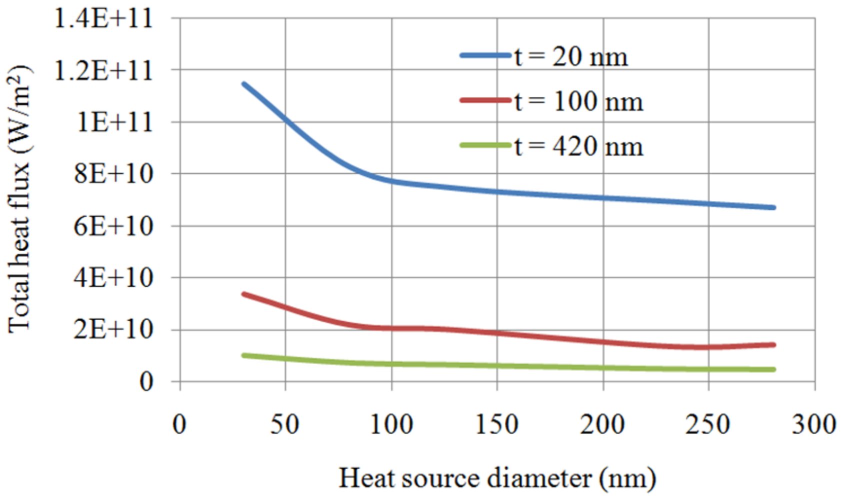

Figure 4- 19: The total heat flux of the heat source as a function of its diameter for silicon thin films with three thicknesses (20 nm, 100 nm and 420 nm).

For the three thicknesses of silicon thin films, the total heat flux decreases with increasing the heat source diameter. A sharp decrease is observed for low diameters. For a thickness of 20 nm, the total heat flux decreases sharply when the heat source diameter vary from 30 nm to 100 nm. It tends to a constant value for diameters larger than 200 nm.

In the frame of the European project, Lancaster University was in charge of creating a platform allowing all partners to have access to previously built models. Therefore our models were sent in order to add them to this platform. This allows SThM users or researchers who work in this domain to have access to material's thermal behavior.

4. Conclusion

The first part of this chapter consisted on studying thermal behavior of Palladium probe as a function of the distance separating it from sample surface. Experimental measurements were performed using the palladium probe under ambient conditions on two samples of copper and glass. Curves of approach and retract toward the samples were performed. From those curves we show the dominance of heat transferred by the probe through air. The evolution of probe response was also studied as a function of the distance separating the tip apex from the sample surface. We highlight on the presence of a resonance phenomenon in amplitude and phase for the 3ω signal which forms a cavity between the probe and the sample. Its intensity depends on the used probe, it is more revealed with the Wollaston than for the Palladium. This phenomenon is correlated to the thermal properties of the surrounding medium (air). The comparison of the normalized evolution of the probe response in amplitude and phase of same frequency for different samples showed that the observed phenomenon is independent of thermal properties of the studied sample. In a further study, this work can be completed by modelling to study more precisely this phenomenon that occurs in the micro/nanoscale and the probe's response in the presence of sample.

The second part consisted on developing numerical models with different methods such as finite element and finite difference to evaluate their domain of validity by using Silicon probe with dimensions around the ballistic heat conduction limit. Therefore a model was developed for Silicon nanoprobe while approaching toward a sample of Silicon. It was developed to have a simplified and fast numerical tool for the interpretation of data when the continuum regime is applicable. The heat flux dissipated by the probe was evaluated via the numerical model and compared to CMI partner results with finite element and finite difference methods. The comparison showed that both methods give practically same results; but from these simulations it is hard to identify which method is more reliable. Therefore in a further study those results should be compared to experimental ones issued directly from SThM measurements.

The last part of this chapter consists on developing modelling tools based on materials library using COMSOL Multiphysics. A heat source of different diameters was placed on the upper surface of Silicon, silicon dioxide, free standing films and polymers with inclusions. The heat flux dissipated from the heat source was evaluated from the modelling. This study allows SThM users to have a prediction about the material’s thermal behavior while performing SThM measurements. Researchers in this domain can have access to these models via a platform created by Lancaster University. They allow the user to change simulation parameters to adapt the built models to their measurement case.

5. References

[1] P. Tovee, M. Pumarol, D. Zeze, Kevin Kjoller, O. Kolosov, Nanoscale spatial resolution probes for scanning thermal microscopy of solid state materials, Journal of App. Phys., (112), 114317 (2012).

[2] E Puyoo, Caractérisation thermique de nanofils de silicium pour des applications à la thermoélectricité, PhD thesis, Bordeaux university (2010)

[3] O. Raphael, N. Trannoy, P. Grossel, Thermal resonance at the microscale in AC scanning thermal microscopy with a thermal resistive probe, Int. Journal of Thermophysics. (33)-1259-1269 (2012).

[4] D. Baillis,J. Randrianalisoa, Prediction of thermal conductivity of nanostructures: Influence of phonon dispersion approximation, Journal of Heat and Mass Transfer (52) 2516-2527, (2009).

[5] P. klapetek, J. Martinek, P. Grolich, M. Valtr, Graphic cards based topography artefacts simulations in Scanning Thermal Microccopy, Int. J. of Heat and Mass Transfer (108), 841-850, (2017)

[6] Glassbrenner, C. J., & Slack, G. A., Thermal conductivity of silicon and germanium from 3 K to the melting point. Physical Review, 134(4A), A1058, (1964).

[7]Shanks, H. R., Maycock, P. D., Sidles, P. H., & Danielson, G. C. Thermal conductivity of silicon from 300 to 1400 K. Physical Review, 130(5), 1743, (1963)..

[8]Anis-ur-Rehman, M., Maqsood, A. Measurement of thermal transport properties with an improved transient plane source technique. International journal of thermophysics, 24(3), 867-883, (2003).

[9] Ohishi, Y., Xie, J., Miyazaki, Y., Aikebaier, Y., Muta, H., Kurosaki, K., &Tada, T. Thermoelectric properties of heavily boron-and phosphorus-doped silicon. Japanese Journal of Applied Physics, 54(7), 071301, (2015).

[10] Data from CMI partner, 2017.

General conclusions and perspectives

These thesis works was dedicated to the characterization of probe's thermal response using scanning thermal microscopy technique to achieve more accurate interpretation of thermal measurements.

Based on literature researches, interactions between the probe-sample system and their surrounding are presented in chapter 1. We focused on the heat losses by the probe to the environment and on studies that treated the surrounding medium between the probe and the sample. Investigations showed that the probe is heated at large distances which can creates a convective phenomenon for the air environment but to date no studies considered natural convection for the surrounding medium between the probe and the sample. This raised the question about considering this assumption in this thesis work. Finally, we presented studies that characterized materials thermal properties at the macro/nanoscale since the probe's thermal response depends on these properties. Researcher's works showed that thermal conductivity of a bulk material is not the same as for thin film material which will be used in our modelling.

The main objective of chapter 2 was to develop a model for the Wollaston probe/sample system. The modelling passes through two steps; the first consisted on developing a model of the Wollaston wire based on experimental data from literature. The numerical model allowed evaluating the heat exchange coefficient to the environment which was estimated to$84000\ W.m^{-2}.K^{-1}$. In the second step, the platinum-rhodium wire was modeled with its realistic geometry using thermo-electric coupling. Based on researcher's works discussed in chapter 1, natural air convection was considered for the surrounding medium between the probe and the sample. We studied the evolution of probe's response toward a sample of copper in the DC operating mode. The comparison of our simulation results to experimental data revealed the main conclusion of this chapter showing the major role of air convection in the heat transfer mechanisms in the probe/sample system. Via the numerical model we was able to evaluate heat fluxes dissipated in the probe-sample system which lead to thermophysical quantities such as probe Joule power and the total thermal conductance. The probe Joule power relative difference was evaluated for different samples of known thermal conductivities. We concluded that the thermal probe is sensitive to thermal conductivities up to 20 $W.m^{-1}.K^{-1}$. The overall thermal conductance at the solid-solid contact was also evaluated for different samples and found to be in the range of 10^{-5} $W.K^{-1}$.

The developed model was used in Chapter 3 to elaborate a methodology for the characterization of the probe thermal signal. We proposed a sample design to be used for this study that was fabricated by VTT. The sample was composed of various steps width ranging from 100 nm to 400 nm covered by SiO_2. We have seen that the sample roughness influence on probe thermal measurements. It was also shown that the probe is sensitive to sample internal structures but cannot distinguish steps width. Therefore we proposed a new sample design with larger steps width. In order to investigate further the thermal signal, we have developed a 3D modelling of the probe-sample system with the realistic dimensions of sample. We were able to reconstitute by modelling the experimental thermal profile. We showed that the thermal signal is not only sensitive to internal structures but also gives volume information which takes into account material’s thermal properties at nanoscale. Due to the developed sample structure with various steps width we were able to estimate the probe spatial resolution which was evaluated to be above 600 nm and below 1 µm for this sample. The developed methodology can be applied for other probes to study in detail the internal structure influence on the probe thermal response. We have also studied a topography free sample composed of buried Si/SiO_2 interface. The thermal signal obtained by the probe was also reconstituted by modelling and pointed out once again on the fact that the thermal signal gives a probed volume depending on material’s thermal properties. This sample can be a powerful tool to characterize other probes. Therefore this study should be followed up by using inverse method to assess material’s thermal conductivities or surface temperature. In the frame of QuantiHeat project we studied single polymers particles of 30 µm in diameter coated with different nanometer thicknesses of silver provided by the industrial company Conpart. The aim of this study is to assess polymers thermal conductivities. We showed that single polymers particle is not adaptive to SThM techniques due to an inappropriate sample preparation. Therefore another set of polymers in an adhesive matrix was studied. We have seen that thermal profiles obtained represent a spherical tendency which seems to be similar to the shape of polymer particles. The thermal conductivity of this sample was evaluated using calibration curves of samples with known thermal conductivities. The thermal conductivity varies between 1.5 and 27 $W.m^{-1}.K^{-1}$due to the silver coating in the scanned volume. The investigation of this sample can be proceeded by developing a 3D model in order to evaluate polymers thermal behavior. Due to a lack in time this couldn't be done in this work but it should be achieved in an upcoming study.

The modelling of steps configuration allowed evaluating the thermal exchange radius b of the probe. We have determined this exchange radius for two different positions of the probe. Although we supposed having the same contact resistance when the probe scans the sample surface, our results showed that b depends on subsurface structures and it varies from 820 nm to 2.2 µm depending on material's thermal properties.

The last Chapter of the thesis was dedicated to the study of probe-sample system with nanoscale probes. We have investigated the probe's thermal response at the third harmonic in AC mode using Palladium probe. We presented a homemade electronic set up that was developed in our laboratory and allows knowing the current that flows in the probe at each moment. The experimental results of probe's response allowed highlighting on a phenomenon specific to AC operating mode which has been already observed with the Wollaston probe in a previous study. This phenomenon is interpreted by thermal wave resonance and shows the presence of interactions between the probe and the sample to distances of several tens of micrometers. It was shown to be independent of materials thermal properties and related to the thermal diffusion length of the surrounding medium (air). It seems that this phenomenon takes place between the cantilever and the sample surface whatever the thermal probe is, but it is less relevant with Palladium probe than with Wollaston one due to the signal range.

In the frame of QuantiHeat project, a study took place to evaluate the validity domain of numerical models of heat transfer in probe/sample. For this we have developed a 3D model for a silicon probe while approaching toward a silicon sample. We have calculated the heat flux dissipated by the probe during the approach. Our results were compared to other numerical methods such as FDM by CMI partners. We have demonstrated that FEM as well as FDM (1 nm) exhibits close results and can be used when the continuum regime is applicable. The reliability of these methods can be determined by comparing them to experimental results issued from SThM measurements that can be done in a further study.

The last part of this chapter was dedicated to elaborate modelling tools to evaluate material's thermal properties based on experimental data using Comsol Multiphysics in the frame of QuantiHeat. We have focused on Silicon and Silicon dioxide bulk materials, polymers with various inclusions and free standing films of Silicon. We have utilized polynomial functions using fitting procedures to evaluate thermal conductivities of materials implemented in the modelling. The simulations allowed to predict material's thermal behavior when a heat source is placed on its surface which is important when performing SThM measurements. These models were implemented in an online platform by Lancaster University. Through this study we was able to offer thermal scientists models that gives an easy access to simulation parameters such as thickness of the materials, ambient temperature that can be changed by the user.

Conclusions générales et perspectives

Ces travaux de thèse ont été consacrés à la microscopie thermique à sonde locale et plus particulièrement à la caractérisation de la réponse thermique de la sonde pour atteindre une interprétation plus fiable des mesures thermiques.

Issues des recherches de la littérature un bilan non exhaustif sur les interactions thermiques entre le système sonde-échantillon et leur environnement est présenté au chapitre 1. Nous nous sommes concentrés sur les études qui ont traité le milieu environnant entre la sonde et l'échantillon (conductif et diffusif). Les investigations ont montré que la sonde parcourue par un courant électrique est chauffée par effet Joule ce qui peut engendrer un phénomène de convection de l'air environnant, mais jusqu'à ce jour aucune étude n'a considéré la convection naturelle pour le milieu entre la sonde et l'échantillon. Cela a soulevé la question compte tenu de cette hypothèse dans ce travail de thèse. Enfin, nous avons présenté les études qui caractérisent les propriétés thermiques des matériaux à l'échelle macro/nanométrique car la réponse thermique de la sonde dépend de ces propriétés. Les travaux passés ont montré que la conductivité thermique d'un matériau massif n'est pas le même que celle d'un film mince ce qui sera pris en compte dans notre modélisation.

L'objectif principal du chapitre 2 a été d'élaboré un modèle numérique réaliste de la sonde en Wollaston et du système sonde/échantillon. La modélisation passe par deux étapes; la première consistait à développer un modèle du filament en Wollaston basé sur des données expérimentales issues de la littérature. Le modèle numérique a permis d'évaluer un coefficient d'échange thermique effectif à travers l'environnement qui a été estimée à $84000\ W/m^2.K$. Pour la deuxième étape, le filament du platine-rhodium a été modélisé en utilisant un couplage thermo-électrique. Nous avons considéré l'hypothèse de la présence de la convection naturelle pour le milieu environnant entre la sonde et l'échantillon. Sur cette base, nous avons étudié l'évolution de la réponse de la sonde s'approchant d'un échantillon de cuivre dans le mode de fonctionnement DC. La comparaison de nos résultats de simulation aux données expérimentales a révélé la principale conclusion de ce chapitre en montrant le rôle majeur de convection de l'air dans les mécanismes de transfert de chaleur dans le système sonde/échantillon. Via le modèle numérique nous avons pu évaluer les flux de chaleur dissipés dans le système sonde-échantillon qui mènent à l'évaluation des grandeurs thermophysiques comme la variation relative de puissance dissipée par effet Joule (ΔP/P) de la sonde et la conductance thermique totale. Cette variation relative a été évaluée pour différents échantillons de conductivités thermiques connues. Nous avons conclu que la sonde thermique est sensible aux conductivités thermiques jusqu'à $20 W.m^{-1}.K^{-1}$. La conductance thermique totale au contact solide-solide a été également évaluée pour différents échantillons et s'avère être de l'ordre de $10^{-5} W.K^{-1}$.

Le modèle a été utilisé dans le chapitre 3 afin d'élaborer une méthodologie pour la caractérisation du signal thermique de la sonde. Nous avons proposé un design d'échantillon nanostructuré qui a été fabriqué par l'institut de Finlande VTT. L'échantillon est composé de différentes largeurs de marche allant de 100 nm à 400 nm recouverts d'une couche de SiO_2. Nous avons vu que la rugosité de l'échantillon influence les mesures thermiques. Nous avons aussi montré que la sonde est sensible aux structures internes de l'échantillon, mais n'est pas capable de distinguer la largeur des marches. Nous avons alors proposé un nouveau design d'échantillon nanostructuré avec des marches plus larges. Afin d'étudier plus précisément le signal thermique, nous avons développé un modèle 3D du système sonde-échantillon prenant en compte les dimensions réalistes de l'échantillon. Nous avons pu reconstruire par modélisation le profil thermique expérimental. Nous avons montré que le signal thermique n'est pas seulement sensible aux structures internes, mais donne également l'information d'un volume sondé lié aux propriétés thermiques des structures internes à l'échelle nanométrique. La structure de l'échantillon développé avec différentes largeurs de marche nous a permis d'estimer la résolution spatiale de sonde qui a été évaluée supérieure à 600 nm et inférieure à 1 µm pour cet échantillon. La méthodologie développée peut être appliquée pour d'autres sondes afin d'étudier en détail l'influence des structures internes sur la réponse thermique de la sonde. Nous avons également étudié un échantillon sans topographie composé d'une interface interne de Si/SiO_2. Le signal thermique obtenu par la sonde a été également reconstitué par modélisation et souligne encore une fois le fait que le signal thermique correspond à un volume sondé dépendant des propriétés thermiques du matériau. Cet échantillon peut être un outil puissant pour caractériser d'autres sondes. C'est pourquoi cette étude doit être poursuivie en utilisant la méthode inverse pour évaluer la conductivité thermique du matériau ou la température de surface. Dans le cadre du projet QuantiHeat nous avons étudié des particules de polymères de 30 µm de diamètre, recouvertes d'une couche nanométrique d'argent de différentes épaisseurs fourni par la compagnie industrielle Compart. Le but de cette étude est d'évaluer les conductivités thermiques de ces polymères. Nous avons montré que les particules en l'état ne sont pas adaptées aux mesures par SThM.

Pour cela un autre lot d'échantillon composé de particules de polymères dans une matrice adhésive a été conçu étudié. Nous avons observé que les profils thermiques obtenues représentent une tendance sphérique qui semble être similaire à la forme de particules de polymère. La conductivité thermique de l'échantillon a été évaluée à l'aide des courbes de calibration ayant des conductivités thermiques connues. La conductivité thermique varie entre 1,5 et 27 $W.m^{-1}.K^{-1}$en raison de la couche d'argent dans le volume sondé. L'investigation de cet échantillon doit être poursuivie par l'élaboration d'un modèle 3D afin d'évaluer le comportement thermique de particules de polymères. Due à un manque de temps, cela ne pouvait être fait dans le cadre de ce travail, mais il devrait être réalisé dans une étude à venir.

La modélisation de la configuration des marches a permis évaluer le rayon d'échange thermique b de la sonde. Nous avons déterminé ce rayon d'échange pour deux positions différentes de la sonde. Bien que nous avons supposé avoir la même résistance de contact lorsque la sonde balaye la surface de l'échantillon, nos résultats ont montré que b dépend des structures internes et qu'il varie de 820 nm à 2,2 µm selon les propriétés thermiques du matériau.

Le dernier chapitre de la thèse a été consacré à l'étude du système sonde-échantillon avec des sondes nanométriques. Nous avons utilisé la sonde Palladium pour étudier la réponse de la sonde à la troisième harmonique en mode AC. Nous avons élaboré un dispositif électronique au sein de notre laboratoire permettant de connaître la tension aux bornes de la sonde à chaque instant. Les résultats expérimentaux de la réponse de la sonde a permis de mettre en évidence un phénomène spécifique au mode de fonctionnement AC qui a déjà été observé avec la sonde de Wollaston dans une étude précédente. Ce phénomène est interprété par une résonance d'ondes thermiques et montre la présence d'interactions entre la sonde et l'échantillon à des distances de plusieurs dizaines de micromètres. Il a été montré être indépendant des propriétés thermiques des matériaux et liée à la longueur de diffusion thermique du milieu environnant (air). Il semble que ce phénomène se produit entre le microlevier et la surface de l'échantillon quelle que soit la sonde thermique, mais il est moins révélé avec la sonde de Palladium due à une intensité de signal plus faible.

Dans le cadre du projet QuantiHeat, une étude a eu lieu pour évaluer le domaine de validité des modèles numériques de transfert de chaleur sonde/échantillon. Pour cela nous avons développé un modèle 3D pour une sonde en Silicium à distance d'un échantillon de Silicium. Nous avons calculé le flux de chaleur dissipé par la sonde pendant l'approche. Nos résultats ont été comparés aux autres méthodes numériques telles que FDM développées par le partenaire CMI. Nous avons démontré que les méthodes FEM comme FDM (1 nm) montrent des résultats relativement proches et peuvent être utilisés lorsque le régime de continuum est applicable. La fiabilité de ces méthodes peut être déterminée en les comparants aux résultats expérimentaux issus de mesures SThM qui peuvent être faites dans une étude postérieure.

La dernière partie de ce chapitre a été dédiée à l'élaboration d'outils de modélisation pour évaluer les propriétés thermiques des matériaux, basées sur des données expérimentales de la littérature, à l'aide de Comsol Multiphysics, et dans le cadre du projet QuantiHeat. Nous nous sommes concentrés sur des matériaux massifs en Silicium et Dioxyde de Silicium, des polymères avec diverses inclusions et des films minces suspendus en Silicium. Nous avons utilisé des fonctions polynômiales en utilisant des procédures d'étalonnage pour évaluer l'évolution des conductivités thermiques des matériaux en fonction de la température qui seront implémentés dans la modélisation. Les simulations ont permis de prédire le comportement thermique du matériau lorsqu'une source chaude est placée sur sa surface, ce qui est important lors des mesures par SThM. Ces modèles ont été implémentés dans une plate-forme en ligne par l'Université de Lancaster. Grâce à cette étude nous avons été en mesure d'offrir pour les thermiciens des modèles qui donnent un accès facile aux paramètres de simulation tels que l'épaisseur des matériaux ou de la température ambiante qui peuvent être modifiés par l'utilisateur.

Appendix

A. Lock in amplifier principle

In order to improve the signal-to-noise ratio and to extract the information contained in the different harmonics, we used a lock in amplifier of type 7265 commercialized by Ortec. The lock in amplifier allows to extract the useful component of the signal at a specific frequency. In our case it will be a multiple n’ of the modulation frequency. The signals and noises to other frequencies will be rejected and doesn’t affect the measurements. Figure 3 represents the schematic diagram of the lock in detection.

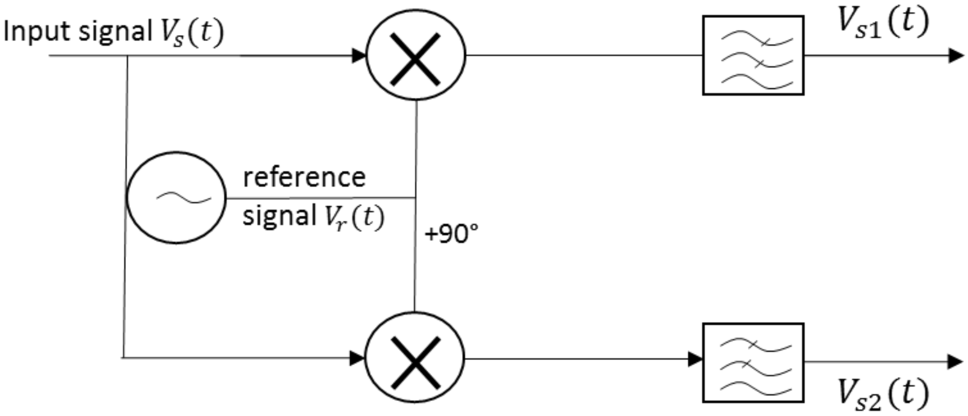

Figure A.1: Schematic representation of the lock in principle: the reference signal is multiplied by the input signal and a π/2 phase shifted form of the reference signal.

In our study the experimental set up is based on a thermo-resistive probe which is simulated by an AC current. The input signal can be decomposed into Fourier series and written as:

$$V_s(t) = \sum_{n=0}^{+\infty} R_n \cos(n\omega_0 t + \theta_n) + b(t) \tag{35}$$

Where R_n and θ_n represents respectively the amplitude and phase of the component n and b(t) represent the noise.. The reference signal passes through a frequency multiplier and can be written as:

$$V_r(t) = A\cos(n'\omega_0 t + \theta_0) \tag{36}$$

Where, ω_0 is the reference pulsation, A and θ_0 represent the amplitude and phase of reference. Thus the frequency multiplier allows then to select a harmonic of n' order of the reference signal. At the output of the multiplier, we obtain:

$$\begin{aligned} V_{s1}(t) = \sum_{n=0}^{+\infty} \frac{R_n A}{2} [&\cos\big((n+n')\omega_0 t + (\theta_n + \theta_0)\big) \\ &+ \cos\big((n-n')\omega_0 t + (\theta_n - \theta_0)\big)] + b(t)A\ \cos(n'\omega_0 t + \theta_0) \end{aligned} \tag{37}$$

Thus, when the selected harmonic n' of the reference signal is equal to the harmonic n of the wanted input signal, the signal $V_{s1}(t)$ present a DC component. After the multiplier, a low-pass filter allows the elimination of the AC and noise components. Since the input signal has always noise distributed over the whole spectrum, the filter cut off frequency must be very low to make the measurements as stable as possible.

The lock in amplifier used in this study is composed of two chains of detection. The first one compares the input signal to the reference signal $V_r(t)$ and the second one to the reference signal shifted by 90°. Thus we obtain, at the output of the filters, the two following tensions:

$$V_{s1}(t) = \frac{R_{n'}A}{2}\cos(\theta_{n'} - \theta_0) \tag{38}$$

$$V_{s2}(t) = \frac{R_{n'}A}{2}\sin(\theta_{n'} - \theta_0) \tag{39}$$

The advantage of this dual detection is to provide the possibility of determining the maximum amplitude of the output voltage$V_s(t)$, while preserving the influence of the phase shift. This amplitude is noted R and it is obtained from the following equation:

$$R = \sqrt{V_{s1}^2 + V_{s2}^2} = \frac{R_{n'}A}{2} \tag{40}$$

The amplitude A of the reference signal is stable over the time, this last relation allows us to follow the evolution of the signal carrying the information. It is also possible to calculate the shift $\Delta\theta = \theta_{n'} - \theta_0$between the reference and the input signal:

$$\frac{V_{s2}(t)}{V_{s1}(t)} = \tan\Delta\theta \tag{41}$$

With

$$\Delta\theta = \tan^{-1}(\frac{V_{s2}}{V_{s1}}) \tag{42}$$

Microscopie thermique à sonde locale : vers une analyse thermique des nanomatériaux

La microscopie thermique est un outil prometteur permettant d'étudier les mesures thermiques de matériaux et les mécanismes de transfert de chaleur aux micro/nanoéchelles. La réponse thermique de la sonde a été étudiée en utilisant deux sondes résistives : Wollaston et Palladium. Un modèle en 3D réaliste a été développé pour la sonde Wollaston et l'échantillon avec leur milieu environnant. La simulation de la sonde prend en compte son support et considère que le milieu environnant est convectif. La réponse de la sonde a été évaluée lors de l'approche vers un échantillon de cuivre. La comparaison avec les résultats expérimentaux montre que la prise en compte de la convection naturelle pour le milieu environnant est une hypothèse valide. Nous présentons ensuite une méthodologie pour étudier le signal thermique de la sonde en contact avec un échantillon nanostructuré. Pour cela, nous avons utilisé un échantillon composé de marches de silicium sous une couche de SiO2. SThM s'avère être un outil puissant pour effectuer l'imagerie sub-surfacique. Nous avons montré que le signal thermique obtenu par la sonde est influencé par la présence de structures internes et correspond à un volume sondé qui tient en compte les propriétés thermiques des matériaux. Avec notre modèle, nous avons pu reconstruire le profil expérimental obtenu par SThM. Pour la sonde en Palladium, la réponse de la sonde a été étudiée expérimentalement sous conditions ambiantes en mode alternatif. L'analyse des résultats a mis en évidence la présence d'un phénomène interpréter comme une résonance d'onde thermique qui prend place au micro/nanoéchelle. Ce phénomène est lié à la longueur de diffusion thermique du milieu environnant (air) et indépendant des propriétés thermiques de l'échantillon.

Mots clés: Microscopie thermique à balayage, Caractérisation thermique, échantillon nanostructuré, sonde thermique, milieu convectif, onde thermique, modèle, expérimental

Thermal Probe Microscopy: Toward a thermal analysis of nanomaterials

Scanning thermal microscopy is a promising tool to investigate material's thermal measurements and heat transfer mechanisms at the micro/nanoscale. The probe thermal response was explored using two different resistive probes: Wollaston and Palladium probes. A 3D realistic model was developed for the Wollaston probe-sample system with their surrounding medium. The simulation of probe takes into account its holder and considers that the surrounding medium between the probe and the sample is convective. The probe's response was evaluated during the approach toward a sample of copper. The comparison with experimental results showed that considering natural air convection for the surrounding medium is a valid assumption. We then present a methodology to characterize the thermal signal of probe in contact with a nanostructured sample. For that, we used a sample composed of buried silicon steps under SiO_2. SThM proves to be a powerful tool to perform subsurface imaging. We showed that the thermal signal obtained by the probe is influenced by the presence of internal structures and corresponds to a scanned volume which takes into account material's thermal properties. With our modelling, we was able to rebuild the experimental profile obtained by SThM. For the Palladium probe, the probe's response was studied experimentally under ambient conditions in the AC mode for different frequencies. The analysis of the results pointed on a phenomenon which can be described as a thermal wave resonance which takes place at micro/nanoscale. This phenomenon was shown to be related to the thermal diffusion length of the surrounding medium (air) and independent of the sample thermal properties.

Keywords: Scanning thermal microscopy, Characterization, nanostructured sample, thermal probe, convective medium, thermal wave, model, experimental

Discipline : MÉCANIQUE DES FLUIDES, ÉNERGÉTIQUE, THERMIQUE, COMBUSTION, ACOUSTIQUE

Spécialité : Energétique et Génie des procédés

Université de Reims Champagne-Ardenne

GRESPI - EA 4694

Campus Moulin de la Housse